Spatio-temporal regulation of mRNA decay revealed by a novel single-molecule dual-color imaging method

Inauguraldissertation

zur

Erlangung der Würde einer Doktorin der Philosophie

vorgelegt der

Philosophisch-Naturwissenschaftlichen Fakultät

der Universität Basel

von

Ivana Horvathova

aus der Tschechischen Republik

Basel, 2018

Genehmigt von der Philosophisch-Naturwissenschaftlichen Fakultät
auf Antrag von:

Prof. Dr. Silvia Arber
(Fakultätsverantwortliche)

Dr. Jeffrey Chao
(Dissertationsleiter)

Prof. Dr. Ramesh Pillai
(Korreferent)

Basel, 12. 12. 2017

Prof. Dr. Martin Spiess
Dekan

ACKNOWLEDGEMENT

First of all, I would like to thank my supervisors throughout my scientific career. Namely, Asst. Prof. Štěpánka Vaňáčová, Ph.D. for guiding me through my first scientific steps during bachelor and master thesis research, Assoc. Prof. Pavel Kovařík, Ph.D. for the first exposure to a foreign scientific environment in his laboratory, and my current mentor, Jeffrey Chao, Ph.D. for the scientific and career advice he gave me during my doctoral studies, for his supervision, and for allowing me to ask the right scientific questions and find the path to address them. He has always been a great source of new challenging ideas with regards to the projects. Furthermore, I very much appreciate all my current and former colleagues from Chao laboratory for creating a very positive and encouraging working environment and for their constructive criticism. By being a part of the Chao laboratory, I had the chance to work with very motivated people who inspire me, and I had the chance to mature scientifically. I have learnt a lot. And I have been lucky to find friends in my colleagues who have proven to be empathic and willing to give a hand when needed. Particularly, I would like to thank my colleague Franka Voigt, Ph.D. for her support in imaging and data analysis and for cooperation in bringing my project to the completion. It was also my pleasure to work with Anna Kotrys, M.Sc. and Caroline Artus-Revel, M.Sc. who valuably contributed to the acquisition and analysis of imaging data, and to biochemical assays, respectively. I also want to acknowledge my colleague Varun Bhaskhar, Ph.D. for proofreading of my thesis.

The mathematical modeling, as a part of my project, was done in collaboration with scientists from a neighboring laboratory. This computer simulation done by Luca Giorgetti, Ph.D. and his doctoral student Yinxiu Zhan, M.Sc. was very refreshing to the project. Also, experts from the core FMI technology platforms were always there to provide an experimental guidance and assistance. Most of the work would not be possible without constant support from our Facility for Advanced Imaging and Microscopy (FAIM), especially without Jan Eglinger, Ph.D. who supported the image analysis, and also Laurent Gelman, Ph.D. and Steven Bourke, M.Sc.. For the sorting of unusually dimly fluorescent cells, I want to acknowledge Hubertus Kohler from the fluorescence activated cell sorting (FACS) facility. And thanks to Michael Stadler from Computational Biology for developing a normalization pipeline for our imaging data.

I would also like to acknowledge my thesis committee members Helge Grosshans, Ph.D., Prof. Ramesh Pillai, Ph.D., my faculty representative Prof. Silvia Arber, Ph.D., and one additional member of the yearly committee meetings, Prof. Witold Filipowicz, Ph.D. for scientific inputs and fruitful discussions. Furthermore, I would like to thank Prof. Jeffrey Kieft, Ph.D. from University of Colorado School of Medicine for providing the sequence of viral elements, being now a core of the imaging system developed during my project, and helpful advice on its usage.

Last but not least, I want to thank my entire family, especially my parents for their endless encouragement. Similarly, I own special thanks also to my sister, Veronika; without her I would not be where I am today. And I would like to acknowledge my friends for supporting me throughout my entire life. In particular, I am deeply grateful to my best friend, Adela, for sharing the same sense of humor. Importantly, I want to cordially thank my partner, Martin, for his constant love and support, scientific discussions and also proofreading of my thesis.

Table of Contents

1. SUMMARY

Discoveries that have been made over past decades emphasized the importance of post-transcriptional control as a means of regulating gene expression. RNA turnover is one of the key aspects of post-transcriptional control that contributes directly towards maintenance of normal cellular homeostasis. Degradation of functional messenger RNAs (mRNAs) is a tightly regulated process and its dysregulation results in either excessive or insufficient amounts of mRNAs within cells that eventually lead to a disease-associated condition. Furthermore, multiple quality control mechanisms eliminate aberrant mRNAs thereby preventing their translation into malfunctioning proteins. The realization of the importance of RNA decay pathways has fueled further research towards understanding the underlying molecular mechanisms in RNA turnover and its regulation.

All protein-coding mRNAs, as well as non-coding RNAs, have distinct half-lives and are ultimately degraded. Previously, many of the factors involved in RNA decay pathways have been identified and studied. Two types of enzymes are shared among RNA decay pathways: exonucleases and endonucleases. The former are further divided into 5′-to-3′ and 3′-to-5′ degrading enzymes and their activation is often dependent on prior removal of terminal stability marks from an RNA molecule. The best-studied exonuclease is Xrn1 that degrades an RNA substrate from the 5′-end to 3′-end. On the other hand, endonucleases cleave an RNA strand to expose the resultant fragments to exonucleases, circumventing the requirement of first removing the stability marks.

Most of our current appreciation of the molecular mechanisms related to the mRNA decay is attributable to the methods that involve ensemble measurements. However, these measurements often result in an averaged outcome from whole population of cells, wherein information about variability among individual cells is lost. In addition, the possibility to get information on the spatio-temporal regulation of mRNA decay is limited using ensemble methods. Hence, accurate dissection of the spatial and temporal regulation of mRNA decay requires development of a single-molecule method that preserves information on cell-to-cell variability. Single-molecule RNA imaging methods have already been used to study several aspects of the mRNA life cycle and they have helped to uncover *in vivo* regulations that were not possible to

observe before. However, a powerful imaging method allowing for an observation of mRNA turnover in real-time at the level of single cells/molecules has been missing.

During my PhD, I established a robust single-molecule imaging technique in order to characterize the spatio-temporal dynamics of RNA turnover within its cellular context. I engineered an mRNA reporter that contains viral tandem pseudo-knots placed between PP7 and MS2 stem-loops. These orthogonal stem-loops can be labeled with spectrally distinct fluorescent proteins. In addition, the viral pseudo-knots block Xrn1-mediated degradation resulting in stabilization of the reporter's 3′-degradation intermediate that is otherwise inherently instable. This stabilized 3′-end contains only the MS2 stem-loop region. Thus, intact mRNAs are labeled with both fluorophores, while incompletely degraded mRNA fragments are labeled only with a single fluorophore. I used the amounts and positions of intact mRNAs and stabilized 3′-ends as readout of mRNA degradation. Therefore, this technique is called 3(Three)′-RNA End Accumulation during Turnover (TREAT).

I applied TREAT to monitor the fates of mRNAs in single fixed and living mammalian cells. Using this method, I measured the kinetics and cell-to-cell variability of mRNA decay in fixed cells. The nuclear export rates and cytoplasmic mRNA half-lives showed that individual degradation events occur independently within the cytoplasm suggesting that there is no burst in mRNA degradation. In addition, I found that transcripts, as well as degradation intermediates, are dispersed throughout cytoplasm and are not enriched within processing bodies in living cells. Imaging of an mRNA biosensor targeted for an endonucleolytic cleavage by the RNA-induced silencing complex (RISC) showed that slicing can be observed in real-time in cytoplasm of living cells but does not occur in nucleus. The slicing events were found to have no spatial preference with respect to the distance from the nucleus.

In addition to the rate of synthesis and the rate of turnover, the levels of mRNAs were found to be affected by the rate of translation as well. Indeed, I have also observed that inhibition of translation by several compounds increases mRNA stability, suggesting that the processes of mRNA degradation and translation are globally interconnected. The cross-talk among three processes central to the mRNA life cycle, transcription, degradation and translation, is becoming increasingly apparent. However, further research is required to obtain a detailed understanding of the molecular interplays in eukaryotic cells. As TREAT system visualizes mRNA from its synthesis in the nucleus through export to degradation in cytoplasm, I anticipate that

this methodology will provide a framework for investigating the entire life history of individual mRNAs in single cells.

2. INTRODUCTION

2.1. THE IMPORTANCE OF mRNA DECAY

A vital aspect of regulated gene expression occurs via the modulation of abundance of messenger RNAs (mRNAs). The levels of all cellular transcripts are determined by the rates of transcription in the nucleus and degradation mostly taking place in the cytoplasm. Constant mRNA levels reflect on equilibrium of transcription and decay while changes in mRNA levels may be caused by alterations in either of them. While the importance of transcription in controlling gene expression is well established, it has become increasingly clear that the regulation of mRNA stability, particularly during cellular transitions, can dramatically influence cytoplasmic mRNA concentrations (Elkon et al., 2010; Friedel et al., 2009; Hao and Baltimore, 2009; Miller et al., 2011; Rabani et al., 2011; Shalem et al., 2011). Moreover, it has been shown that up to 50% of changes in gene expression occur at the level of mRNA stability (Cacace et al., 2012; Cheadle et al., 2005; Garcia-Martinez et al., 2004; Schwanhausser et al., 2011). In dynamic processes such as embryonic development, cell differentiation and cellular stress responses, cells have to possess adequate amounts of particular mRNAs at a given time that can serve as templates for synthesis of proteins that are required for the physiological process. Understanding whether dynamic changes in mRNA levels are due to changes in mRNA transcription or changes in mRNA decay is not trivial. The transcriptome is composed of mRNAs of different lifetimes, however their susceptibility to degradation may change significantly thereby affecting protein synthesis. A long lifetime of an mRNA enables a cell to produce more proteins from that particular mRNA. When a rapid reduction in protein expression is needed, discontinuation of transcription can reflect only slowly on the levels of mRNAs with long half-lives. Therefore, active degradation of these mRNAs must be triggered to halt protein production. By an active recruitment of a degradation machinery to otherwise stable mRNAs within appropriate time, a cell ensures to adjust the mRNA levels. In contrast, for mRNAs with intrinsically short half-lives, the decrease in transcription rate can be the main contributor towards diminished mRNA levels. In another scenario, when a cell needs to preserve energy resources or the mRNAs themselves, decay pathways can be stopped for a time period needed to decide about the cellular fate.

The importance of mRNA decay can be illustrated on a specialized RNA degradation program that has been discovered to function during early development in metazoa. The developmental stages have to be tightly regulated by changes in gene expression pattern to establish a new cellular program. After the fusion of specialized differentiated cells, an oocyte and a spermatozoon, the derived zygote has to undergo a reprograming event to become a pluripotent embryo. This process is referred to as maternal-to-zygotic transition (MZT) and requires the both zygotic genome activation (ZGA) and the degradation of maternal products. During early embryogenesis, cellular functions are dependent primarily on maternal transcripts and proteins while there is little to no transcription of mRNA from the zygotic genome. Subsequently, the newly formed zygotic genome begins to be transcribed while mechanisms that destabilize and clear the maternal mRNA are activated in a coordinated manner. The proper orchestration of maternal mRNA clearance is critical for normal embryogenesis (reviewed in Yartseva and Giraldez, 2015).

2.2. LIFE CYCLE OF MRNA IN A NUTSHELL

The transcription of RNA is executed via DNA-programmed-RNA polymerase. The best studied is RNA polymerase II (Pol II) that transcribes protein coding as well as some non-coding genes. In principle, Pol II is recruited to a promoter region on DNA by transcription factors to form preinitiation complex (PIC). Additional elements often required for Pol II recruitment and thus initiation of the transcription are *cis*-acting enhancers, and *trans*-acing activators and co-activators. Once Pol II is recruited to its target gene, it starts scanning the sequence downstream of the promoter to find a transcription start site. Shortly after transcription initiates, a protective cap composed of 7-methylguanosine is co-transcriptionally deposited onto the 5′-end of the emerging transcript. Cap-binding proteins stabilize the emerging mRNA and heterogeneous nuclear ribonucleoproteins (hnRNPs) associate with the nascent transcript so that splicing, the maturation process that removes introns, can occur during transcription elongation or soon after the release of the nascent transcript (Coulon et al., 2014; Martin et al., 2013). After Pol II has transcribed the cleavage and polyadenylation signal, these regulatory sequences are recognized by factors that cleave the transcript at a predefined 3′-site, which is followed by transcription termination. The exposed 3′-end is further polyadenylated, which in turn stabilizes the mature transcript (reviewed

in Neve et al., 2017). A poly(A)-tail containing transcript packaged into an mRNA ribonucleoprotein (mRNP) is then exported to the cytoplasm. After export, a repertoire of mRNA binding proteins remodels the mRNP to favor the binding of cytoplasmic factors, such as eukaryotic initiation factors (eIFs) to start translation (reviewed in Muller-McNicoll and Neugebauer, 2013). The dynamic remodeling is thought to facilitate the formation of a circular conformation of mRNA held by the interaction of eIF4G to both the cap-binding eIF4E and the poly(A)-binding protein (PABP), thus forming a bridge between 5′- and 3′-termini (Wells et al., 1998). This circularization is proposed to promote the cycling of ribosomes on the mRNA leading to time-efficient translation (reviewed in Gallie, 1998). Apart from translation, mRNA-associated proteins can influence the rate of mRNA degradation either directly by promoting or precluding binding of decay factors or indirectly by influencing the cellular location.

2.3. CYTOPLASMIC MRNA DECAY PATHWAYS

2.3.1. Bulk decay of mRNAs

Degradation of mRNAs is a multistep process that requires an orchestrated series of enzymatic reactions (reviewed in Garneau et al., 2007). If an mRNA is locked in a circular form, then decircularization proceeds removal of protective hallmarks – the cap and poly(A)-tail. For most mRNAs, shortening of the poly(A)-tail is thought to be the first and rate-limiting step in mRNA decay and requires the consecutive actions of the Pan2-Pan3 and Ccr4-Not-Caf1 complexes (reviewed in Chen and Shyu, 2011; Funakoshi et al., 2007; Yamashita et al., 2005). The existence of additional deadenylases, such as poly(A)-specific ribonuclease PARN, expands the repertoire of poly(A)-tail length regulators in eukaryotes (reviewed in Godwin et al., 2013). The relative contribution of the deadenylases to overall poly(A)-tail length regulation is not entirely clear. Deadenylated transcripts are fed into one of the exonucleolytic degradation pathways (Figure 1). Following deadenylation, Lsm1-7-Pat1 complex binds to shortened 3′-terminal adenosine extension and recruits the decapping enzymes Dcp1-Dcp2 to the 5′-end. As a next step, Dcp1-Dcp2 hydrolyzes the 5′-cap structure (Dunckley and Parker, 1999; Lykke-Andersen, 2002; van Dijk et al., 2002). Decapping generates a transcript with 5′-monophosphate that serves as a substrate for Xrn1 (5′-to-3′ exonuclease), which rapidly degrades the transcript in a processive fashion (Chang et al., 2011; Jinek et al., 2011; Stevens, 1980). Currently, Xrn1-

mediated degradation is believed to be the dominant eukaryotic cytoplasmic decay pathway, perhaps through the coupling of Xrn1 to Dcp1-Dcp2 by the scaffold protein and enhancer of decapping 4 (Edc4) (reviewed in Chang et al., 2014a; Jones et al., 2012). On the other hand, the mammalian cytoplasmic exosome complex, including the catalytic subunit Dis3-like exonuclease (Dis3l), degrades the mRNA in 3′-to-5′ direction upon deadenylation (reviewed in Lykke-Andersen et al., 2011). The activity of the exosome in the cytoplasm depends on the presence of a specific activator in form of the hetero-tetramer Ski complex (Halbach et al., 2013). Alternatively, Dis3l2 is another cytoplasmic exonuclease that acts independently of the exosome and Ski complex and degrades RNAs from the 3′-end (Astuti et al., 2012). Following 3′-to-5′ decay, the remaining mRNA fragment with its 5′-cap is degraded by scavenger decapping enzyme (DcpS). This enzyme is capable of efficiently hydrolyzing capped RNA substrate when its length does not exceed 10nt (reviewed in Milac et al., 2014). Selection for Dis3l2 pathway is often achieved by the non-templated addition of a uridine tract to the 3′-end of a deadenylated mRNA, which provides a binding site for Dis3l2 to initiate or even reinitiate the degradation (Chang et al., 2013a; Malecki et al., 2013).

Intriguingly, the current model that deadenylation is a prerequisite for bulk mRNA degradation has been challenged by several observations. First, an addition of non-templated uridine-rich stretches to the 3′-termini of a polyadenylated mRNA alone triggers mRNA instability in *Schizosaccharomyces pombe (S.p.)* (Rissland and Norbury, 2009). The uridylation attracts Dis3l2 that is required for such pathway activity. Besides Dis3l2, uridylation of poly(A)-tailed transcripts has been proposed to render vulnerability to the Xrn1-nucleolytic attack by recruitment of Lsm1-7 heptameric complex to uridylated 3′-end (Rissland and Norbury, 2009). Further, the observation that Xrn1-mediated decay and Dis3l2-mediated decay probably cooperate in *S.p.* only highlights the apparent complexity of mRNA degradation pathways in eukaryotic cells (Malecki et al., 2013). This cooperation is underscored by the interaction of both nucleases with one another and with polysomes in human cells, suggesting that degradation pathways might be coupled to the ongoing translation. Moreover, high-throughput sequencing has revealed numerous mRNA targets shared by Dis3l2 and Xrn1 indicating cooperation of these two enzymes in RNA catalysis (Lubas et al., 2013). Altogether, both uridylation and deadenylation may play partially redundant roles in triggering RNA degradation, and it remains to be determined whether

deadenylation-independent exonuclease attack of poly(A)-tailed mRNAs can operate in mammalian cells.

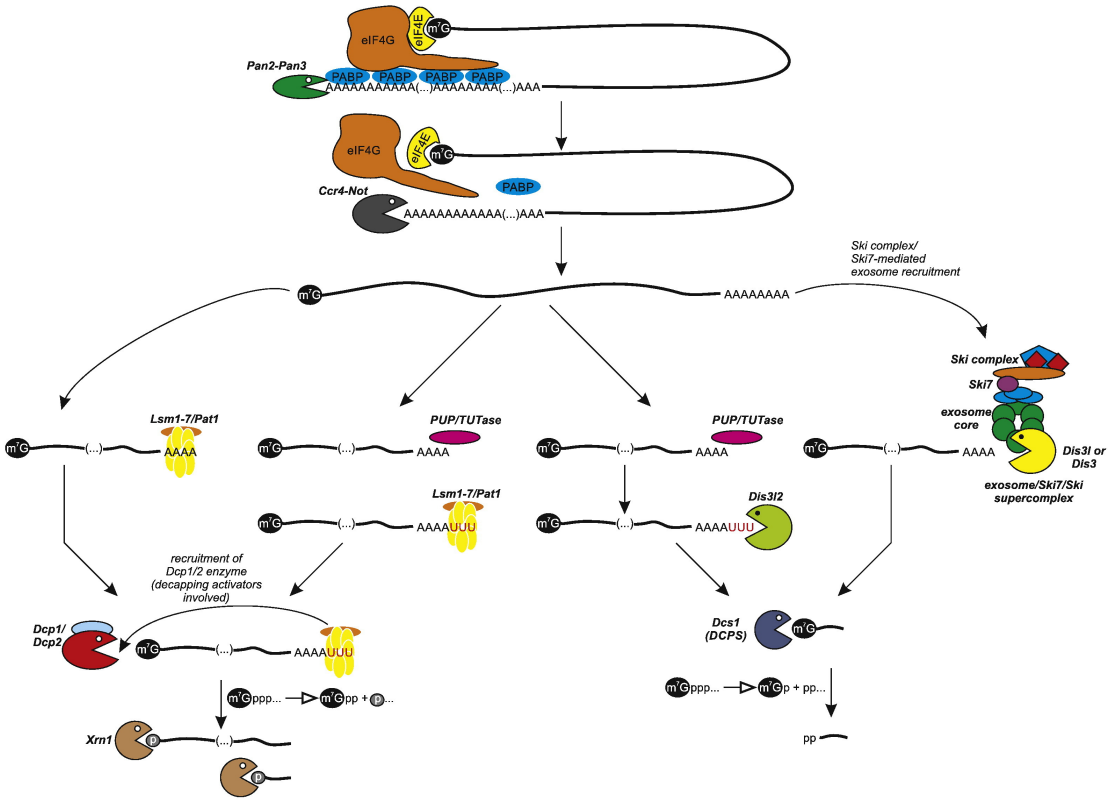

Figure 1. Overview of major degradation pathways of poly(A)-tailed mRNAs (adapted from the review Labno et al., 2016a)

Step-wise deadenylation is executed by the Pan2-Pan3 and Ccr4-Not complexes. The displacement of PABPs releases the circular form of mRNA held by bridging contacts between cap-binding eIF4E and eIF4G proteins. The degradation can proceed by recruitment of 5′-to-3′ degradation factors after the binding of the Lsm1-7-Pat1 complex at the 3′-end activating the decapping complex composed of Dcp1-Dcp2. The unprotected 5′-end is then degraded by Xrn1. Deadenylated mRNAs that have been uridylated by terminal uridyl-transferases (TUTases) are either fed into the Xrn-1 dependent pathway, or targeted by the 3′-to-5′ exoribonuclease Dis3l2. Degradation of deadenylated mRNA can also occur in the 3′-to-5′ direction by the exosome complex recruited by Ski complex.

2.3.2. Small RNA-mediated mRNA decay

Transcripts can contain regulatory sequences targeting them for an accelerated decay. The regulation of targeted RNA degradation is, in part, ensured by highly conserved and widespread post-transcriptional gene silencing (PTGS) through microRNAs (miRNAs) or small-interfering RNAs (siRNAs). These small RNAs (sRNAs, usually ~22 nt) are loaded onto an Argonaute (Ago) protein to guide the RNA-induced silencing complex (RISC) to mRNAs in a sequence-specific manner. The degree of sequence complementarity between sRNA and mRNA governs which mode of silencing is activated. Perfect or near-perfect complementarity triggers an endonucleolytic cleavage of a target mRNA whereas imperfect pairing elicits, translational repression often coupled with destabilization by exonucleolytic degradation (reviewed in Carthew and Sontheimer, 2009).

miRNAs are genomically encoded and originate from Pol II-mediated transcription of genes, referred to as MIR genes. Transcribed primary (pri)-miRNAs are stabilized by a 5′-cap and 3′-poly(A)-tail. Subsequently, the pri-miRNA is trimmed into a stem-loop precursor (pre)-miRNA by the RNase III enzyme Drosha operating in a complex with the dsRNA-binding protein DiGeorge syndrome critical region 8 (DGCR8) (Kwon et al., 2016). The pre-miRNA is further processed into a mature miRNA duplex by Dicer, another RNase III enzyme, in complex with its cofactors, the protein activator of the interferon-induced protein kinase (PACT) and the TAR RNA binding protein (TRBP) (reviewed in Carthew and Sontheimer, 2009; Kok et al., 2007). Alternatively, non-canonical miRNAs can also originate from precursors called mirtrons, arising from introns. This pathway bypasses the Drosha processing (Berezikov et al., 2007; Okamura et al., 2007; Ruby et al., 2007). In mammals, mature miRNAs are associated with all four Ago proteins (Ago1-4), but only Ago2 displays endonuclease activity (Liu et al., 2004; Meister et al., 2004). A single strand, commonly referred to as a guide strand, from the duplex miRNA is selected for the incorporation into a mature RISC complex. This is governed by the thermodynamic profile of the duplex termini (Khvorova et al., 2003; Schwarz et al., 2003). The limited base pairing prevents most animal miRNAs from cleaving the target mRNA and, instead, causes destabilization of the target transcript by base pairing to its 3′-untranslated region (UTR) (Lim et al., 2005; Wu et al., 2006). miRNA-mediated PTGS depends on recruitment of GW182 (also known as TNRC6) that in turn specifically binds to the Ccr4-Not complex eventually leading to translational repression and/or mRNA

deadenylation followed by exonucleolytic decay (Chekulaeva et al., 2011; Liu et al., 2005). Interestingly, while miRNA-directed cleavage of mRNAs is common in plants, there are only a few such examples of animal miRNAs that extensively pair with their targets to trigger a cleavage (Xu et al., 2016; Yekta et al., 2004). In mammals, miRNAs are predicted to control the activity of ~60% of all protein coding genes (Friedman et al., 2009). Although all four vertebrate Ago proteins seem to have overlapping functions, the individual capacities and selectivity for various miRNAs remains unclear (Su et al., 2009).

Unlike miRNAs, the origin of siRNAs is generally an exogenous viral RNA. Other sources of siRNAs exist, for instance repeat-associated transcripts of centromeres and transposons (reviewed in Carthew and Sontheimer, 2009). However, members of endogenous class of siRNAs (endo-siRNAs) are generated from intrinsic, long, double stranded transcripts (Hamilton et al., 2002; Yang and Kazazian, 2006). Biogenesis of siRNAs starts with long double stranded precursor RNAs formed either through intramolecular base pairing or by the activities of RNA-dependent RNA polymerase (RdRP). Dicer processes the precursors into mature siRNA duplexes. A guide siRNA strand is selected that fully matches the sequence of a target mRNA to facilitate an endocleavage. Given that only Ago2 displays endonuclease activity, it acts as the core effector of siRNAs-mediated PTGS (Figure 2) (Liu et al., 2004; Meister et al., 2004). The Ago2 cleavage site on a target RNA is located between 10th and 11th nucleotides from the 5′-terminus of the siRNA guide strand (Elbashir et al., 2001). The resulting 3′-end cleavage product bears 5′-monophosphate and it is therefore rapidly recognized by Xrn1 for rapid degradation. On the other hand, the 5′-end cleavage product exposes its 3′-terminus to the activity of exosome and it is degraded in a processive manner (Orban and Izaurralde, 2005). A second decay pathway has been implicated in the degradation of 5′-end cleavage fragments. The exposed 3′-terminus can be extended by the activity of a particular terminal uridylyl-transferase (TUTase) that can in turn stimulate Dis3l2-mediate degradation (Shen and Goodman, 2004; Ustianenko et al., 2016; Xu et al., 2016). Nevertheless, siRNA can be found associated to other paralogs of the Argonaute protein family than Ago2 and have been proposed to influence transcriptional gene silencing (TGS) (Janowski et al., 2006; Kim et al., 2006). siRNAs are commonly used as a means to modulate the expression of a desired gene as a laboratory technique, often referred to as RNA intereference (RNAi). RNAi is triggered by artificial introduction of siRNA duplexes into cells or by expression of short-hairpin RNAs that enter the sRNA biogenesis pathway to become siRNAs.

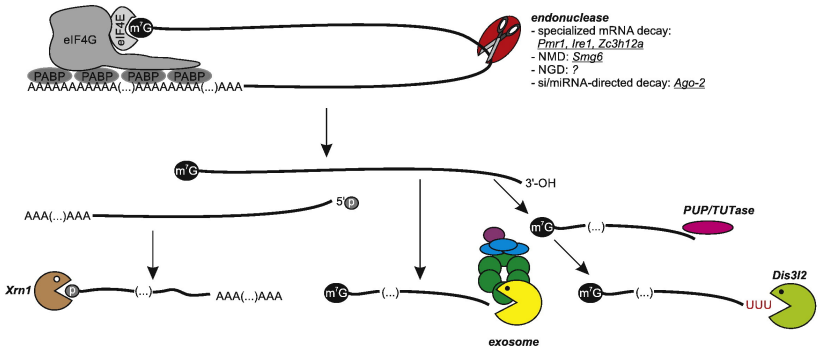

Figure 2. Degradation initiated by endocleavage of poly(A)-tailed mRNAs (adapted from the review Labno et al., 2016a)

Internal cleavage by endonucleases occurs without prior deadenylation or decapping, which results in release of fragments with unprotected 3′- and 5′-ends. The fragments can be degraded in the 5′-to-3′ direction by Xrn1 and in the 3′-to-5′ direction by the exosome complex or by Dis3l2 after non-templated uridylation of the exposed 3′-end.

A third class of small RNAs functioning in TGS (as well as PTGS) are piwi-interacting RNAs (piRNAs). piRNAs have special biogenesis processes that significantly differ from miRNA or siRNA pathways. Piwi proteins belong to a different clade of evolutionarily conserved Argonaute family. piRNAs are derived from both transposons and genes and are only found in animals (reviewed in Siomi et al., 2011). These types of sRNAs are highly enriched in the germline tissues where they silence mobile DNA elements, thereby contributing towards genome integrity (reviewed in Weick and Miska, 2014). piRNAs were reported to have a specialized function in gonads, however, information regarding their presence and role in somatic tissue is scarce.

2.3.3. Endonuclease-initiated mRNA decay

RNA degradation can be initiated by an internal cleavage without prior removal of protective 5′-cap and 3′-poly(A)-tail. This is executed by endonucleases that expose the unprotected ends of cleaved fragments to exonucleases. Some endonucleases have been implicated in processing of various RNA species while other endonucleases regulate the stability of selected mRNA targets. The activation of endonucleases is often dependent on specific signals such as stress stimuli (reviewed in Tomecki and

Dziembowski, 2010). One endonuclease is Ago2, the core factor of RISC, that has been described in the previous section. Here, I will focus on other endonucleases that modulate the stability of mRNAs.

The following overview demonstrates the diversity of endonucleases and their functions in mRNA decay in eukaryotes. First of all, Smg6 (suppressor with a morphogenetic effect on genitalia 6) is an endonuclease effector implicated in a surveillance mechanism and can cleave mRNAs near premature termination codons (PTCs) during non-sense mediated decay (NMD) (Eberle et al., 2009; Huntzinger et al., 2008). Second endonuclease, Ire1 (inositol-requiring enzyme 1), is an endoplasmic reticulum (ER) transmembrane protein. In general, proteins translated by ER-bound ribosomes are mostly targeted to the ER itself, to other organelles, or destined for secretion (reviewed in Bravo et al., 2013). In the case of ER-stress, unfolded proteins accumulate in the ER lumen and are sensed by the Ire1 protein. Consequently, Ire1 gets activated by autophosphorylation and acts as an endonuclease on many of ER-associated mRNAs to initiate their degradation. This is referred to as regulated Ire1-dependent decay (RIDD). The increased turnover of ER-bound mRNAs, provides lower influx of nascent proteins into the ER lumen and at the same time releases the translational machinery for synthesis of proteins that are crucial to response to the stress, such as chaperons. Hence, Ire1 helps to restore the balance within the ER during the unfolded protein response (UPR), and thus Ire1 contributes to avoiding apoptosis (Oikawa et al., 2010; Tirasophon et al., 2000). A third example of an endonuclease is Regnase1 (also known as ZC3H12A or MCPIP1) that specifically recognizes stem-loop structures present in 3'-UTR of cytokine mRNAs, such as tumor-necrosis factor α (TNF-α) and interleukin 6 (IL6). However, the cleavage sites have been mapped to occur outside of the stem-loop region (Boehm et al., 2016). The synthesis of Regnase1 is induced by macrophages and monocytes and has an essential role in preventing immune disorders (Matsushita et al., 2009; Mino et al., 2015). Next, Pmr1 (polysomal ribonuclease 1)-mediated mRNA decay depends on the binding of Pmr1 to a polysome-bound substrate mRNA (Yang and Schoenberg, 2004). Other site-specific nucleases G3BP (Ras-GTPase activating protein SH3 domain-binding protein) and Ape1 (apurinic/apyrimidinic endonuclease 1) cleave *c*-Myc mRNA, and cleavage of *α*-globin mRNA is carried out by an erythroid-enriched endonuclease (Barnes et al., 2009; Tourriere et al., 2001; Wang and Kiledjian, 2000). As part of the body's innate immune defense, the endonuclease RNaseL can be induced in response to viral infection in order to unspecifically degrade RNAs within

the cell and thereby limit the synthesis of both viral and cellular proteins (Bisbal and Silverman, 2007). In *Xenopus laevis,* another endonuclease XendoU localizes to ER and cleaves the mRNA without any apparent sequence specificity, however, it is thought to function in a calcium-dependent manner. Human cells possess a XendoU homolog that promotes ER remodeling by inducing the eviction of ribosome together with mRNPs from the ER membrane (Schwarz and Blower, 2014). The growing list of endoribonucleases with either general or specialized mRNA targeting emphasizes a larger role in mRNA metabolism than has been previously anticipated, nevertheless, there are still many questions that remain to be answered.

2.3.4. mRNA surveillance mechanisms

Quality control mechanisms are pathways that prevent erroneous mRNAs from serving as templates for translation (reviewed in Garneau et al., 2007). These surveillance mechanisms first detect the erroneous mRNA followed by recruitment of nucleases that are shared with bulk mRNA degradation. Non-sense mediated decay (NMD) is the most understood mRNA surveillance pathway that targets newly synthesized mammalian mRNAs bearing a premature termination codon (PTC). The PTC is a stop codon positioned upstream of the normal termination codon, and it typically induces NMD when spaced by 50 nt or more from the nearest exon junction complexes (EJC). In the nucleus, EJCs are deposited ~20-24 nt upstream of exon-exon junction generated by splicing and transported to the cytoplasm together with the mRNA (reviewed in Le Hir et al., 2016). NMD is presumed to act during the pioneer round of translation and its task is to eliminate PTC-containing mRNAs in order to prevent synthesis of truncated proteins. An essential NMD factor, up-frameshift 1 (Upf1), interacts with cap binding protein 80 (CBP80) that is, in general, translocated with newly synthetized mRNA from nucleus. Through a cascade of protein-protein interactions, Upf1 gets phosphorylated and depending on the site of phosphorylation, either the Smg6 or Smg5-Smg7 complex is recruited. The endonuclease Smg6, already described in the previous paragraph, mediates a cleavage of the NMD target followed by Xrn1- and exosome-mediated degradation. In parallel, the pathway involving Smg5-Smg7 initiates degradation by deadenylation and/or decapping releasing the mRNA body for exonucleolytic cleavage from either site (reviewed in Maquat et al., 2010; Nicholson and Muhlemann, 2010).

Besides NMD, other quality control mechanisms including no-go decay (NGD) and non-stop decay (NSD) ensure fidelity of mRNAs. NGD degrades faulty mRNAs by endonucleolytic cleavage near sites where ribosomes have stalled. The responsible endonuclease has yet to be identified. Similar to other decay pathways initiated by endonucleases, the cleaved mRNA fragments are further degraded by the combined actions of exonucleases from either side. On the other hand, NSD functions on mRNAs lacking a stop codon, which results in translation proceeding through the poly(A)-tail potentially till the very 3′-end. As a result of translation through the poly(A)-tail, the ribosome adds a C-terminal poly-lysine tract to the nascent polypeptide. This can trigger ribosome stalling and subsequent dissociation due to unfavorable electrostatic forces between the positively charged poly-lysine peptide and the negatively charged exit tunnel of the ribosome (Ito-Harashima et al., 2007; Lu et al., 2007). Moreover, PABPs are likely displaced from poly(A)-tail by the translating ribosome, leading to the promotion of decapping and Xrn1-mediated decay. However, recruitment of exosome to NSG substrates is not ruled out. Both control mechanisms, NGD and NSD, release sequestered ribosomes and other translation factors, which can engage in translation of other mRNA (reviewed in Ghosh and Jacobson, 2010).

2.3.5. Regulatory *cis*-elements

Additional mRNA decay pathways have also been identified that enable regulation of the stability of mRNA molecules bearing specific *cis*-regulatory elements. Among these, the most studied is the AU-rich elements (ARE)-mediated decay. Similarly to the vast majority of miRNA sites, many AREs are found in 3′-UTRs of transcripts. The ARE-containing transcriptome encodes for proto-oncogenes (for example, *c*-Fos) and inflammatory mediators (for example, TNFα, IL1, IL2, IL3, granulocyte macrophage colony-stimulating factor (GMCSF)). In combination with their cognate binding proteins (BPs), AREs have important physiological and pathological functions. In general, ARE-BPs (for instance, tristetraprolin (TTP), butyrate response factor 1 and 2 (BRF1 and BRF2, respectively), KH-type splicing regulatory protein (KSRP) and AU-rich binding factor 1 (AUF1)) function as adaptor proteins to recruit the degradation machinery to the target mRNA. Association and dissociation of the adaptor protein to the AREs is regulated by their phosphorylation state (Briata et al., 2005; Clement et al., 2011; Mahtani et al., 2001; Schmidlin et al.,

2004; Wilson et al., 2003). The decay of ARE-containing mRNAs begins with poly(A)-tail shortening and the mRNA body is subsequently targeted for decay by both the 5′-to-3′ and 3′-to-5′ decay machineries (Murray and Schoenberg, 2007; Yamashita et al., 2005). However, the factors of the 5′-to-3′ decay machinery, Xrn1 and Lsm1, were shown to be essential for ARE-mediated decay (AMD) (Stoecklin et al., 2006). Importantly, ARE-BPs can also have a stabilizing effect. Another protein binding AREs, named human antigen R (HuR), counteracts the effect of the destabilizing ARE-BPs by competing for the binding sites, and thus promotes mRNA stability (Brennan and Steitz, 2001). Phosphorylation status not only modulates the affinity of ARE-BPs to mRNAs but also their nucleocytoplasmic shuttling presumably both in unbound and mRNA-bound forms (Brook et al., 2006; Lee et al., 2011). Phosphorylation at different sites of HuR controls its subcellular distribution depending on the cell-cycle stage. HuR is retained in the nucleus at late G2 phase by cyclin-dependent kinase 1 (Cdk1) phosphorylation and HuR regulates stability of the cyclin mRNAs (Kim et al., 2008). In contrast, phosphorylation at other sites can promote the translocation of HuR into cytoplasm (Doller et al., 2008; Doller et al., 2007; Lafarga et al., 2009).

The second most studied *cis*-regulatory elements that induce instability of mRNA are GU-rich elements (GREs). These regulatory elements are enriched in the 3'-UTR of human transcripts that exhibit rapid mRNA turnover (reviewed in Vlasova-St Louis and Bohjanen, 2011). GREs confer affinity to CUG-binding protein 1 (CUGBP1), which mediates subsequent transcript deadenylation by recruiting PARN deadenylase and thus degradation (Moraes et al., 2006; Vlasova et al., 2008).

In *Drosophila*, degradation pathways for mRNA clearance of maternal transcripts during the MZT have been extensively studied. One of the characterized decay pathways for a large subset of maternal mRNAs depends on a conserved protein called Smaug that recognizes a stem-loop structure within these mRNAs and recruits the Ccr4-Not complex to initiate poly(A)-tail shortening and subsequent mRNA elimination (Tadros et al., 2007). Interestingly, the majority of stem-loop structures with affinity to Smaug can be found within coding regions, and only some occur in 3′-UTRs as revealed by a transcriptome-wide mapping (Chen et al., 2014a).

A specialized degradation pathway is elicited by Staufen1 (Stau1) on mRNAs that harbor Stau1-binding site within their 3′-UTR. Stau1-mediated mRNA decay (SMD) is also dependent on a direct interaction of Stau1 with the key NMD factor Upf1, and the downstream series of events seems to be analogous to NMD (reviewed in

Park and Maquat, 2013). Stau1 thus competes for Upf1 binding with other proteins including other NMD factors.

Specific stem-loop sequence, referred to as the iron-responsive element (IRE), is found in the transferrin receptor mRNA, ferritin mRNA, and other mRNAs whose products are involved in iron homeostasis in animal cells. In cooperation with *trans*-acting iron regulatory proteins (IRPs), *cis*-acting IRE is responsible for the control of translation initiation or mRNA stability. The mRNA of ferritin (an iron storage protein) contains one IRE in its 5′-UTR. When iron concentration is low, IRPs bind the IRE in the ferritin mRNA reducing its translation. In contrast, binding of IRPs to multiple IREs in the 3′-UTR of the transferrin receptor (involved in iron acquisition) leads to increased mRNA stability by preventing endocleavage within the stem-loops sequence of IREs and subsequent degradation (reviewed in Muckenthaler et al., 2017).

2.3.6. Decay of replication-dependent histone mRNAs

An exceptional case is the cell-cycle-regulated decay of replication-dependent histone mRNAs. The degradation rate of these histone mRNAs peaks at the end of S phase, which demonstrates the coordination of histone protein synthesis with DNA replication. This unique post-transcriptional regulation is possible owing to the specific architecture of histone mRNAs, including the presence of a conserved stem-loop (SL) instead of poly(A)-tail. The 3′-end positioned element can be bound by a specific SL binding protein (SLBP) and by the Eri1 exoribonuclease (reviewed in Marzluff et al., 2008; Tan et al., 2013). Initiation of degradation is achieved by the interaction of SLBP with TUTase-4 or TUTase-7 which add an oligo(U)-tail to the 3′-terminus, thereby recruiting the Lsm1-7 complex (Lackey et al., 2016; Mullen and Marzluff, 2008; Schmidt et al., 2011). Upon Lsm1-7 binding, decapping and subsequent Xrn1-mediated decay (3′-to-5′) and/or 3′-to-5′ decay by Eri1 in cooperation with exosome occur. It has been suggested that the 3′-to-5′ decay directionality dominates, and thus the degradation occurs in a biphasic mode. First, repetitive rounds of Eri1-mediated decay and TUTase-dependent uridylation allow for SL removal (Hoefig et al., 2013). The second degradation step is executed by the exosome complex (Mullen and Marzluff, 2008). At the end of S phase, when histone mRNA translation terminates, the stem-loop bound SLBP interacts with Upf1 suggesting recruitment of other NMD factors as well (Kaygun and Marzluff, 2005). Although the molecular mechanism how

Upf1 facilitates the histone mRNA degradation in not known, researchers suggested that the helicase activity of Upf1 opens the SL structure enabling faster exonucleolytic attack from the 3′-end (Hoefig et al., 2013). Recently, even Dis3l2 was shown to play a role in decay of replication-dependent histone mRNAs (Labno et al., 2016b; Lubas et al., 2013). How the multiple degradative enzymes work in concert to degrade histone mRNA timely requires further investigation.

2.3. COMPARTMENTALIZATION OF CYTOPLASMIC MRNA DECAY EVENTS

2.3.1. Processing bodies

Many subcellular locations have a specialized function. However, it is not well established how cytoplasmic granules or organelles are implicated in RNA degradation. Membraneless cytoplasmic compartments, termed processing bodies (PBs), were discovered as Xrn1-containing foci in a mouse fibroblast cell line (Bashkirov et al., 1997). Their size ranges from 100nm to 300nm in diameter. Besides Xrn1, these cytoplasmic foci also accumulate mRNA decapping factors, deadenylases, Ago proteins, GW182, mRNAs, miRNAs, NMD and AMD factors, and others, suggesting their coordinated action (Figure 3). Moreover, the cytoplasmic exosome complex as well as its adaptor Ski complex are excluded from PBs. This indicates that PBs principally concentrate players of the 5′-to-3′ degradation machinery. Interestingly, PBs lack most of the translation factors including eIF4A and PABPs, however, still contain the cap binding eIF4E. The absence of many translational factors indicates that these have to dissociate from mRNPs before or immediately after they enter or aggregate to form PBs. In correlation with this, mRNAs that localize to PBs are translationally silenced (reviewed in Kulkarni et al., 2010).

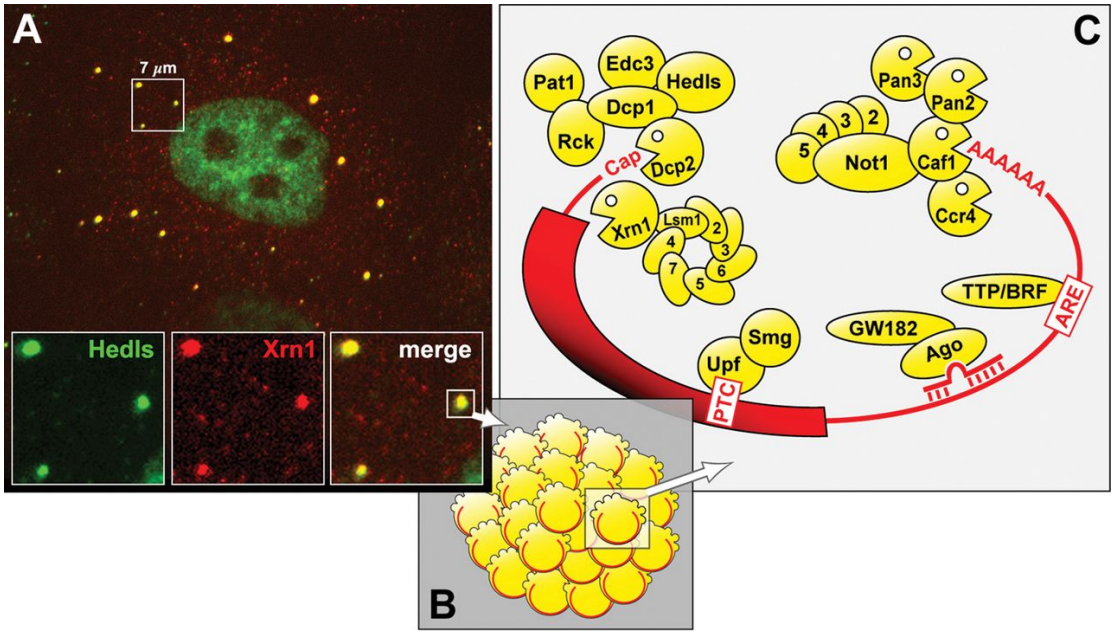

Figure 3. Features and composition of processing bodies (reviewed in Kulkarni et al., 2010)

A*) Components of PBs, Xrn1 in red and Hedls (also known as Edc4) in green, visualized by immunofluorescence staining in African green monkey COS7 kidney cells.* ***B****) Schematic representation of mRNPs assembled into a PB.* ***C****) PBs contain translationally silenced mRNAs that may bear cis-elements in form of a miRNA site, a PTC, or an ARE. Protein factors involved in recognizing PTCs (Upf and Smg), factors associated with miRNAs (Ago and GW182) or bound to AREs (TTP, BRF) also localize to PBs. Furthermore, PBs harbor deadenylase complexes (Pan2-Pan3, Ccr4-Not-Caf1), the decapping enzyme Dcp2 together with its activators (Dcp1, Rck, Hedls, Edc3 and Pat1) as well as the 5′-to-3′ exonuclease Xrn1 that is associated with the Lsm1–7 complex.*

There is a long-standing debate over the role of PBs; whether they only store the repressed mRNAs, particularly during cellular stresses, or if they also contribute to mRNA degradation. Owing to the absence of PABPs from PBs and the presence of enzymes involved in deadenylation, researchers have assumed that the mRNAs localized to PBs have only short poly(A)-tail, if any (Kedersha et al., 2005). Indeed, oligo-(dT) probe visualized poly(A)-containing mRNAs residing in PBs only upon Xrn1 depletion (Aizer et al., 2014; Cougot et al., 2004). Moreover, microscopically visible PBs disappear when deadenylation is blocked supporting the notion that deadenylation is a prerequisite for PB formation (Cougot et al., 2004; Sheth and Parker, 2003; Zheng et al., 2008). Since the degradation processes are functional in

cells with disrupted PBs and since the inhibition of miRNA biogenesis causes disappearance of PBs, the formation of microscopically detectable PBs has been proposed to be a consequence, not the cause, of mRNA degradation including miRNA-mediated gene silencing (Eulalio et al., 2007; Stalder and Muhlemann, 2009). On the other hand, PBs are more prominent when Xrn1 or Dcp2 is deleted and mRNAs accumulate to higher extend suggesting inhibited degradation of accumulated mRNAs (Cougot et al., 2004; Eulalio et al., 2007; Sheth and Parker, 2003). In addition, mRNA decay intermediates have been trapped in yeast PBs proposing possible regulation of mRNA degradation in these compact cytoplasmic environments (Sheth and Parker, 2003). Quantitative analysis of fluorescently tagged mRNA reporters during amino acid starvation proposed a dual role of PBs – mRNA degradation and storage (Aizer et al., 2014). However, direct evidence for PBs as decay factories in mammals has not yet been presented and the high concentration of degradation enzymes in particular spots does not necessarily suggest their local activity.

PBs are highly dynamic spherical structures. The number and size of visible PBs varies depending on the translational activity of a cell, which may be compromised by various cellular stresses (Brengues et al., 2005; Teixeira et al., 2005). In addition, PBs number and size changes throughout the cell cycle with enlarged and more abundant PBs in late S and G2 phases. But these foci disappear in mitotic phase (Eystathioy et al., 2002; Sivan et al., 2007; Yang et al., 2004). Although Xrn1 is found concentrated in discrete PBs, it is also found concurrently throughout the cytoplasm. This, along with a recent finding of the co-translational degradation of mRNAs, correlates with the notion that PBs are dispensable for mRNA degradation (Eulalio et al., 2007; Pelechano et al., 2015; Stalder and Muhlemann, 2009). Nevertheless, it is challenging to rule out a possible existence of submicroscopic PBs that would provide increased local concentration of degradative factors and potential mini-factories for mRNA degradation.

2.3.2. Stress granules

Another microscopically detectable cytoplasmic aggregates, stress granules (SGs), were first observed in the cytoplasm of tomato cells (Nover et al., 1989). Similar to PBs, SGs are not constricted by a membrane and accumulate translationally repressed mRNAs. In addition, mitotic cells are unable to assemble SGs when

ribosomes are stalled on the mRNAs (Sivan et al., 2007). In contrast to PBs, SGs are often larger (up to microns in diameter) amorphous structures appearing only in response to translational arrest (such as stress) and they dissolve completely when translation is restored. Non-translating mRNAs within SGs are bound by the 40S ribosomal subunit and translation initiation factors. Furthermore, SGs harbor G3BP and PABPs, the latter suggesting poly(A)-tail integrity of recruited mRNAs (reviewed in Anderson and Kedersha, 2008).

2.3.3. Processing bodies docking to stress granules

Both of the dynamic structures, PBs and SGs, share non-translating mRNAs together with multiple protein factors (for instance Xrn1, HuR, eIF4E, TTP, BRF1, cytoplasmic polyadenylation element-binding protein 1 (CPEB1), RISC components, T-cell internal antigen-1 (TIA-1) and TIA-1-related (TIAR)) and are frequently located adjacent to each other, indicating a possible cargo exchange (Kedersha et al., 2005; Wilczynska et al., 2005). Intriguingly, PBs and SGs are formed independently in mammalian cells since abrogation of one does not restrain assembly of the other (Kedersha et al., 2005; Serman et al., 2007). Physically connected to surrounding cytoplasm, PBs and SGs have no membrane to preclude flux of molecules in and out. Indeed, mRNAs can exit both PBs and SGs and assemble into polysomes to re-engage in translation (Bhattacharyya et al., 2006; Brengues et al., 2005). It remains to be determined whether mRNPs can move from PBs to SGs, from SGs to PBs or in both directions as their tethering indicates. A sorting model, called mRNA triage, has been proposed wherein translationally stalled mRNAs assemble with other factors to form SGs. From SGs, mRNPs are sorted to reinitiate translation in cytosol, to be stored in SGs, or to be transferred into PBs for potential degradation (reviewed in Anderson and Kedersha, 2008).

Commonly, environmental stresses are sensed by cellular kinases and results in eIF2α phosphorylation leading to cap-dependent translation inhibition followed by polysome disassembly (reviewed in Anderson and Kedersha, 2008). The translational arrest is potentially selective as a study focused on ER stress on a global level showed that translation of 25% of mRNAs was significantly suppressed, while translation of another 25% of mRNAs was significantly enhanced (Kawai et al., 2004). During stress conditions, proteins necessary for stress adaptation, such as heat-shock protein 70

and 90 (Hsp70 and Hsp90, respectively) are preferentially synthetized, while many other RNAs are selectively recruited to SGs for translational arrest in order to conserve limited resources (e.g. many mRNAs coding for housekeeping proteins) (Kedersha and Anderson, 2002; Stohr et al., 2006). Up to 20% of total cellular mRNAs are represented by transcripts with several nucleotides long 5′-terminal oligopyrimidine motif (5′-TOP) within a context of unstructured 5′-UTR. This CU-rich motif is found in vast majority of transcripts encoding components of translational machinery and housekeeping genes, referring to their collective regulation (reviewed in Hamilton et al., 2006). Upon amino acid starvation, translational regulation of 5′-TOP-containing mRNAs has been shown to be dependent on TIA-1 and TIAR, factors promoting nucleation of SGs (Damgaard and Lykke-Andersen, 2011). However, transcripts containing 5′-TOP tract were shown to localize also into PBs during arsenite stress (Halstead et al., 2015). Stress-induced stabilization is particularly evident for ARE-containing mRNAs, where the accumulation of HuR in stress granules and PBs is proposed to protect these transcripts by displacing destabilizing ARE-BPs (reviewed in von Roretz et al., 2011). The link between both compartments appears to be a part of the integrated stress response enabling to survive adverse environmental conditions by, at least, selectively regulating the protein expression. It is of high importance to reveal the underlying regulations in order to describe the functional link between mRNA degradation, storage, and translation in response to environmental cues.

Condensation of mRNPs can be driven by a phenomenon known as liquid-liquid phase transition (reviewed in Banani et al., 2017). The potential of some mRNPs to assemble into PBs and SGs is partly provided by prion-like self-interacting domains, often present in aggregates-associated proteins. Thus the formation of small aggregates could serve as a platform for assembly of bigger structures as it was suggested for PB-nucleation initiated by Edc3, Pat1 and Lsm4 proteins (Decker et al., 2007; Mazzoni et al., 2007; Pilkington and Parker, 2008; Reijns et al., 2008). One possible mechanism of SG-assembly is through the self-aggregation of prion-like domains in the RNA binding proteins TIA-1 and TIAR (Gilks et al., 2004). Live imaging experiments showed association of PBs to cytoskeleton, which may affect the localization of the aggregates. Rather stationary PBs were associated with actin bundles, whereas others displaying mobility were connected to microtubules (Aizer et al., 2008; Gallina et al., 2013; Sweet et al., 2011). It is still an open question if PBs with different motilities could function differently. SGs are less mobile than PBs, yet they constantly change shape, fuse or divide (Kedersha et al., 2005). The dynamics of both

membraneless entities, PBs and SGs, were proposed to be partly governed by dynein and kinesin, the motor proteins traversing along microtubules (Loschi et al., 2009). Although the role of the cytoskeleton in assembly and movement of PBs and SGs remains poorly understood, it may be responsible for bringing these two compartments into proximity to cooperate and exchange mRNAs destined for storage or degradation and exchange the cargo.

2.3.4. Endoplasmic reticulum

PBs were first implicated as sites of post-transcriptional RNA silencing due to presence of target mRNA, miRNA and Ago proteins in these foci (Jagannath and Wood, 2009; Jakymiw et al., 2005; Liu et al., 2005; Pillai et al., 2005). Nevertheless, subsequent examinations found microscopically visible PBs to be dispensable for miRNA-mediated gene silencing, raising the notion that the localization of the RNA silencing machinery and target mRNAs to PBs is rather a consequence than the cause of RNA silencing activity (Chu and Rana, 2006; Eulalio et al., 2007). More recently, emerging evidence revealed connection between sRNA-mediated gene silencing and rough endoplasmic reticulum (rER) (Barman and Bhattacharyya, 2015; Li et al., 2013a; Sahoo et al., 2017; Stalder et al., 2013; Wu et al., 2013). Extensive subcellular fractionation showed that miRNA- and siRNA-loaded human Ago2 population co-sediments on the ER membrane together with the triad of RISC-factors: Dicer, PACT, TRBP (Haase et al., 2005; Kok et al., 2007; Stalder et al., 2013). It is PACT and TRBP that anchors RISC to outer ER membrane in an RNA-independent manner. Stalder *et al*. has proposed that loading of miRNA and siRNA into RISC, encounter of the target mRNA, and Ago2-mediated slicing are nucleated at the rER. Furthermore, nucleation of RISC loading and mRNA slicing at the ER membrane is not qualitatively essential but physiologically important for the kinetics and efficacy of this process (Stalder et al., 2013).

Continuous with the outer layer of the nuclear envelope, the rER compartment constantly binds and releases ribosomes from its membrane, creating the dotted pattern on its surface. Towards cell periphery, ER changes its character from membranous sheets of rER to tubular structure of smooth ER lacking ribosomes. The classic view holds that mRNAs encoding cytosolic or nucleoplasmic proteins are translated on cytosolic ribosomes, whereas mRNAs encoding secretory or membrane

proteins are translated on the rER. This view is under reconsideration as recent observations suggest that rER may serve for translation of broad range of mRNAs (Chen et al., 2011; Lerner et al., 2003; Pyhtila et al., 2008; Reid and Nicchitta, 2012). In addition to the ER-anchored Ire1 endonuclease that is activated upon ER-stress (described in 2.1.3.), the spatial coincidence of functional RISC complexes and translation machineries suggests that translation and degradation of mRNA may generally function in concert at the rER.

2.4. NUCLEAR RNA DECAY

While most of the mRNA degradation machineries reside in the cytoplasm, there are also nuclear RNA degradation pathways. In the nucleus, Xrn1-related exonuclease, Xrn2, is involved in the processive degradation of nuclear RNAs as well as ribosomal RNA maturation, transcriptional termination and quality control of mRNA capping (Fang et al., 2005; Jiao et al., 2010; Kim et al., 2004; Miki et al., 2017; West et al., 2004). As opposed to nuclear localization of Xrn2, Xrn1 has typically been assumed to localize exclusively to the cytoplasm. Interestingly, recent investigations in yeasts suggest that Xrn1 shuttles to the nucleus assembled in complexes with other factors and show that disruption of Xrn1 catalytic activity compromises transcription (Haimovich et al., 2013; Medina et al., 2014). However, the exact role of Xrn1 in the nucleus remains to be determined.

One dominant protein complex implicated in accurate processing of nuclear RNA precursors, in nuclear turnover of aberrant RNAs and products of pervasive transcription is the nuclear form of exosome complex. Furthermore, nuclear exosome is also implicated in control of expression levels of some mRNAs. In contrast to cytoplasmic exosome complex containing the exonuclease Dis3l besides the core 9 subunits, the nucleoplasmic exosome complex contains catalytic units in form of Dis3 and Rrp6 proteins. Given the plethora of exosome substrates in the nucleus, many cofactors were identified to bring the exosome to different classes of substrates (reviewed in Chlebowski et al., 2013).

Besides cytoplasmic function in PTGS, it is becoming evident that sRNAs also have specific nuclear functions and have been proposed to play a role in transcriptional gene silencing (TGS) or in transcriptional gene activation (TGA) in mammalian cells

(reviewed in Catalanotto et al., 2016). Western blots of nuclear fractions and immunostaining have revealed the presence of Ago proteins, Dicer, TRBP, and TNRC6 in cell nuclei, where they combine to form multiprotein complexes (Gagnon et al., 2014; Nishi et al., 2013; Ohrt et al., 2008; Rudel et al., 2008; Weinmann et al., 2009). In parallel, miRNAs have been detected in the nuclear compartment through microarray analysis and sRNA deep sequencing of nuclear extracts (Gagnon et al., 2014; Jeffries et al., 2011; Liao et al., 2010). Gagnon and coworkers found that the nuclear Ago2 programmed with exogenous siRNAs retains its catalytic activity and is able to cleave a nuclear long noncoding RNA, metastasis-associated lung adenocarcinoma transcript 1 (MALAT1), inducing its degradation. Surprisingly, RISC-loading and maturation factors, for instance Hsp90, Translin, TRAX, were found to be excluded from nucleus (Gagnon et al., 2014). The current hypothesis is that the sRNA-Ago2 assembly occurs outside the nucleus, where some critical loading factors are present. Once established, the minimal RISC may subsequently be imported into the nucleus. However, it still remains elusive if these sRNA-associated protein complexes play a role in mRNA degradation in the nucleus mimicking their cytoplasmic function.

Altogether, the nuclear envelope allows more molecules than previously anticipated to localize back to the nucleus. This blurs the dogmatic view on compartmentalized gene expression regulation in eukaryotes and opens new possibilities to unravel the complicated molecular network behind the fundamental cellular processes.

2.5. MODULATION OF MRNA STABILITY BY OTHER ASPECTS

There are several other important aspects of mRNA stability modulation. Among them, alternative polyadenylation and signaling pathways are well-established topics, whereas the impact of mRNA methylation on its stability has emerged only recently. Most of human precursors of mRNAs feature multiple cleavage and polyadenylation signal sequences in their 3′-UTR. These signals provide a means to vary the 3′-end of mature mRNAs. As most of the *cis*-acting elements that regulate mRNA half-life are situated within 3′-UTRs, an mRNA containing shorter 3′-UTR is less likely to possess one or more of these elements when compared to its isoform with a longer 3′-UTR (reviewed in Elkon et al., 2013). Thus, the alternative

polyadenylation contributes to the complexity of transcriptome by creating isoforms of different vulnerability to stability regulators.

A list of stimuli eliciting signaling pathways that regulate mRNA stability is expanding. Cellular signaling networks are important for rapid response to external stimuli (UV radiation, heat shock, hypoxia, nutrient deprivation, oxidative stress) and intrinsic factors (cytokines, growth factors, cellular stress mediators, hormones) to trigger post-translational modifications (PTMs) of RNA-binding proteins by phosphorylation, ubiquitination, methylation, acetylation etc. These modifications are essential for either changes in general abundance of RNA-binding proteins, or changes of their binding properties. Thus, rapid remodeling of dynamic RNPs changes the regulation of mRNA turnover and translation. The examples of prominent signaling cascades are: p38 mitogen-activated protein kinase (MAPK), which regulates phosphorylation of e.g. TTP; c-Jun N-terminal kinase (JNK); extracellular signal-regulated kinases (ERK); AMP-activated kinase (AMPK); mammalian target of rapamycin (mTOR) (reviewed in Thapar and Denmon, 2013). Other kinase pathways phosphorylate eIF2α. These are protein kinase R (PKR), which responds to viral infection, PKR-like endoplasmic reticulum kinase (PERK) is triggered by ER-stress, general control nonderepressible 2 (GCN2) kinase is activated upon amino acid starvation, and heme-regulated initiation factor 2α kinase (HRI) senses oxidative stress by arsenite (Barber, 2005; Damgaard and Lykke-Andersen, 2011; Harding et al., 2000; McEwen et al., 2005). One of the fundamental biological questions that needs to be answered in detail is how the gene expression is regulated in response to extrinsic stresses and what are the molecular factors that play a role in these signaling pathways.

Besides modifications of RNA binding proteins, mRNA itself can be modified post-transcriptionally. The fate of an mRNA can be modulated by depositing an N6-methyl group onto an adenosine (m^6A), which turned out to be the most abundant modification in eukaryotic mRNAs and long non-coding RNAs (Liu and Pan, 2016). This reversible modification is typically enriched in long exons, near stop codons, and in the 3′-UTR (Dominissini et al., 2012; Meyer et al., 2012). As 3′-UTR is rich in *cis*-regulatory elements, this hints that sequence methylation might have an impact on mRNA stability. Despite the identification of several components of this system, including methyltransferases (called “writers), demethylases (referred to as “erasers”), and m^6A interacting proteins (“readers”), the mechanisms by which methylation

regulates mRNA functions are currently being extensively studied (reviewed in Meyer and Jaffrey, 2014).

2.6. mRNA DECAY-TRANSCRIPTION FEEDBACK LOOP

Emerging evidence is changing researcher's view on the central dogma of molecular biology as a compartmentalized one-directional process. The recent findings favor a model where all eukaryotic cellular processes do not happen in isolation but rather are integrated in a circular gene expression system. In addition, the nuclear envelope appears permeable for decay factors in both directions.

Xrn1 has been recently implicated as a key factor in mediating the buffering between the rates of transcription and mRNA decay in order to maintain appropriate levels of gene expression in yeast (Bregman et al., 2011; Haimovich et al., 2013; Medina et al., 2014; Sun et al., 2013; Trcek et al., 2011). Different mechanistic explanations of how Xrn1 contributes to buffering of mRNA levels were provided. One report suggests that downregulation of mRNA degradation triggers the expression of transcription repressor Nrg1 that subsequently downregulates mRNA synthesis, while the second report implies that decay factors associate with chromatin and affects transcription initiation and elongation (Haimovich et al., 2013; Sun et al., 2013). Conversely, reduced mRNA synthesis leads to decreased rates of mRNA turnover (Sun et al., 2013; Sun et al., 2012). Shown by Haimovich *et al.*, Xrn1 shuttles between nucleus and cytoplasm, which is in line with its proposed dual function, in synthesis and degradation (Haimovich et al., 2013). Subsequently, it was shown that Xrn1 enhances transcription rate with a bias towards the most actively transcribed genes, including components of translation machinery (Medina et al., 2014). Further research is needed to clarify how the interconnection between the decay and transcription is mediated and to determine if such coupling of RNA synthesis-degradation occurs in higher eukaryotes.

Herpesvirus-encoded endonuclease, called SOX, degrades mammalian host mRNAs in cytoplasm, which is sensed by cell and triggers a feedback mechanism in the nucleus by repressing RNA PoI II-transcription of cellular genes but not viral genes. Intriguingly, Xrn1 catalytic activity is required for this transcriptional feedback (Abernathy et al., 2015). This is in parallel to findings in yeast indicating that Xrn1-

linked transcriptional regulation is a conserved feature. Noteworthy, rotavirus infection forces exonuclease Xrn1 along with the decapping enzyme Dcp1a to relocalize from cytoplasm to nucleus perhaps as a consequence of PB disruption (Bhowmick et al., 2015). The precise function of Xrn1 in the mutual feedback between mRNA synthesis and degradation, however, still remains elusive.

2.7. COUPLING MRNA DECAY AND TRANSLATION

Discovery of the interaction between the PABP and the eIF4F complex led to the hypothesis that the circular conformation of mRNA promotes translation. In addition, it was also thought to contribute towards mRNA stability by restricting access of the free ends to exonucleases. Altogether, this led to the idea that translation and degradation might be spatio-temporally uncoupled. However, several lines of evidence indicate that mRNA degradation is intimately coupled to translation. First, multiple mRNA quality control pathways depend on ongoing translation (reviewed in Garneau et al., 2007). The next connection between mRNA decay rates and active translation is reflected by the observation that the codon content of the transcript has some impact on how quickly it is degraded. It has been found recently that mRNAs comprising optimal codons have long half-lives. Optimal codons can be decoded by the ribosome more efficiently due to optimal abundance of a particular charged tRNA, and thus are translated faster. On the other hand, transcripts composed of suboptimal codons, undergoing slower translation, are significantly less stable (Presnyak et al., 2015). Recently, in yeast, Dhh1 was identified as the sensor of translation elongation rate and couples translation to mRNA decay. Messages containing suboptimal codons associate with higher number of Dhh1 proteins causing destabilization of the mRNAs (Radhakrishnan et al., 2016). This phenomenon has been demonstrated so far in yeast, but whether such a mechanism for fine-tuning gene expression exists in higher eukaryotes is yet to be determined. Mammalian Dhh1 homolog, Ddx6, was shown to interact with Ccr4-Not complex, which may potentially recruit downstream degradation effector proteins (Chen et al., 2014b; Mathys et al., 2014; Ozgur et al., 2015). Ribosome pausing on poly(A)-stretches during translation that may lead to accelerated mRNA degradation has been also shown in both invertebrate and vertebrate cells (Arthur et al., 2015). Lastly, another yeast study based on a genome-wide sequencing, which identifies 5′-monophosphorylated molecules that are mRNA degradation

intermediates *in vivo*, revealed that degradation by Xrn1 followed last translating ribosome as seen by characteristic 3-nucleotide periodicity in sequenced coding regions. This footprint is a result of general co-translational 5′-to-3′ mRNA degradation pathway suggesting that the ribosomes do not have to dissociate from an mRNA before the degradation is initiated (Pelechano et al., 2015).

Another link between degradation and translation can be seen due to the existence of PBs and SGs, which can be physically connected to each other and potentially exchange non-translating transcripts in-between these two entities. Moreover, SGs contain many translation factors that PBs lack. On the contrary, multiple degradation factors reside in PBs, but most of them are present in SGs as well, including Xrn1 (reviewed in Decker and Parker, 2012).

2.8. THE PIVOTAL EXORIBONUCLEASE XRN1

Much of the known molecular underpinnings of Xrn1-mediated decay come from studies in the yeast *Saccharomyces cerevisiae (S.c.).* Orthologs of Xrn1 have been identified in most key model organisms as well as in humans. Studies using higher eukaryotes have enhanced our current understanding of molecular mechanisms and biological roles of Xrn1 in multicellular organisms. The majority of the cytoplasmic decay mechanisms involve Xrn1 activity in cooperation with its interacting partners as described in the previous sections.

The first crystal structure of the multi-domain Xrn1 enzyme comes from yeast *Kluyveromyces lactis* (Chang et al., 2011). Concurrently, the mechanism of action of the Xrn1 enzyme was strongly supported by the crystal structure of *Drosophila melanogaster* Xrn1 in complex with an RNA substrate (Jinek et al., 2011). This crystal structure elucidated the molecular mechanism of the exclusive recognition of 5′-monophosphate by Xrn1, and thus the processive manner of Xrn1-mediated RNA degradation. Xrn1 binds the 5′-terminal trinucleotide of a substrate and by processive translocation by one nucleotide it releases nucleoside monophosphate. Furthermore, Xrn1 requires initial recognition of a single-stranded 5′-overhangs in order to degrade structured RNAs. The capability of melting an RNA substrate containing secondary structures is ATP-independent. Of note, the catalytic mechanism of Xrn1 requires

divalent cations as shown by biochemical assays and coordination of Mg^{2+} by Xrn1 residues at the active site (Jinek et al., 2011).

2.9. XRN1-ASSOCIATED DISEASES

Although the molecular mechanism of Xrn1-mediated RNA degradation has been well dissected, less is known about its specific role in cellular processes underlying human diseases. The relationship of evolutionarily highly conserved Xrn1 and pathogenesis can be derived from phenotypes seen in model organisms. Xrn1 deletion causes growth and sporulation defects, and impaired DNA recombination in *S.c* (reviewed in Jones et al., 2012). In favor of the notion that the Xrn1-mediated decay pathway prevails in cytoplasm is the genome-wide increase of mRNA stability upon deletion of Xrn1 (Haimovich et al., 2013; Sun et al., 2013). The fact that Xrn1 is not entirely indispensable for yeast cells points towards redundant activities of different mRNA decay pathways operating in the cytoplasm. In eukaryotic multicellular organisms, homologues of Xrn1 are involved in developmental processes and have been shown to be key controllers in apoptosis (Jones et al., 2016; Newbury and Woollard, 2004; Waldron et al., 2015). Other decay mechanisms are not capable of fully compensating for the loss of Xrn1 in *Ceanorhabditis elegans* as RNAi-mediated knockdown in this organism leads to embryonic lethality (Newbury and Woollard, 2004). In line with this, Xrn1 null mutants in *Drosophila melanogaster* die during early development (Jones et al., 2016). Furthermore, the Xrn1 homolog in *Drosophila* has been shown to be required for male fertility (Zabolotskaya et al., 2008). Finally, reduced Xrn1 mRNA level has been measured in osteosarcoma cell lines as well as samples from patients suffering from this form of bone tumor implying that lower levels of Xrn1 lead to increased cell proliferation (Zhang et al., 2002). A cell line derived from human lung carcinoma (A549) with CRISPR (clustered regularly interspaced short palindromic repeat)/Cas9 (CRISPR-associated)-mediated Xrn1 knockout was viable but resistant to dsDNA vaccinia virus (VACV) infection (Liu and Moss, 2016). Moreover, RNAi-mediated Xrn1 knockdown in human fibroblast cells infected with VACV showed an increased accumulation of dsRNA, activation of PKR kinase and RNaseL endonuclease, and an inhibition of viral gene expression, which suggests that Xrn1 plays an important role in a viral life cycle (Burgess and Mohr, 2015),

2.9.1. The role of Xrn1 in life cycle of RNA viruses

Growing evidence indicates that RNA viruses have evolved several strategies to interface and/or avoid the cellular RNA degradation machineries and thus promote a productive infection. Disruption of the cellular RNA decay machineries is one of the key strategies that can have a variety of benefits for the virus. For example, the lack of degradation pathways can lead to a temporal stabilization of viral transcripts and can thus help the virus to propagate. Some viral transcripts appear to hijack cellular RNA binding proteins, such as HuR and PABP, to stabilize their transcripts (Palusa et al., 2012; Sokoloski et al., 2010). RNA viruses may also interfere with cellular pathways in order to affect mounting of an effective innate immune response (reviewed in Dickson and Wilusz, 2011).

Xrn1 also appears to be a key factor involved in the host response to viral infection and has been implicated in pathogenesis of many viral families. Recently, several studies have reported that the activity of Xrn1 is specifically inhibited by certain members of (+)ssRNA *Flaviviridae* family, such as Hepatitis C virus from genus *Hepacivirus,* Dengue Fever virus, West Nile virus, Yellow Fever virus, Japanese Encephalitis virus, Murray Valley Encephalitis, and most recently Zika virus from genus *Flavivirus* (reviewed in Fernandez-Garcia et al., 2009; reviewed in Li et al., 2015). As Xrn1 is a key enzyme in the control of *Flaviviridae* infection, it presents an opportunity for the development of antiviral treatment and vaccines. However, there is still much work to be done to properly understand the way in which Xrn1 regulates the cellular pathways and their link to disease progression.

2.9.2. Arthropod-borne flaviviruses

Arthropod-borne members of *Flavivirus* genus are usually transmitted to humans through insect vectors such as mosquitos or occasionally ticks (Kuno et al., 1998). Flaviviral genome contains conserved and highly structured 5′- and 3′-UTRs with single open reading frame (ORF) encoding multiple viral proteins that facilitate assembly of new viral particles. The flaviviral RNA is 5′-capped but lacks polyadenylated 3′-termini, instead, it terminates in a stem-loop element, which protects the viral RNA from the nuclease attack at the 3′-end attack. Recent observations have elucidated the molecular mechanism whereby most of the flaviviruses inhibit Xrn1,

eventually shedding light on the disease mechanism of flaviviral infections. As revealed from a crystal structure and biochemical assays, genomic RNA of flaviviruses contains two discrete Xrn1-resistant RNA (xrRNA) elements within the 3′-UTR. The xrRNA is based on stem-loop structure assembling into interwoven pseudo-knots (PKs) that creates ring-like conformation blocking the progression of Xrn1 by sequestering the 5′-end of the remaining RNA („molecular brace“) (Chapman et al., 2014a; Chapman et al., 2014b). In turn, the 5′-end is not accessible for the Xrn1 active site as more than 3 nucleotides of single-stranded RNA are required for Xrn1 to efficiently load onto a substrate (Jinek et al., 2011). This steric hindrance caused by the pseudo-knot structure leads to generation of small subgenomic flaviviral RNAs (sfRNAs) in the host cytoplasm (Figure 4). A single nucleotide mutation in the Dengue viral RNA disrupts the structure of xrRNA and allows the enzyme to completely destroy the RNA, thus revealing this element to be functionally critical for Xrn1 resistance (Chapman et al., 2014b).

The stabilized non-coding sfRNAs have been reported to bind and to sequester Xrn1, and thus to interfere with the global cellular levels of RNAs by reducing the cellular 5′-to-3′ degradation capability (Chapman et al., 2014a; Chapman et al., 2014b; Moon et al., 2012). The first mRNAs being affected by the disruption of Xrn1 degradation pathway are short-lived mRNAs such as transcription factors involved in oncogenesis (e.g. c-Myc, c-Fos) and angiogenesis (e.g. vascular endothelial growth factor A (VEGFA)) (Moon et al., 2015a), cytokines and factors involved in innate immunity leading to inflammatory symptoms (Moon et al., 2012). Thus, the stabilization of otherwise inherently instable mRNAs may contribute to development of a disease state. Intriguingly, the molecular brace must not shelter the 3′-end in order to be readily denatured by enzymes acting in 3′-to-5′ manner, such as the viral RdRP, which is known to replicate the viral genome.

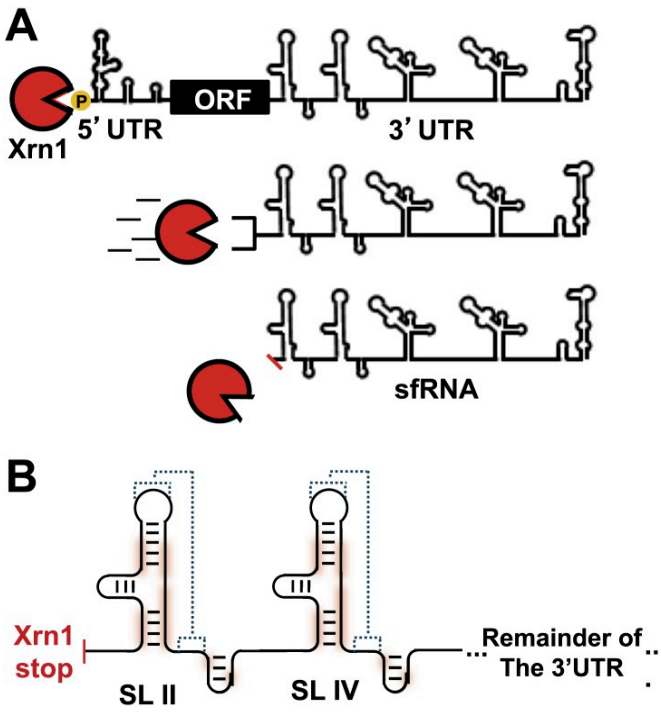

Figure 4. Scheme of incomplete degradation of the flaviviral genomic RNA by the 5′-to-3′ exonuclease Xrn1 governed by stem-loop regions (Chapman et al., 2014b)

A) *Xrn1 initiates degradation on decapped 5′-monophosphorylated substrates of flaviviral RNA. The 5′-UTR and ORF are efficiently degraded, however, the 3′-UTR harbors the stem-loop region thereby blocking Xrn1 activity. This block results in formation of sfRNA.* ***B****) The two stem-loop region that form pseudo-knots is responsible for stopping Xrn1 activity. The intramolecular interactions forming the pseudo-knots are depicted by dotted lines.*

Flaviviral infection results in accumulation of both the genomic as well as subgenomic flaviviral RNAs (sfRNAs). The latter are associated with infection-induced cytopathicity in cell cultures and pathogenicity in mice (Funk et al., 2010; Pijlman et al., 2008; Schuessler et al., 2012). The sfRNA is multifunctional and affects several pathways in infected cells: (i) alters mRNA degradation patterns (Moon et al., 2012); (ii) modulates sRNA-mediated gene silencing (Moon et al., 2015a; Schnettler et al., 2012); (iii) disrupts the interferon-induced antiviral response (Bidet et al., 2014; Chang et al., 2013b; Manokaran et al., 2015; Schuessler et al., 2012); (iv) interacts with the viral replication process (Fan et al., 2011); (v) serves as a decoy for cellular proteins involved in RNA regulation (Bidet et al., 2014; Moon et al., 2015a). The described ability of sfRNAs to resist Xrn1-mediated degradation is surprising as Xrn1 has a

helicase-like domain (Jinek et al., 2011) and can degrade highly structured RNAs (Chang et al., 2011; reviewed in Nagarajan et al., 2013). Thus, sfRNA formation results from an RNA fold that interacts directly with Xrn1, presenting the enzyme with a structure that confounds its helicase activity. The molecular detail of the sfRNA-Xrn1 interaction remains relatively unexplored. It seems that specific characteristics of the structured elements within 3′-UTR of variety of viral RNAs may modulate the robustness of Xrn1 resistance in different hosts (Chapman et al., 2014a; Chapman et al., 2014b; Villordo et al., 2015).

2.9.3. Hepatitis C

Similarly to arthropod-borne flaviviruses, a highly structured region occurs within 5′-UTR of related Hepatitis C virus (HCV). This region stalls Xrn1 and reduces its overall activity (Moon et al., 2015a). Interestingly, Xrn1 stalls near the viral internal ribosome entry site (IRES) that is required for cap-independent translation initiation (reviewed in Niepmann, 2013). HCV uses bipartite strategy how to protect its transcripts against Xrn1. The second way how HCV evolved to inhibit the action of Xrn1 is through exploiting host-expressing liver-specific mir-122 that binds to two sites at 5′-UTR of the viral RNA (Cox et al., 2013; Jopling et al., 2008; Jopling et al., 2005; Li et al., 2013b; Machlin et al., 2011). Intriguingly, this binding of mir-122 in a complex with Ago2 does not elicit degradation of viral transcripts, as typical for miRNAs, but prevents its Xrn1-mediated degradation and actually stimulates the viral gene expression in an unconventional fashion (Conrad et al., 2013; Mortimer and Doudna, 2013; Shimakami et al., 2012; Thibault et al., 2015). Resembling the other flaviviruses, HCV 3′-terminal stem-loop structures are refractory to exosomal decay. Thus, understanding viral life-cycle regulation at the molecular level of RNA can have profound implications in the development of anti-viral drugs. This is illustrated by experimental treatment targeting miR-122 by an inhibitor in form of a complementary modified antisense oligonucleotide that is effective in compromising HCV replication (Janssen et al., 2013; Lanford et al., 2010).

2.10. METHODS TO STUDY MRNA DECAY

Our knowledge of RNA decay pathways in the cytoplasm of eukaryotic cells has increased significantly in recent decades mostly due to substantial technological

advances. Among others, genome-wide inhibitor-free approaches for determining RNA stabilities in mammalian cells have been fundamental. In these methods, endogenous transcripts are pulse-labeled by modified nucleotides (most frequently 4-thiouridine (4sU) or 5-bromouridine (5BrU) as analogs of uridine) with minimal adverse effects on gene expression, RNA decay, protein stability and cell viability (Kenzelmann et al., 2007; Melvin et al., 1978,Woodford, 1988 #339). This is often followed by affinity purification and analysis of labeled *de novo* RNAs in a time series. Another way to estimate endogenous mRNA decay kinetics is to apply transcription inhibitors such as actinomycin D (actD) to block cellular RNA synthesis followed by a measurement of RNA levels over time. The advantage of this approach is that the whole transcriptome can be examined at once. However, the drawback of using actD is that this drug can negatively impact the cellular physiology, including mRNA metabolism, and that complicates the data interpretation (Harrold et al., 1991; Seiser et al., 1995). This limitation can be overcome by use of a reporter gene that specifically responds to administration of a compound facilitating transcription of the given reporter gene at a given time. The transcriptional pulsing approach often employs tetracycline (or its analogue doxycycline) (Tet)-inducible promoter to drive highly robust but transient transcription of a reporter gene in mammalian cells (Loflin et al., 1999; Xu et al., 1998). In the absence of further transcription, the changes in the abundance of an mRNA reporter can be accurately monitored. Owing to the extreme instability of decay intermediates *in vivo*, most methodologies fail to assess precise relationship between an mRNA and its decay intermediate. To decipher the mechanisms modulating RNA decay, ability to chase the mature form of an mRNA and its decay intermediate in parallel is essential.

2.10.1. Bulk measurements of mRNA decay

Several methods have been used in the past to measure mRNA half-life from a population of cells. The above described pulse-chase approaches can precede cell lysis followed by extraction of total RNA that can eventually serve as an input for a downstream analysis by biochemical methods. One of the semi-quantitative methods to assess relative abundances of transcripts is northern blotting. The basis of northern blot relies on size-separation of isolated total RNA in a gel, transfer of resolved RNAs to a membrane, and detection of a specific RNA by hybridization of labeled nucleotide

probe. Classically, the probe can be labeled radioactively as it was used, for instance, in the study of Orban & Izaurralde. After actD treatment, intact reporter mRNA could be distinguished from its degradation intermediates based on the size of detected RNAs on a northern blot over a time-course, and half-lives value could be derived using this information (Orban and Izaurralde, 2005). Due to ease of handling, fluorescent or digoxigenin-labeled probes often substitute radioactive probes nowadays. Another semi-quantitative method for a bulk measurement is reverse transcription followed by target amplification via a polymerase chain reaction (RT-PCR). The disadvantages of RT-PCR are that the reaction product is evaluated at the end point when the reaction may have transited to a plateau phase and that only a set of mRNAs can be questioned at the same time. An alternation of RT-PCR is its quantitative version (RT-qPCR). It provides real-time quantification of a target in the exponential phase during amplification.

For multiplex analysis of transcript abundances, DNA microarrays were developed. Microarrays have been used to determine relative abundance of predetermined large number of expressed genes simultaneously. In this method, the extracted mRNA is reverse transcribed into complementary DNA (cDNA) fragments, which are fluorescently labeled, and subsequently hybridized to an imprinted DNA pattern on a chip. Measurement of fluorescent intensity across the ordered array indicates the abundance of a chosen set of sequences. For example, using microarrays, it has been shown that mRNAs encoding housekeeping proteins tend to have considerably longer half-lives than those encoding regulatory proteins (Yang et al., 2003). Nowadays, next-generation-sequencing advances allow for routine large-scale profiling of gene expression in any organism. In combination with RNA labeling approaches, high-throughput sequencing provides a genome-wide measurement of mRNA abundances. A recently developed technique, called SLAM-seq, uses combination of 4sU incorporation and alkylation chemistry coupled to RNA sequencing. Applied to mouse embryonic stem cells, SLAM-seq provided global and transcript-specific insights into pluripotency-associated gene expression and gave a mechanistic insight into mRNA decay pathways (Herzog et al., 2017).

2.10.2. Current single-molecule techniques to study mRNA

Conventional bulk methods to measure mRNA turnover, such as qPCR, result in averaged output from many cells, and thus lead to a loss of information about spatial regulation of RNA turnover and cell-to-cell variability. Therefore, single-cell methods are important for distinguishing observations from bulk measurements, especially in the context of gene expression noise and of complex function of a tissue. To reveal cellular heterogeneity in RNA metabolism, a single-cell RNA-sequencing (scRNA-seq) method and its variations have been developed (reviewed in Kolodziejczyk et al., 2015). Nevertheless, scRNA-seq is still technically challenging because it often suffers from incomplete RNA conversion into cDNA and from cDNA amplification noise. Moreover, scRNA-seq does not contain any spatial information and masks the molecular dynamic processes. Similar drawbacks are encountered in analysis of known candidate genes by single-cell RT-qPCR, although this approach also allows uncovering potential heterogeneities within a population of cells (Bengtsson et al., 2008).

The spatial information can be preserved by high-resolution fluorescent microscopy of single molecules within an intact cell providing absolute quantities and positions of RNA molecules. Single-molecule approaches have provided invaluable insight into various aspects of RNA life cycle over the past years. Two imaging techniques that are commonly used to visualize mRNA particles are: single molecule fluorescent *in situ* hybridization (smFISH) and single-particle tracking (SPT) in live-cell imaging. The former relies on hybridization of multiple fluorescent sequence-specific probes to an mRNA molecule of interest within fixed cells. More than one RNA species can be observed at the same time by smFISH method (Raj et al., 2008). As an example, using smFISH, Trcek *et al.* studied the spatial and temporal regulation of NMD and found that the majority of the PTC-containing transcripts are degraded soon after export (Trcek et al., 2013). Given the fact that smFISH can be combined with immunostaining for simultaneous detection of functionally associated proteins, smFISH is a highly powerful method to study mRNA metabolism at single transcript resolution. Among live-cell imaging approaches, MS2 and related PP7 labeling systems are broadly utilized to track mRNAs (Medioni et al., 2012), The system of MS2 and PP7 is based on orthogonal high-affinity interactions of MS2 bacteriophage coat protein (MCP) or PP7 bacteriophage coat protein (PCP) with the respective cognate RNA hairpin (Figure 5) (Chao et al., 2008). The coat proteins are fused to spectrally

distinct fluorophores to allow for two-color simultaneous imaging. Inherently, the coat-proteins form homodimers to bind their respective stem-loop. To amplify the signal, fluorescent protein is often introduced in tandem and, in addition, each RNA stem-loop is integrated into an RNA reporter in the form of a cassette containing multiple repeats.

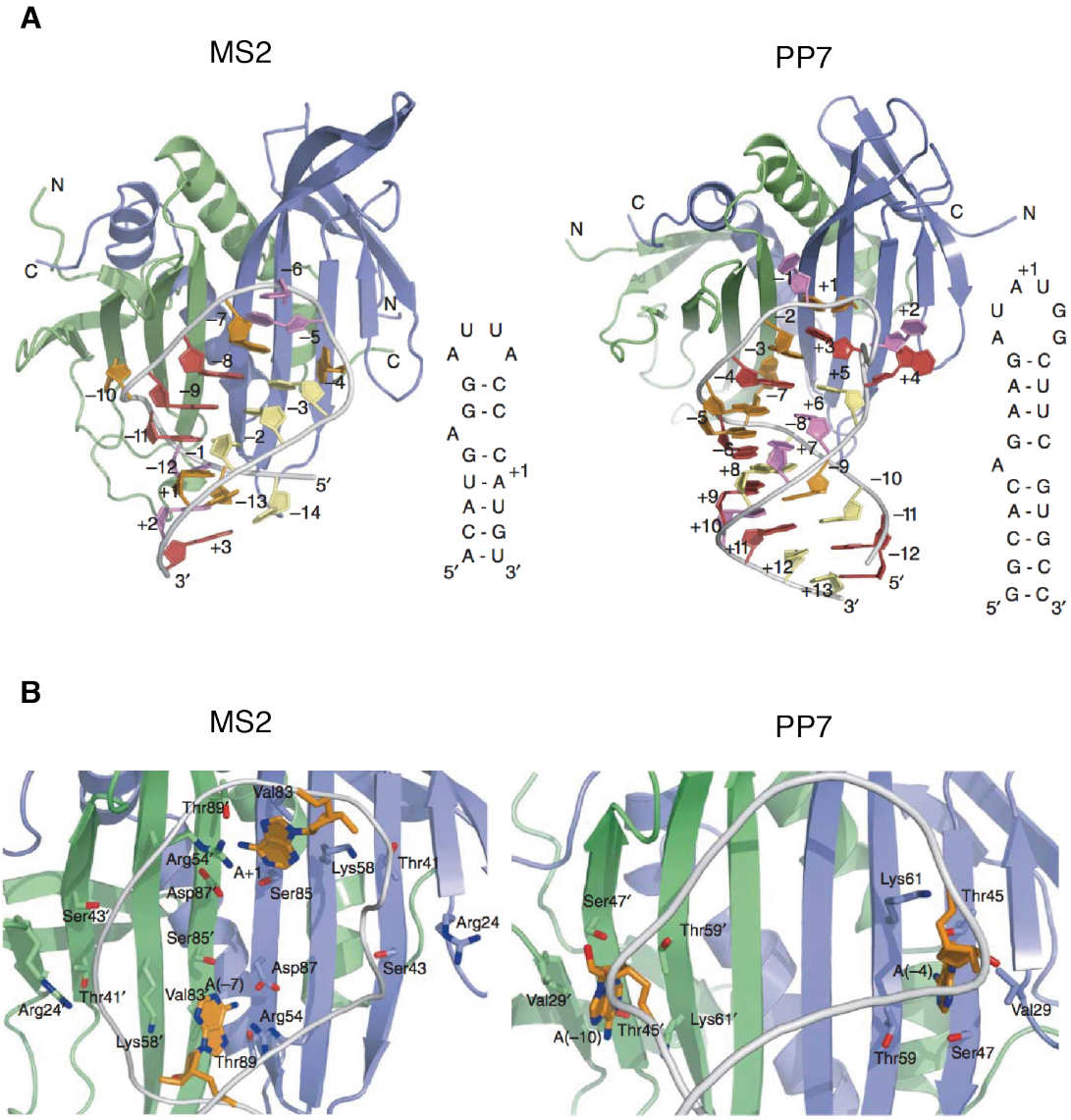

Figure 5. Orthogonal dual-labeling system of MS2 and PP7 coat proteins in complexes with cognate RNA stem-loop (adapted from Chao et al., 2008)

A) *Sequence and structure representation of the MS2 and PP7 system. In both structures, the RNA stem-loop binds across the extended beta-sheet surface formed by the coat protein dimer (blue, green).* ***B****) The orientation of the adenine recognition pockets is rotated with respect to the dimer axis between the MS2 and PP7 coat proteins. Cartoon shows the position of the phosphate backbone in gray and bound adenosines are shown in orange.*

Single-molecule approaches have revisited some of the previous findings from bulk measurements, and thus have complemented cellular and biochemical methods by providing spatio-temporal information including variance among cells. The advent of MS2-MCP labeling system in the Singer laboratory enabled tracking the movement of *ASH1* mRNA into the daughter cell in budding yeast and paved the way for development of series of single-color and later multiple-color imaging methods (Bertrand et al., 1998). The pioneering work employing simultaneous two-color imaging system with single-molecule resolution has been pivotal for discovery of the intrinsic transcriptional noise of an endogenously expressed yeast gene. Each allele of this gene was tagged by one of the coat proteins, MS2 or PP7, respectively, in living yeast cells (Hocine et al., 2013). Single-molecule imaging has also illuminated the dynamics of RNA transcription and identified the novel phenomenon of stochastic transcriptional bursting, which is the primary cause of expression noise in cells and tissue (Larson et al., 2013; Larson et al., 2011). Next, differential labeling of introns and exons allowed for mRNA splicing to be monitored in the nucleus of living cells pointing towards occurrence of both co-transcriptional splicing and splicing after release from transcription site (Coulon et al., 2014; Martin et al., 2013). In another study, spatially resolved kinetics of nuclear mRNA export revealed a three-step model consisting of docking to nuclear pore, transport and release in mammalian cells (Grunwald and Singer, 2010). In living *Drosophila* oocytes, *oskar* mRNA has been shown to be transported to the posterior pole actively along microtubules (Zimyanin et al., 2008). To differentiate the untranslated mRNA molecule from a translated mRNA, a clever biosensor called TRICK, which stands for translating RNA imaging by coat protein knock-off, was developed. TRICK enables to observe the first round of translation in living cells (Halstead et al., 2015). Dynamics of translation has been recently described in living cells by innovative approach wherein fluorescently labeled mRNA particles were imaged simultaneously with a cognate nascent polypeptide chain. Here, the emerging peptide is visualized by binding of fluorescent single-chain antibodies to a number of N-terminal epitopes (Morisaki et al., 2016; Wang et al., 2016; Wu et al., 2016; Yan et al., 2016).

The advent of innovative single-molecule methods to observe various aspects of mRNA lives represent significant shift towards quantitative understanding of RNA metabolism. However, the RNA field has been waiting for a single-molecule method that would allow for real-time imaging of mRNA degradation dynamics and kinetics to be measured.

3. AIM OF THE THESIS

Although many of the molecular pathways and proteins involved in mRNA degradation are known, our understanding of when and where the degradation events occur within cells is limited. The main aim of my doctoral research project was to develop a single-molecule imaging method to interrogate mRNA degradation in individual cells by fluorescent microscopy.

There are two major hurdles for studying RNA turnover at single-molecule resolution using an imaging approach.

I. *Inherent instability of degradation intermediates*

The inherent instability of RNA degradation intermediates was demonstrated by Orban & Izaurralde who measured half-life of the cleavage products arising from RISC-initiated degradation in *Drosophila* cells. In this study, RNAi-mediated depletion of Xrn1 strongly stabilized otherwise short-lived ($t_{1/2}$ < 15 min) 3′-degradation intermediate (Orban and Izaurralde, 2005). However, RNAi has many pitfalls: (i) off-target effects of RNAi-mediated gene silencing, (ii) variability due to different transfection efficiencies, (iii) disturbances in cellular homeostasis due to knockdown of the major RNA decay factor. To circumvent these pitfalls, I intended to find an alternative way that would specifically increase stability of degradation intermediates arising from a particular reporter.

II. *Lack of a robust system to differentially label and image intact RNAs and degradation intermediates*

Fluorescent proteins and dyes often lose their fluorescence upon extended exposure to light. This phenomenon is known as photobleaching and depends on the kind of fluorophore and molecular environment. Mostly due to reactions with molecular oxygen, photochemical modifications of a fluorophore in an excited state result in the irreversible loss of its ability to fluoresce. Hence, in a single-labeled system, the loss of signal could be due to degradation of the mRNA or due to photobleaching. To this end, I was motivated to develop, validate and employ a dual-color imaging method wherein mRNA degradation intermediates are stabilized and can be fluorescently distinguished from intact mRNAs.

Xrn1 is the major cytoplasmic 5′-to-3′ exoribonuclease that is implicated in the majority of RNA degradation pathways in eukaryotes. Thus, Xrn1 is placed at a pivotal position in mRNA stability control. Design of a reporter monitoring Xrn1-mediated degradation in both living and fixed cells is therefore of high importance for the research community. To this aim, I stabilized degradation intermediates of an mRNA reporter generated by Xrn1 by placing flaviviral Xrn1-resistant RNA elements within the 3′-UTR of the reporter. To visualize the intact mRNA as well as its degradation intermediate, the designed reporter contained the orthogonal MS2/PP7 labeling system in such a way that the intact mRNAs are dual-colored while the degradation intermediates are single-colored.

To study the spatio-temporal regulation of mRNA decay with single-molecule precision, I aimed to generate an inducible system allowing for a temporal control over transcription of the reporter gene from a single genomic locus. At the same time, this induction ensures transcription at a level compatible with single-molecule detection. Using this approach, the goal of my PhD project was to monitor the fates of individual mRNAs in single living and fixed mammalian cells in order to obtain a comprehensive analysis and quantitative understanding of the mechanisms that regulate mRNA turnover.

GENERAL OBJECTIVES and PARTICULAR QUESTIONS:

- **What are *in vivo* kinetics and dynamics of mRNA decay?**
  - When and where does mRNA degradation occur?
  - Can mRNA degradation occur in bursts?
  - What is the nature of cell-to-cell variability in counts of mRNAs?
  - Do processing bodies play a role in mRNA degradation?
  - What is the impact of translation inhibition on mRNA degradation?
- **How is Ago2-mediated cleavage of mRNA regulated in time and space?**
  - How long does it take to cleave an mRNA?
  - Where does the cleavage occur?
- **How is spatio-temporal regulation of mRNAs influenced by *cis*-elements such as AU-rich elements and 5′-TOP?**

4. RESULTS

The results from my doctoral research are compiled into the publication titled “The Dynamics of mRNA Turnover Revealed by Single-Molecule Imaging in Single Cells” that is attached to this thesis.

Technology

Molecular Cell

The Dynamics of mRNA Turnover Revealed by Single-Molecule Imaging in Single Cells

Graphical Abstract

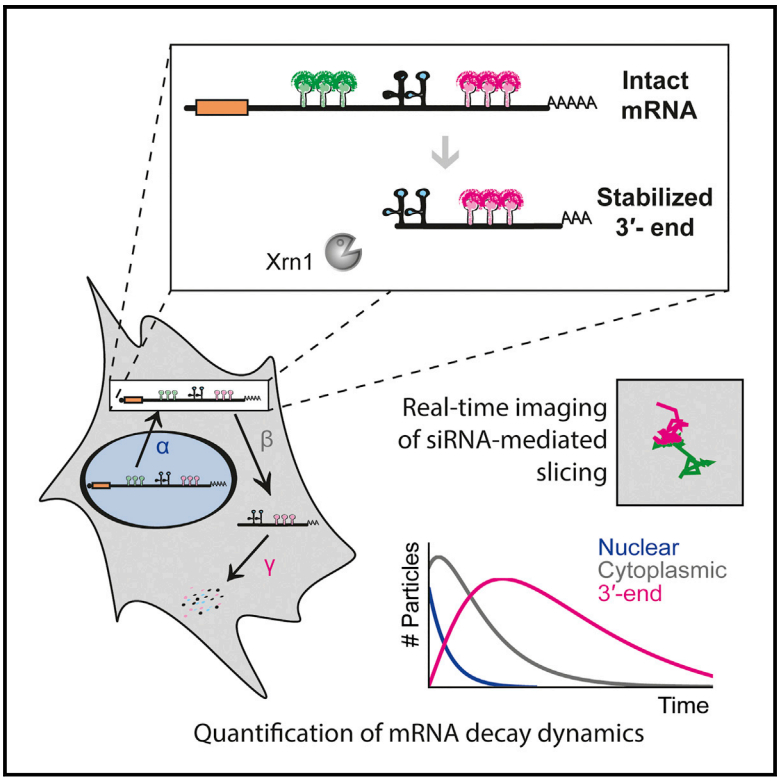

Authors

Ivana Horvathova, Franka Voigt, Anna V. Kotrys, ..., Michael B. Stadler, Luca Giorgetti, Jeffrey A. Chao

Correspondence

jeffrey.chao@fmi.ch

In Brief

RNA degradation plays a fundamental role in regulating gene expression. Horvathova et al. developed a fluorescence microscopy methodology that enables the dynamics of RNA degradation to be quantified with single-molecule resolution in fixed and living cells. This allows the entire life of mRNAs from birth to death to be visualized.

Highlights

- TREAT enables single-mRNA imaging of RNA degradation in single cells
- TREAT mRNA degradation does not burst
- Real-time observation of Ago2 slicing of TREAT mRNAs
- TREAT mRNAs are not degraded in P-bodies

Horvathova et al., 2017, Molecular Cell *68*, 1–11
November 2, 2017
https://doi.org/10.1016/j.molcel.2017.09.030

CellPress

Please cite this article in press as: Horvathova et al., The Dynamics of mRNA Turnover Revealed by Single-Molecule Imaging in Single Cells, Molecular Cell (2017), https://doi.org/10.1016/j.molcel.2017.09.030

Molecular Cell
Technology

CellPress

The Dynamics of mRNA Turnover Revealed by Single-Molecule Imaging in Single Cells

Ivana Horvathova,[1,2,4] Franka Voigt,[1,4] Anna V. Kotrys,[1] Yinxiu Zhan,[1,2] Caroline G. Artus-Revel,[1] Jan Eglinger,[1] Michael B. Stadler,[1,3] Luca Giorgetti,[1] and Jeffrey A. Chao[1,5,*]
[1]Friedrich Miescher Institute for Biomedical Research, 4058 Basel, Switzerland
[2]University of Basel, 4003 Basel, Switzerland
[3]Swiss Institute of Bioinformatics, 4058 Basel, Switzerland
[4]These authors contributed equally
[5]Lead Contact
*Correspondence: jeffrey.chao@fmi.ch
https://doi.org/10.1016/j.molcel.2017.09.030

SUMMARY

RNA degradation plays a fundamental role in regulating gene expression. In order to characterize the spatiotemporal dynamics of RNA turnover in single cells, we developed a fluorescent biosensor based on dual-color, single-molecule RNA imaging that allows intact transcripts to be distinguished from stabilized degradation intermediates. Using this method, we measured mRNA decay in single cells and found that individual degradation events occur independently within the cytosol and are not enriched within processing bodies. We show that slicing of an mRNA targeted for endonucleolytic cleavage by the RNA-induced silencing complex can be observed in real time in living cells. This methodology provides a framework for investigating the entire life history of individual mRNAs from birth to death in single cells.

INTRODUCTION

Gene expression is regulated by the abundance of mRNA. The levels of all cellular transcripts are determined by the balance between the rates of transcription in the nucleus and degradation in the cytoplasm. The life of an mRNA begins when it emerges from RNA Pol II and is recognized by factors that are responsible for its capping, splicing, and polyadenylation. The mature transcript is then exported to the cytoplasm where it can be transported, translated, and eventually degraded. While the importance of transcription in controlling gene expression is well established, it has become increasingly clear that the regulation of mRNA stability, particularly during development or rapid changes in environmental conditions, can dramatically influence mRNA levels (Elkon et al., 2010; Friedel et al., 2009; Hao and Baltimore, 2009; Miller et al., 2011; Rabani et al., 2011). RNA degradation also plays a crucial role in mRNA quality control that safeguards cells from the deleterious effects of aberrant transcripts (Isken and Maquat, 2007).

Degradation of mRNAs is a multi-step process that requires an orchestrated series of enzymatic reactions (Garneau et al., 2007). For most mRNAs, shortening of the poly(A) tail is thought to be the first step in mRNA decay and requires the consecutive actions of the Pan2-Pan3 and the Ccr4-Caf1-Tob complexes (Funakoshi et al., 2007; Yamashita et al., 2005). Following deadenylation, the 5′-cap structure is hydrolyzed by the Dcp1-Dcp2 complex (Dunckley and Parker, 1999; Lykke-Andersen, 2002; van Dijk et al., 2002). The body of the transcript can then be degraded by Xrn1 (5′-to-3′ exonuclease) or the cytoplasmic exosome complex (3′-to-5′ exonuclease) (Garneau et al., 2007). Currently, Xrn1-mediated degradation is believed to be the dominant cytoplasmic decay pathway, perhaps through the coupling of Xrn1 to Dcp1-Dcp2 by the scaffold protein Edc4 (Chang et al., 2014). Additional mRNA decay pathways have also been identified that enable regulation of mRNA stability (e.g., AU-rich elements, miRNAs) or quality control (Garneau et al., 2007; Schoenberg and Maquat, 2012).

While many of the proteins and pathways involved in mRNA degradation have been elucidated, our understanding of when and where these events occur within cells has not kept pace. Single-molecule fluorescent *in situ* hybridization (smFISH) has enabled some aspects of mRNA degradation to be characterized, but the loss of signal resulting directly from the process being studied has prevented this approach from being widely applied (Kramer, 2017; Trcek et al., 2011, 2013). Here, we describe a single-molecule fluorescent microscopy methodology for measuring the spatial and temporal dynamics of mRNA degradation in fixed and living single cells.

DESIGN

Recently, a viral RNA pseudo-knot (PK) structure was identified in flaviviruses that blocks Xrn1 by sequestering the 5′-phosphate from the enzyme, thereby preventing further degradation of the viral genome (Kieft et al., 2015). We took advantage of this feature to engineer a single-molecule mRNA turnover biosensor that contains a 3′ UTR with the tandem PKs from the Kunjin strain of West Nile virus placed between the orthogonal PP7 and MS2 bacteriophage stem loops (Chapman et al., 2014a; Hocine et al., 2013) (Figure 1A). Since the MS2 stem loops are protected from

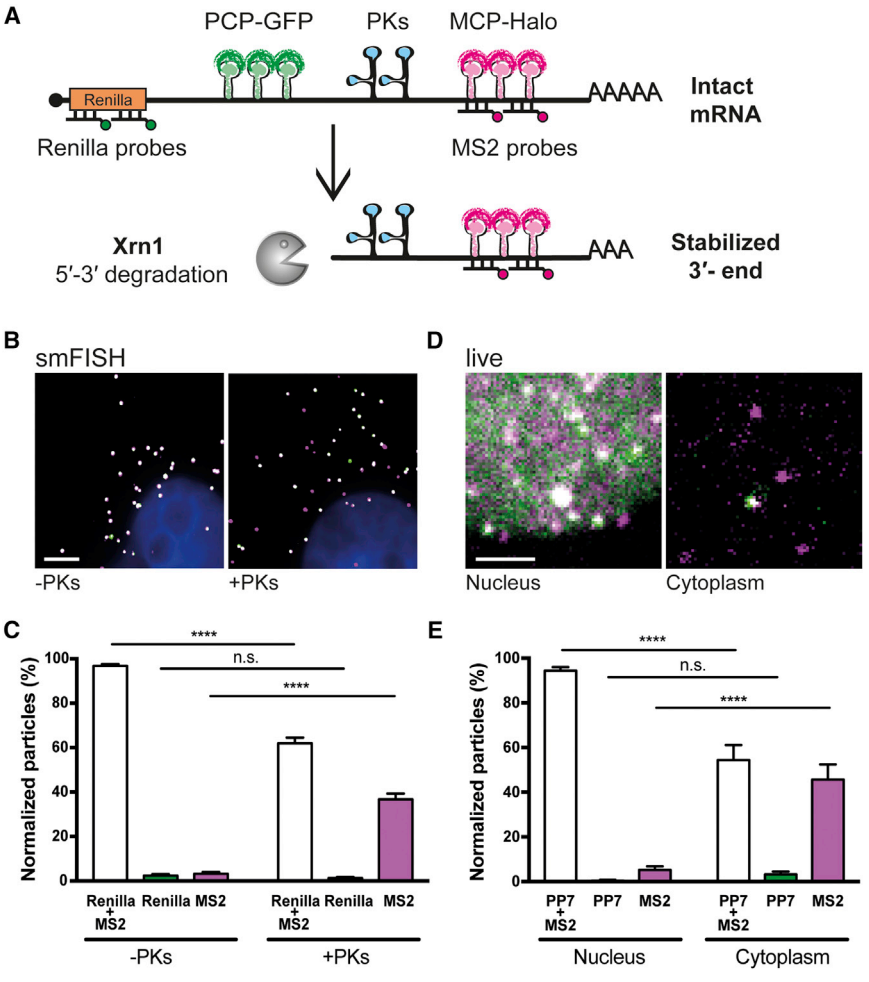

Figure 1. TREAT Imaging of mRNA Degradation in Single Cells

(A) Schematic of the intact TREAT reporter mRNA and its stabilized degradation fragment. *Renilla* luciferase is in the open reading frame, and the 3′ UTR contains two viral pseudo-knots (PKs, blue) that are flanked by PP7 (green) and MS2 (magenta) stem loops. The stabilized 3′ end (MS2 stem loops only) arises from partial degradation by Xrn1 that is blocked by the PKs. In fixed cells, smFISH probes can be targeted to *Renilla* luciferase and MS2 stem loops, and in live cells, PP7 and MS2 coat proteins (PCP and MCP, respectively) can be fused to spectrally distinct fluorescent proteins.

(B) Representative smFISH images of HeLa cells stably expressing control (−PKs) or TREAT (+PKs) reporters hybridized with *Renilla* (green) and MS2 (magenta) probes. Cells were induced by addition of doxycycline for 2 hr and fixed 2 hr after induction was stopped. Scale bar, 2 μm.

(C) Viral PKs are required for accumulation of stabilized 3′ ends. Quantitative analysis of smFISH reveals that the fraction of intact transcripts (*Renilla* + MS2, white) decreases while the fraction of stabilized 3′ ends (MS2, magenta) increases in cells expressing TREAT reporter (10,810 particles, 62 cells) compared to control reporter (3,465 particles, 66 cells) (p values, **** < 0.0001; n.s., not significant; unpaired t test). Graph shows mean ± SEM.

(D) Representative live-cell images of a HeLa cell line stably expressing the TREAT reporter with NLS-PCP-GFP and NLS-MCP-Halo. Intact mRNAs are dual labeled with NLS-MCP-Halo (magenta) and NLS-PCP-GFP (green) and appear as white spots, whereas stabilized 3′ ends are labeled by only NLS-MCP-Halo.

(E) TREAT mRNAs are degraded in the cytoplasm. Quantification of intact and degraded RNAs in the nucleus (388 particles, 11 cells) and cytoplasm (594 particles, 12 cells) was performed using two-color SPT, and co-localization analysis was normalized by detection efficiencies in both channels. p values, **** < 0.0001; n.s., not significant; unpaired t test.

Xrn1-mediated degradation by the PKs, this biosensor allows discrimination between intact (PP7 and MS2) transcripts and stabilized 3′ end degradation intermediates (MS2 only) in living cells that express the PP7 coat protein (PCP) and MS2 coat protein (MCP) fused to spectrally distinct fluorescent proteins. Similarly, smFISH probes can be targeted to the two distinct regions of the transcript in order to image mRNA decay in fixed cells. We refer to this technique as 3(*three*)′-*R*NA *e*nd *a*ccumulation during *t*urnover (TREAT).

RESULTS

Development of TREAT for Imaging mRNA Degradation

In order to monitor physiological mRNA decay, expression of the TREAT reporter should not disrupt Xrn1-mediated degradation. While Xrn1 does not form a stable complex with the viral PKs, it has been reported that overexpression of the entire Kunjin flaviviral subgenomic RNA, which contains the PKs and other structured RNA elements, results in stabilization of endogenous mRNAs (Chapman et al., 2014b; Moon et al., 2012). The stability of endogenous c-Myc mRNA measured by RT-qPCR was similar in HeLa cells that expressed the TREAT reporter and cells that did not express it (Figure S1A). Importantly, the PKs also did not alter the stability or translation of the TREAT reporter compared to a control lacking these elements (Figures S1B and S1C). To validate the potential of the PKs to block Xrn1 from fully degrading the TREAT reporter, we determined the size of TREAT and control transcripts by northern blot. A probe complementary to a sequence in the 3′ UTR in both types of transcripts demonstrated that accumulation of the specific degradation intermediate occurred only in the presence of the PKs (Figure S2). Importantly, co-expression of NLS-MCP-Halo and NLS-PCP-GFP did not stabilize alternative degradation intermediates of the reporters without PKs as reported in yeast (Figure S2) (Garcia and Parker, 2015; Heinrich et al., 2017). Taken as a whole, the presence of the viral PKs in the TREAT reporter does not perturb RNA degradation in either *cis* or *trans* in HeLa cells.

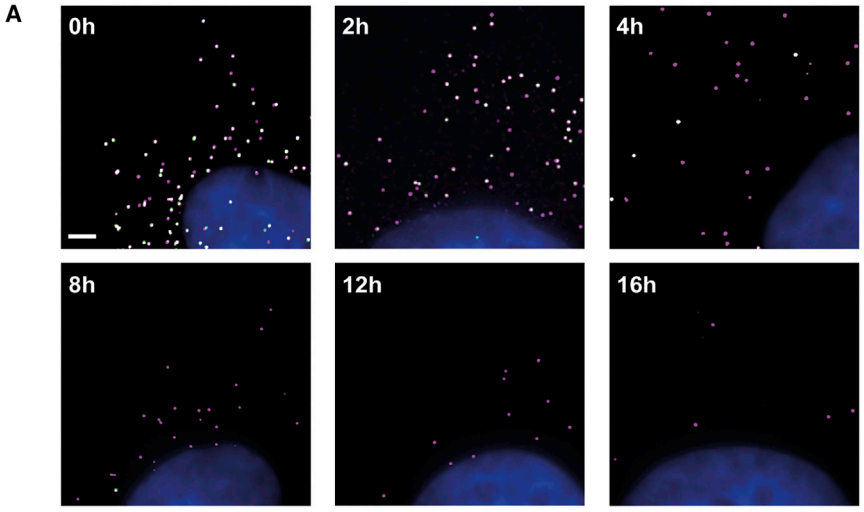

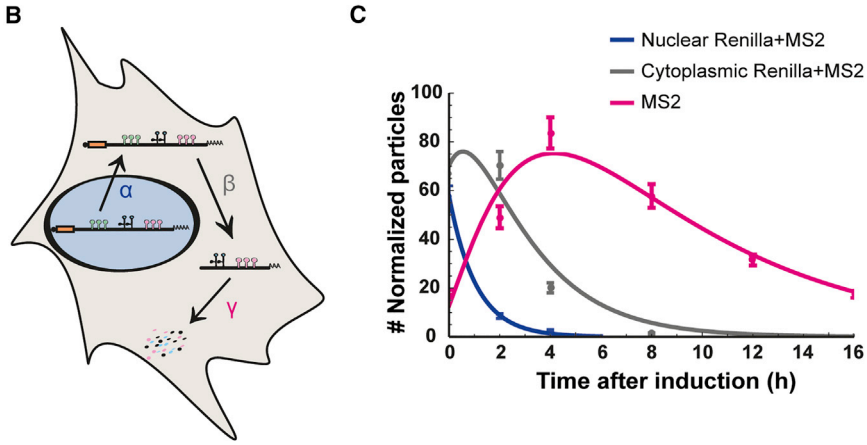

Figure 2. Half-Life Measurement of TREAT mRNAs in Single Cells

(A) Representative smFISH images of the TREAT reporter in HeLa cells. Cells were induced for 2 hr with doxycycline and fixed at successive time points (0, 2, 4, 8, 12, 16 hr) after induction was stopped. Images show that the stabilized 3′ end (MS2, magenta) accumulates within cells while the number of intact TREAT mRNAs (*Renilla* + MS2, white) decreases over time. Scale bar, 2 μm.

(B) Schematic model of the TREAT mRNA life cycle within a cell with depicted rates: α, nuclear export rate; β, degradation rate of the TREAT transcript; γ, stabilized 3′ end degradation rate.

(C) Counts of intact mRNAs (nuclear or cytoplasmic) and stabilized 3′ ends were obtained from the quantitative analysis of smFISH data at fixation time points (> 120 cells per time point in two biological replicates). Data were fit to the model to calculate the experimental rate constants (α, β, γ). All error bars indicate SEM.

The TREAT reporter was integrated into a single genomic locus in doxycycline-inducible HeLa cells that stably express NLS-PCP-GFP and NLS-MCP-Halo to monitor mRNA turnover in single cells. The ability of TREAT to detect mRNA degradation requires quantification of the co-localization of fluorescent signals positioned 5′ and 3′ of the PKs. To this aim, a control reporter without PKs was used to benchmark co-localization and determine detection efficiencies in both fixed and living cells, since only intact two-color transcripts should be detected with this construct (Figure S3, Movie S1). In fixed cells, smFISH probes targeting the *Renilla* luciferase coding sequence and MS2 stem loops demonstrated that introduction of the PKs into the TREAT reporter enabled detection of an increase in the fraction of MS2-only particles (Figures 1B and 1C). Importantly, there was no change in the number of *Renilla*-only particles, indicating the effect of the PKs was specific for the stabilized 3′ end. In live cells, single-particle tracking (SPT) of TREAT mRNAs in the nucleus demonstrated that the majority of transcripts are intact (> 94%) (Figures 1D and 1E, Movie S2). In the cytoplasm, however, SPT and co-localization analysis of TREAT transcripts revealed two distinct populations of RNA, intact mRNAs (MS2 and PP7) and stabilized 3′ ends (MS2 only) (Figures 1D and 1E). Similar to the fixed-cell data, there was no increase in the number of PP7-only-labeled particles. These experiments demonstrated that TREAT can measure mRNA turnover with single-molecule resolution in both fixed and living cells.

TREAT Measurement of mRNA Degradation in Single Cells

We measured the kinetics of TREAT mRNA degradation in single cells using smFISH. Expression of the reporter was induced for 2 hr with doxycycline, and cells were fixed at successive time points after induction was stopped (Figure 2A). The turnover of intact TREAT mRNAs and the stabilized 3′ ends in the cytoplasm can be described by

$$\frac{d[\mathrm{Nuc}]}{dt} = -\alpha[\mathrm{Nuc}]$$

$$\frac{d[\mathrm{Cyt}]}{dt} = \alpha[\mathrm{Nuc}] - \beta[\mathrm{Cyt}]$$

$$\frac{d[\mathrm{Deg}]}{dt} = \beta[\mathrm{Cyt}] - \gamma[\mathrm{Deg}],$$

where *Nuc* is the number of intact nuclear mRNAs, α is the export rate of mRNAs to the cytoplasm, *Cyt* is the number of intact cytoplasmic mRNAs, β is the decay rate of the intact cytoplasmic mRNA, *Deg* is the number of stabilized 3′ ends, and γ is the decay rate of the stabilized 3′ ends (Figure 2B). Fitting the evolution of the mean numbers of RNA species in time to this model resulted in an export time of 0.74 ± 0.05 hr and degradation half-lives of 1.63 ± 0.24 hr (cytoplasmic intact mRNA) and 4.39 ± 0.47 hr (stabilized 3′ end) (Figure 2C). RNAi knockdown

of Xrn1 increased the half-life of the TREAT reporter while knockdown of Rrp40, an exosome core subunit, had no effect, indicating that Xrn1-mediated degradation is indeed the dominant decay pathway for TREAT transcripts (Figure S4).

Single-cell measurements enabled the observation that transcription is not a simple Poisson process and can occur in bursts; however, it has not yet been possible to determine if similar dynamics also occur during mRNA turnover (Raj and van Oudenaarden, 2008). During analysis of the smFISH images, we observed considerable cell-to-cell variation in the abundance of stabilized 3′ ends in individual cells. The ratio of the variance to the mean (Fano factor) of the number of stabilized 3′ ends at each time point was greater than one, which is indicative of possible deviations from Poisson processes. To determine the nature of this variability, we used a discrete stochastic approach to solve the master equation associated with the model described above and generated the probability distribution of intact mRNAs and stabilized 3′ ends based upon their distribution at the initial time point. Simulation of the RNA populations at later time points, assuming that the turnover of intact and degraded mRNA are single-step Poisson processes governed by the measured decay rates, was in good agreement with the experimental data (Figure S5). Virtually all of the variability in the number of stabilized 3′ ends of the TREAT transcript could be accounted for by the initial cell-to-cell heterogeneity in mRNA numbers that results from variable levels of transcription in individual cells. This indicates that the degradation of each TREAT transcript occurs independently within the cell.

Real-Time Observation of mRNA Degradation in Living Cells

Due to the difference in timescales between the half-life of the TREAT mRNA (1.6 hr) and our live-cell experiments (5–10 s), it was challenging to directly detect TREAT degradation events in live cells. In order to generate a TREAT reporter that would be more rapidly degraded, we incorporated an siRNA sequence derived from Firefly luciferase between the PP7 stem loops and the PKs and stably expressed the corresponding shRNA in the HeLa cell line used for imaging (Figure 3A). Using smFISH, the cytoplasmic half-life of the TREAT siRNA reporter was determined to be ~7.5 min, while the export time and degradation of the stabilized 3′ ends were not changed (Figure 3B). We were also able to detect the transient appearance of the 5′ end of the transcript in the cytoplasm generated by Ago2-mediated endonucleolytic cleavage, which was degraded with a half-life of ~9.7 min. Similar to our modeling of the variability of TREAT reporter degradation, we also did not detect degradation bursts for TREAT siRNA transcripts (Figure S6).

In order to identify the cellular site of slicing, we imaged the TREAT siRNA reporter in live cells. While RNAi factors have been detected in the nuclei of mammalian cells, they were found to be inactive and unable to degrade nuclear transcripts (Zeng and Cullen, 2002). Recently, however, it has been suggested that Ago2 can be active in mammalian cell nuclei and was shown to degrade the nuclear lncRNA Malat1 (Gagnon et al., 2014). We quantified the co-localization of nuclear TREAT siRNA transcripts and did not observe a change in the number of intact transcripts, 5′ ends, or stabilized 3′ ends compared to a non-sliced control, indicating that the short half-life of TREAT siRNA transcripts was not due to increased nuclear degradation (Figures 3C and 3D).

To quantify cytoplasmic slicing, we developed an automated SPT and co-localization algorithm to identify degradation events within our movies. We reasoned that slicing could be visualized as either the rapid disappearance of the 5′ signal (NLS-PCP-GFP) from a dual-labeled transcript or the spatial separation of the 5′ signal (NLS-PCP-GFP) and 3′ signal (NLS-MCP-Halo) after endonucleolytic cleavage (Figure 4A). Loss of the 5′ signal (NLS-PCP-GFP) from a transcript could arise from either slicing or photo-bleaching. We measured the slope of the loss of NLS-PCP-GFP and did not detect any significant outliers for intact TREAT siRNA transcripts compared to a non-sliced control (Figure 4B). We did, however, detect slicing decay events (n = 17) where intact mRNAs were observed to sever into 5′ ends (PP7) and 3′ ends (MS2) that then spatially move apart from one another and could be independently tracked (Figure 4C, Movie S3). Since the 5′ end is not immediately degraded and can separate from its 3′ end after Ago2-mediated endonucleolytic cleavage, this suggests that there is not a tight coupling between slicing and the downstream degradation of the decay intermediates. We measured the cytoplasmic position of slicing events from the nucleus and found that their distribution was similar to non-sliced control transcripts, indicating that slicing does not preferentially occur in a specific location, but is homogenously distributed throughout the cell (Figure 4D).

P-Bodies Are Not Sites of TREAT mRNA Degradation

Phase transitions have been implicated in an increasing number of diverse biological phenomena; however, their underlying molecular mechanisms are not well understood (Banani et al., 2017). Processing bodies (P-bodies), evolutionarily conserved membrane-less cytoplasmic compartments that are formed by the condensation of RNA-binding proteins and mRNAs, were one of the first phase transitions to be identified (Jain and Parker, 2013). Since they are enriched for proteins involved in many aspects of mRNA turnover, including decapping factors, deadenylases, and Xrn1, it was initially proposed that they functioned as cellular sites of active mRNA degradation (Cougot et al., 2004; Sheth and Parker, 2003). Subsequently, it was shown that microscopically visible P-bodies accounted for only a small fraction (~0.3%) of the cytoplasmic volume and were not required for degradation of transcripts, indicating that mRNA turnover does not require compartmentalization (Chu and Rana, 2006; Eulalio et al., 2007; Leung et al., 2006; Stoecklin et al., 2006). Whether mRNA decay, however, was more efficient or inhibited within P-bodies remained an open question. It has also been suggested that P-bodies function as sites of mRNA storage during cellular stress from which mRNAs return to the cytoplasm for translation upon recovery (Bhattacharyya et al., 2006; Brengues et al., 2005). Since the TREAT reporter can directly report on the cellular site of mRNA decay, we set out to clarify the role of P-bodies in this process.

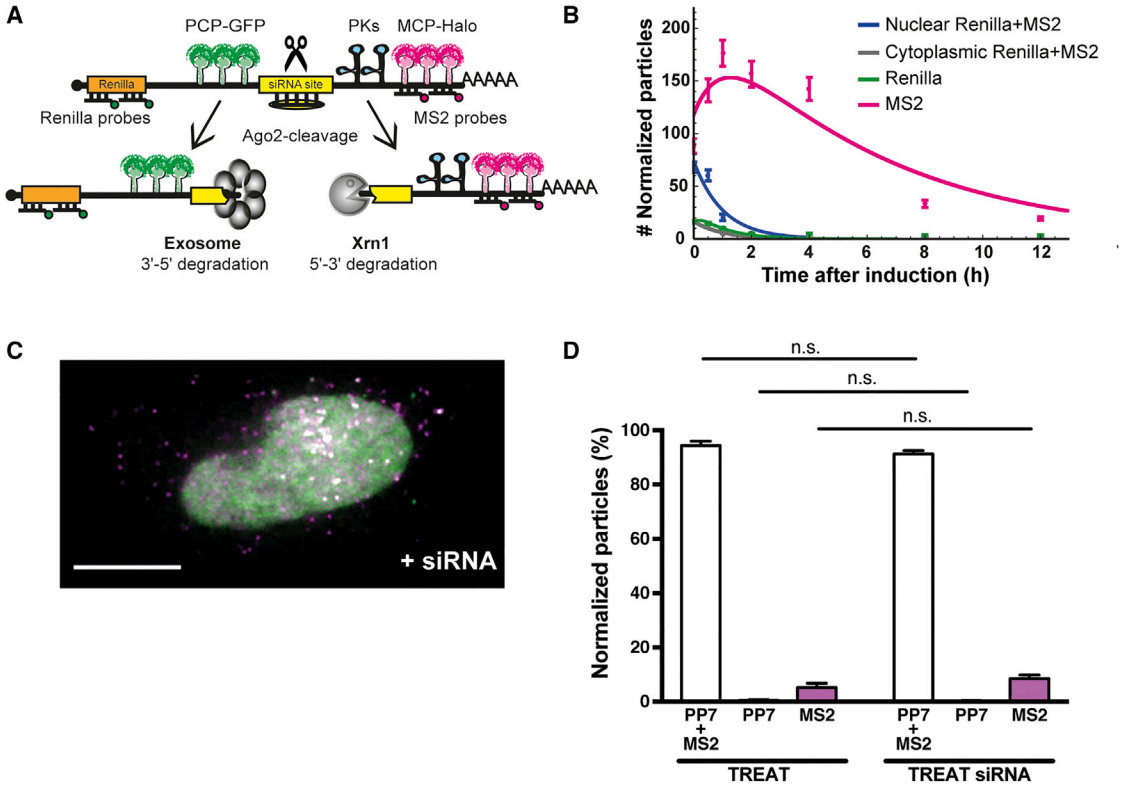

Figure 3. TREAT siRNA Transcripts Are Rapidly Degraded in the Cytoplasm

(A) Schematic of TREAT siRNA reporter and slicing degradation fragments. An siRNA target sequence was placed between the PP7 stem loops and the PKs in the 3′ UTR. After expression of the cognate siRNA, endonucleolytic cleavage results in a 5′ end containing PP7 stem loops and the stabilized 3′ end containing MS2 stem loops.

(B) Measurement of TREAT siRNA reporter stability. Counts of intact mRNA (nuclear or cytoplasmic), 5′ ends, and stabilized 3′ ends were obtained from quantification of smFISH data (> 190 cells per time point in two biological replicates).

(C) Representative live-cell image of HeLa cells expressing TREAT siRNA reporter labeled with NLS-PCP-GFP (green) and NLS-MCP-Halo (magenta). Intact mRNAs are dual labeled with NLS-PCP-GFP (green) and NLS-MCP-Halo (magenta) and appear as white spots. Scale bar, 10 μm.

(D) Quantification of co-localization of NLS-PCP-GFP and NLS-MCP-Halo for TREAT siRNA reporter in the nucleus (534 particles, 14 cells) compared to nuclear TREAT data (388 particles, 11 cells) (p values: n.s., not significant; unpaired t test).

A HeLa cell line was generated that stably expresses a SNAP-Dcp1a fluorescent fusion protein, which labels P-bodies, in combination with NLS-PCP-GFP and NLS-MCP-Halo, which allowed imaging of P-bodies and TREAT reporter mRNAs in living cells (Kedersha and Anderson, 2007). The number of SNAP-Dcp1a-labeled P-bodies detected by live-cell imaging was similar to the number of endogenous P-bodies detected by immunofluorescence against DDX6, an established P-body marker, and the foci formed by SNAP-Dcp1a also co-localized with endogenous Xrn1 (Figure S7). We then assessed the co-localization of intact and degraded TREAT transcripts with P-bodies in living cells. Simultaneous acquisition of the TREAT reporter in two channels (NLS-PCP-GFP, NLS-MCP-Halo) was followed by imaging of P-bodies (SNAP-Dcp1a). P-bodies were segmented and used to generate distance maps where positions within P-bodies were defined as positive values while locations outside received negative values. P-body co-localization of intact and degraded TREAT transcripts was measured at each time point. A cumulative P-body localization index was calculated from three consecutive frames (3 × 50 ms) in order to account for spurious co-localization. This index was negative for all intact TREAT transcripts and stabilized 3′ ends, indicating that neither species accumulated in P-bodies (Figures 5A and 5B, Movie S4).

Transcripts that contain an AU-rich element (ARE) within their 3′ UTRs undergo rapid degradation, and this *cis*-acting element has also been shown to promote the association of mRNAs with P-bodies (Franks and Lykke-Andersen, 2007). We modified the TREAT reporter to include the TNF-α ARE between the PP7 stem loops and the viral PKs (Figure 5C). The half-life of TREAT TNF-α ARE reporter transcripts was reduced to ~30 min, which is consistent with the role of the ARE on mRNA stability (Figure S8). Interestingly, we also found that the nuclear export rate and the degradation of the stabilized 3′ ends was faster for the TREAT TNF-α ARE reporter. We detected a small number of intact TREAT ARE transcripts with positive cumulative P-body localization values; however, we found no evidence for the accumulation of degraded fragments within P-bodies (Figures 5C and 5D, Movie S5). To confirm that the RNAs within P-bodies were not a mixture of

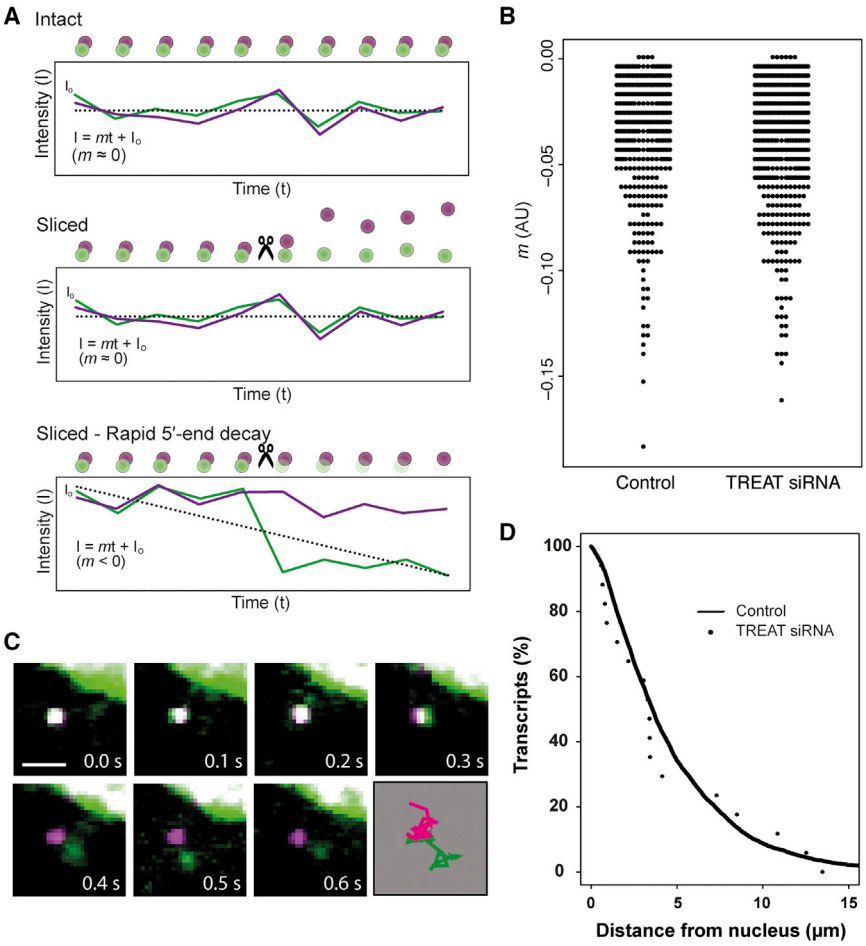

Figure 4. TREAT Imaging of siRNA-Mediated Endonucleolytic Cleavage in Live Cells

(A) Cartoons depicting potential slicing scenarios in live cells. Non-sliced: Dual-labeled transcripts have green and magenta signals that co-localize and do not change in fluorescence intensity (I) over time (t) compared to initial intensity (I_0). Dotted lines show theoretical linear fits to the bleach-corrected fluorescence intensity of the green signal curves. The slope (m) of the linear regression was used to quantify intensity changes. Sliced: Dual-labeled transcripts are cleaved between green and magenta signals that can independently be tracked. Sliced and rapid 5′ end decay: After slicing of a dual-labeled transcript, the green signal is rapidly lost.

(B) Beeswarm plot of the slopes (m) of the linear regressions of the bleach-corrected NLS-PCP-GFP intensities of dual-labeled particles (> 5 frames) collected for the TREAT siRNA reporter (575 particles, 681 cells) as well as the non-sliced control (361 particles, 125 cells). Populations do not differ in their outlier composition. In control data, 5% of m are less than −0.093, and an almost identical fraction of TREAT siRNA reporters (5.4%) are also within this threshold.

(C) Time sequence showing a slicing event in a live cell. A dual-colored intact mRNA (PP7 + MS2) is observed for several consecutive frames followed by slicing and spatial separation of the 5′ (PP7, green) and 3′ (MS2, magenta) fragments. Time series projection of two-channel SPT shows co-localization and separation of signals.

(D) Distribution of slicing events in the cytoplasm. The location of slicing events (black dots) relative to the nucleus is similar to the positions of control transcripts (black line). p value = 0.74; Kolmogorov-Smirnov test. All error bars indicate SEM. Scale bar, 1 μm.

intact mRNAs and stabilized 3′ ends resulting from active degradation, we compared the ratio of the fluorescence intensity of NLS-PCP-GFP to NLS-MCP-Halo for RNAs in P-bodies with intact transcripts that remained in the cytosol (Figure 5E). The RNAs in P-bodies and intact mRNAs in the cytosol had similar ratios, indicating that RNAs within P-bodies were intact and were not undergoing degradation.

Since the number of P-bodies is low in unstressed cells, we stressed cells with arsenite for 1 hr to increase the number and size of P-bodies. It has been proposed previously that cellular transcripts may be triaged through stress granules into P-bodies for degradation during stress (Anderson et al., 2015; Decker and Parker, 2012). During arsenite stress, we detected only intact TREAT mRNAs and not stabilized 3′ ends with positive cumulative P-body localization values (Figures 6A and 6B, Movie S6). To increase the association of mRNAs with P-bodies, we added a 5′-TOP sequence to the TREAT reporter, because this *cis*-element was shown to promote the interaction of mRNAs with P-bodies during arsenite stress (Halstead et al., 2015). Similarly, only intact 5′-TOP TREAT transcripts were found within P-bodies during stress (Figures 6C and 6D, Movie S7). Further experiments will be required to determine if P-bodies are sites of specialized mRNA degradation, but our data suggest that these cellular compartments are not general sites of active mRNA turnover during normal cell growth or stress.

Translation Inhibition Stabilizes TREAT mRNAs

While analyzing the spatial position of TREAT transcripts during stress, we observed an increase in the total number of intact mRNAs within cells (Figures 7A and 7B). Since only a small percentage of TREAT reporter transcripts accumulate in P-bodies or stress granules during arsenite stress, this increase in stability cannot be explained by these cellular compartments serving as protective storage sites. Because arsenite stress inhibits general translation via eIF2α phosphorylation, we tested the effect of several other translation inhibitors, which target distinct stages of protein synthesis, for their effects on mRNA stability. TREAT transcripts were induced for 2 hr with doxycycline followed by addition of harringtonine, cycloheximide, or puromycin (Figure 7C). Similar to arsenite, these translation inhibitors caused a dramatic stabilization of TREAT transcripts (Figure 7D). The effect was more pronounced after 4 hr of treatment with translation inhibitors, as

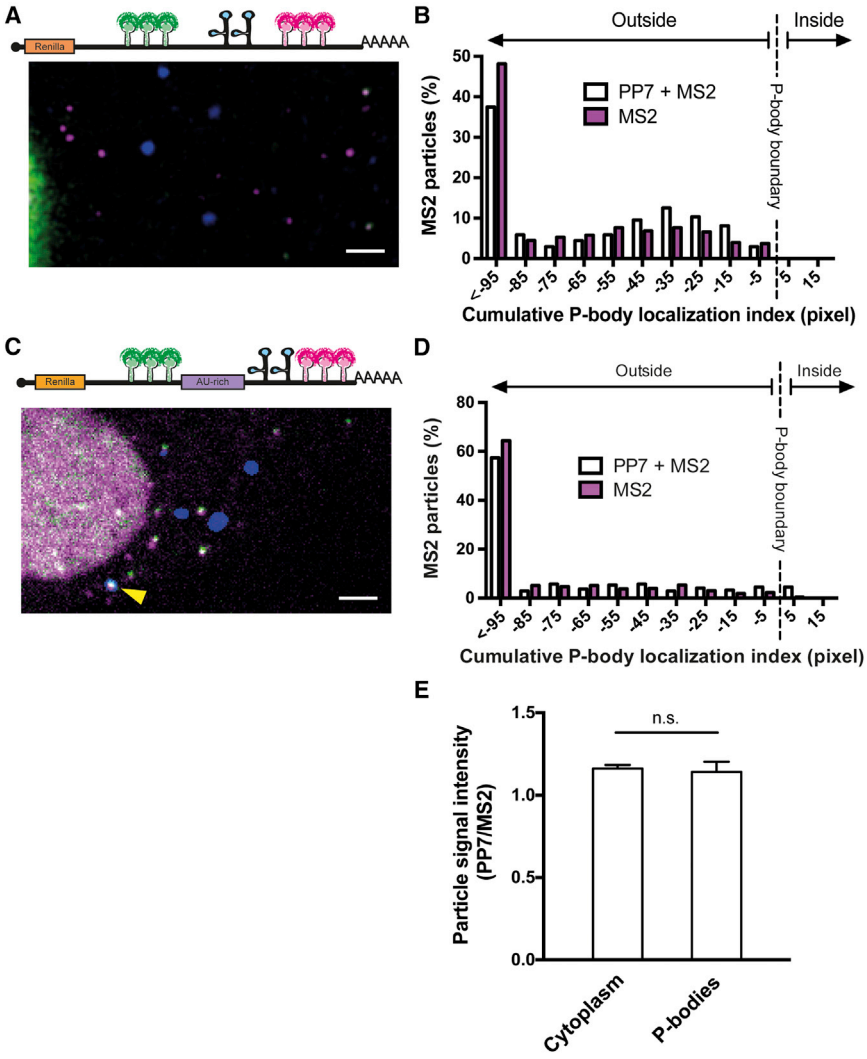

Figure 5. TREAT Transcripts Are Not Degraded in P-Bodies

(A) Representative live-cell image of TREAT reporter in HeLa cells expressing NLS-MCP-Halo (magenta), NLS-PCP-GFP (green), and SNAP-Dcp1a (blue).

(B) TREAT transcripts do not accumulate in P-bodies. Two-channel SPT identified intact (PP7 + MS2) and stabilized 3′ ends (MS2) (516 particles, 27 cells) in cells. The position in pixels of all RNAs with respect to P-bodies was measured, and the cumulative P-body localization index was calculated from three successive frames (3 × 50 ms).

(C) Representative live-cell image of TREAT TNF-α ARE reporter in HeLa cells expressing NLS-MCP-Halo (magenta), NLS-PCP-GFP (green), and SNAP-Dcp1a (blue). The yellow arrowhead points to an intact TREAT mRNA bound to a P-body.

(D) Low accumulation of intact TREAT TNF-α ARE transcripts within P-bodies. SPT identified intact (PP7 + MS2) and stabilized 3′ ends (MS2) (772 particles, 55 cells).

(E) Intact mRNAs in P-bodies are not undergoing degradation. The ratio of the fluorescent intensity of NLS-PCP-GFP and NLS-MCP-Halo was similar for all dual-colored mRNAs in P-bodies and cytosol (n.s., not significant; unpaired t test). Histograms are plotted with bin widths of 10 pixels. Scale bars, 5 μm. Error bars indicate SEM.

degradation remained completely blocked. While harringtonine and cycloheximide could immobilize ribosomes on TREAT transcripts, thereby blocking Xrn1 degradation, puromycin causes disassociation of ribosomes from transcripts. Our data indicate that any inhibition of translation results in stabilization of TREAT mRNAs.

The global inhibition of mRNA degradation we observed during arsenite stress is consistent with a general inhibition of decay resulting from proteolytic degradation of Tob and Pan3, which are the factors responsible for recruitment of deadenylases to transcripts (Yamagishi et al., 2014). Inhibition of deadenylation has also been observed in yeast and mammalian cells in response to a variety of cellular stresses, suggesting that this may be a conserved pathway that is activated when translation is inhibited (Gowrishankar et al., 2006; Hilgers et al., 2006). Alternatively, the release factor eRF3 has also been shown to compete with Tob/Pan3 for PABPC1, suggesting a possible direct coupling between translation and mRNA decay (Funakoshi et al., 2007; Yamagishi et al., 2014).

DISCUSSION

Single-molecule measurements of the mRNA life cycle have profoundly altered our understanding of gene expression; however, it has not yet been possible to directly measure how these processes are inter-connected within single cells. The continued development of multicolored RNA biosensors will enable a more sophisticated investigation of the coupling between transcription, translation, and mRNA degradation. A variety of orthogonal fluorescent proteins and RNA-labeling methods exist that would enable translation (TRICK) and mRNA turnover (TREAT) to be imaged simultaneously in three channels (Chen et al., 2009; Daigle and Ellenberg, 2007; Grimm et al., 2015; Halstead et al., 2015). Similarly, TREAT could also be coupled with the recently developed methods for nascent polypeptide imaging that would allow the relationship between translation and mRNA turnover to be understood in greater detail (Morisaki et al., 2016; Pichon et al., 2016; Wang et al., 2016; Wu et al., 2016; Yan et al., 2016). A complete accounting of an individual transcript's life from birth to death is now possible.

Limitations

Previously, overexpression or viral infection of RNAs containing Xrn1-blocking PKs was shown to affect degradation of endogenous mRNAs (Moon et al., 2012). While TREAT and a conceptually similar approach using Xrn1-resistant RNA elements did not

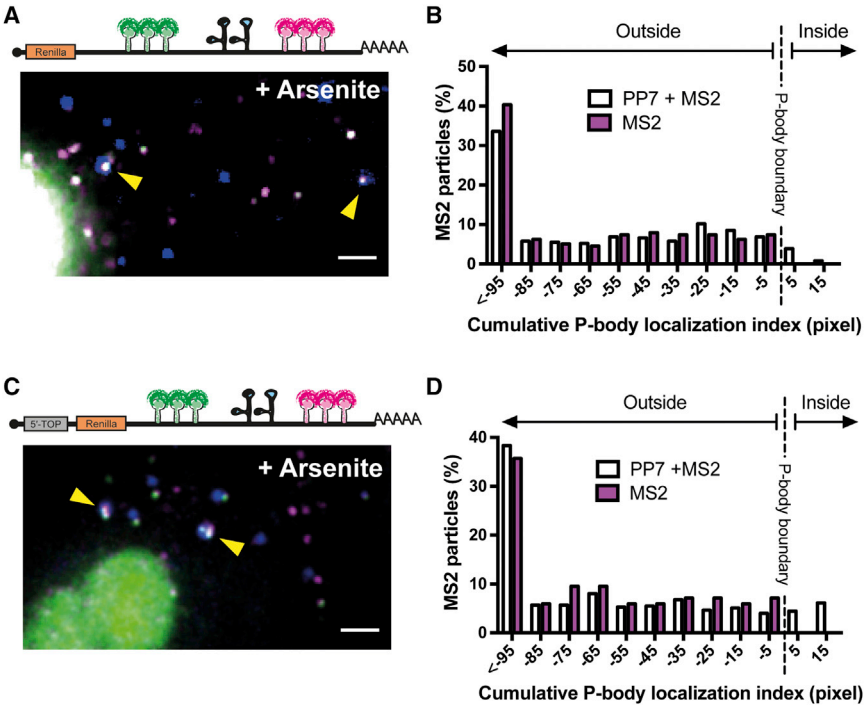

Figure 6. TREAT Transcripts Are Not Degraded in P-Bodies during Stress

(A) Representative live-cell image of TREAT reporter in HeLa cells expressing NLS-MCP-Halo (magenta), NLS-PCP-GFP (green), and SNAP-Dcp1a (blue) as a P-body marker stressed with arsenite (500 μM) for 1 hr.

(B) Intact TREAT transcripts accumulate in P-bodies during arsenite stress. SPT experiments were performed to identify intact (MS2 + PP7, white) and stabilized 3′ ends (MS2 only, magenta) in arsenite-stressed cells (539 particles, 19 cells).

(C) Representative live-cell image of 5′-TOP TREAT reporter in HeLa cells expressing NLS-MCP-Halo (magenta), NLS-PCP-GFP (green), and SNAP-Dcp1a (blue) as a P-body marker stressed with arsenite (500 μM) for 1 hr.

(D) Intact 5′-TOP TREAT transcripts accumulate in P-bodies during arsenite stress to a greater extent than TREAT transcripts. SPT experiments were performed to identify intact (MS2 + PP7, white) and stabilized 3′ ends (MS2 only, magenta) in arsenite-stressed (556 particles, 22 cells) cells. Histograms are plotted with bin widths of 10 pixels and centered at shown values. Scale bar, 5 μm.

detect inhibition of endogenous mRNA decay, this effect could be concentration dependent (Boehm et al., 2016). It will be an important control when establishing TREAT in other experimental systems that the approach itself does not influence mRNA degradation.

In order to directly detect mRNA decay events in live cells, we incorporated an siRNA target sequence within the TREAT reporter to shorten the half-life of the transcript. Continued development of automated SPT and analysis routines will enable the detection of decay events for more stable transcripts. Furthermore, tethering of TREAT reporter mRNAs to cytoplasmic structures (e.g., membranes via addition of a CAAX prenylation sequence to MCP) can immobilize the transcript and has been shown to allow monitoring of individual mRNAs for extended time periods (Yan et al., 2016). While restricting mobility of mRNAs may not be appropriate for all applications of TREAT, it will overcome limitations in decay detection due to movement of RNAs. Alternatively, advances in the speed and sensitivity of

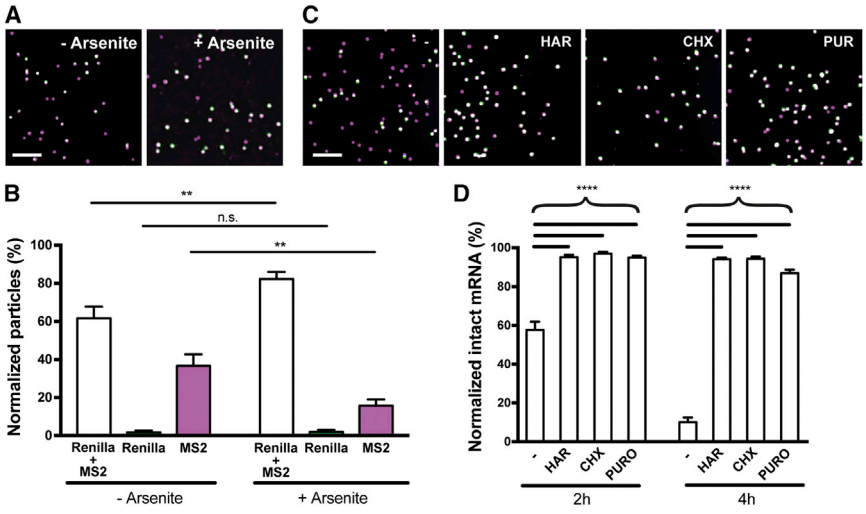

Figure 7. Stabilization of TREAT Transcripts during Stress and Translation Inhibition

(A) Representative smFISH images of the TREAT reporter in HeLa cells with and without arsenite stress. HeLa cells were induced for 2 hr with doxycycline and then treated with 500 μM arsenite for another 2 hr. Intact mRNAs (*Renilla* + MS2, white) and stabilized 3′ ends (MS2, magenta) were measured by smFISH.

(B) Intact mRNAs are stabilized in arsenite-stressed cells (16 cells) compared to unstressed cells (8 cells).

(C) Representative smFISH images of the TREAT reporter in HeLa cells treated with translational inhibitors. HeLa cells were induced for 2 hr with doxycycline followed by addition of translational inhibitors harringtonine (5 μM), cycloheximide (100 μg mL^{-1}), and puromycin (100 μg mL^{-1}) for 2 or 4 hr.

(D) Quantification of smFISH of HeLa cells treated with translational inhibitors shows stabilization of TREAT mRNAs. Shown are untreated (2 hr, 20 cells; 4 hr, 23 cells), harringtonine (2 hr, 34 cells; 4 hr, 37 cells), cycloheximide (2 hr, 38 cells; 4 hr, 38 cells), and puromycin (2 hr, 39 cells; 4 hr, 36 hr). Graph shows mean ± SEM. p values: ** < 0.01, **** < 0.0001; n.s., not significant; unpaired t test. Scale bars, 5 μm.

multi-color, multi-focal plane microscopy may enable single mRNAs to be observed continuously while freely moving in the cytosol (Abrahamsson et al., 2013).

STAR★METHODS

Detailed methods are provided in the online version of this paper and include the following:

- KEY RESOURCES TABLE
- CONTACT FOR REAGENT AND RESOURCE SHARING
- EXPERIMENTAL MODEL AND SUBJECT DETAILS
  - Cell lines and tissue culture
- METHOD DETAILS
  - Plasmid construction
  - HeLa stable cell line construction
  - Northern Blot
  - RT-qPCR
  - Renilla luciferase assay
  - siRNA transfection
  - Western Blotting
  - Single-molecule FISH
  - Detection of mRNA spots from smFISH and co-localization analysis
  - Correction of co-localization data for detection efficiency
  - Modeling of mRNA half-lives from smFISH measurements
  - Stochastic simulation of mRNA decay
  - Immunofluorescence
  - Live-cell imaging of TREAT mRNAs
- QUANTIFICATION AND STATISTICAL ANALYSIS
  - Single particle tracking of mRNAs in live cells and track co-localization
  - Live-cell slicing analysis
  - Quantification and co-localization of mRNAs in P-bodies in living cells
  - Statistical Analysis
- DATA AND SOFTWARE AVAILABILITY

SUPPLEMENTAL INFORMATION

Supplemental Information includes eight figures, seven movies, one file of detailed protocols, and the track-based co-localization workflow used to identify intact and stabilized 3′ end TREAT reporter mRNAs and can be found with this article online at https://doi.org/10.1016/j.molcel.2017.09.030.

AUTHOR CONTRIBUTIONS

I.H. and F.V. performed experiments and analyzed data with help from A.V.K. and C.G.A.-R. (northern blot and smFISH) and J.E. (image analysis). Y.Z. and L.G. performed the mathematical modeling, and M.B.S. contributed to data normalization. J.A.C. wrote the manuscript with input from all of the authors.

ACKNOWLEDGMENTS

This work was supported by the Novartis Research Foundation (J.A.C., L.G.), the Swiss National Science Foundation grant 31003A_156477 (J.A.C), the SNF-NCCR RNA & Disease (J.A.C.), and the SystemsX.ch/MetastasiX project (M.B.S.). The authors thank J. Kieft (UC Denver) for advice on viral pseudoknots, K. Schönig (CIMH) for the parental HeLa 11ht cell line, L. Lavis (Janelia Farm) for providing Halo and SNAP dyes, T. Lionnet (Janelia Farm) for providing access to AIRLOCALIZE detection software, and J. Lykke-Andersen (UCSD) for sharing plasmids containing TNF-α AU-rich element and RPL32 5′-TOP sequences. We acknowledge L. Gelman and S. Bourke (FMI) for microscopy support and H. Kohler (FMI) for cell sorting. The authors thank W. Filipowicz, H. Grosshans, T. Lionnet, R. Singer, and D. Schübeler for their helpful suggestions.

Received: August 22, 2017
Revised: September 8, 2017
Accepted: September 21, 2017
Published: October 19, 2017

REFERENCES

Abrahamsson, S., Chen, J., Hajj, B., Stallinga, S., Katsov, A.Y., Wisniewski, J., Mizuguchi, G., Soule, P., Mueller, F., Dugast Darzacq, C., et al. (2013). Fast multicolor 3D imaging using aberration-corrected multifocus microscopy. Nat. Methods *10*, 60–63.

Anderson, P., Kedersha, N., and Ivanov, P. (2015). Stress granules, P-bodies and cancer. Biochim. Biophys. Acta *1849*, 861–870.

Banani, S.F., Lee, H.O., Hyman, A.A., and Rosen, M.K. (2017). Biomolecular condensates: organizers of cellular biochemistry. Nat. Rev. Mol. Cell Biol. *18*, 285–298.

Beard, C., Hochedlinger, K., Plath, K., Wutz, A., and Jaenisch, R. (2006). Efficient method to generate single-copy transgenic mice by site-specific integration in embryonic stem cells. Genesis *44*, 23–28.

Berg, H.C. (1993). Random Walks in Biology (Princeton University Press).

Berthold, M.R., Cebron, N., Dill, F., Gabriel, T.R., Kötter, T., Meinl, T., Ohl, P., Thiel, K., and Wiswede, B. (2009). KNIME - The Konstanz Information Miner: Version 2.0 and Beyond. ACM SIGKDD Explorations Newsletter *11*, 26–31.

Bhattacharyya, S.N., Habermacher, R., Martine, U., Closs, E.I., and Filipowicz, W. (2006). Relief of microRNA-mediated translational repression in human cells subjected to stress. Cell *125*, 1111–1124.

Boehm, V., Gerbracht, J.V., Marx, M.C., and Gehring, N.H. (2016). Interrogating the degradation pathways of unstable mRNAs with XRN1-resistant sequences. Nat. Commun. *7*, 13691.

Brengues, M., Teixeira, D., and Parker, R. (2005). Movement of eukaryotic mRNAs between polysomes and cytoplasmic processing bodies. Science *310*, 486–489.

Chang, C.T., Bercovich, N., Loh, B., Jonas, S., and Izaurralde, E. (2014). The activation of the decapping enzyme DCP2 by DCP1 occurs on the EDC4 scaffold and involves a conserved loop in DCP1. Nucleic Acids Res. *42*, 5217–5233.

Chapman, E.G., Costantino, D.A., Rabe, J.L., Moon, S.L., Wilusz, J., Nix, J.C., and Kieft, J.S. (2014a). The structural basis of pathogenic subgenomic flavivirus RNA (sfRNA) production. Science *344*, 307–310.

Chapman, E.G., Moon, S.L., Wilusz, J., and Kieft, J.S. (2014b). RNA structures that resist degradation by Xrn1 produce a pathogenic Dengue virus RNA. eLife *3*, e01892.

Chen, J., Nikolaitchik, O., Singh, J., Wright, A., Bencsics, C.E., Coffin, J.M., Ni, N., Lockett, S., Pathak, V.K., and Hu, W.S. (2009). High efficiency of HIV-1 genomic RNA packaging and heterozygote formation revealed by single virion analysis. Proc. Natl. Acad. Sci. USA *106*, 13535–13540.

Chu, C.Y., and Rana, T.M. (2006). Translation repression in human cells by microRNA-induced gene silencing requires RCK/p54. PLoS Biol. *4*, e210.

Cougot, N., Babajko, S., and Séraphin, B. (2004). Cytoplasmic foci are sites of mRNA decay in human cells. J. Cell Biol. *165*, 31–40.

Daigle, N., and Ellenberg, J. (2007). LambdaN-GFP: an RNA reporter system for live-cell imaging. Nat. Methods *4*, 633–636.

Damgaard, C.K., and Lykke-Andersen, J. (2011). Translational coregulation of 5'TOP mRNAs by TIA-1 and TIAR. Genes Dev. *25*, 2057–2068.

Decker, C.J., and Parker, R. (2012). P-bodies and stress granules: possible roles in the control of translation and mRNA degradation. Cold Spring Harb. Perspect. Biol. *4*, a012286.

Dunckley, T., and Parker, R. (1999). The DCP2 protein is required for mRNA decapping in Saccharomyces cerevisiae and contains a functional MutT motif. EMBO J. *18*, 5411–5422.

Elkon, R., Zlotorynski, E., Zeller, K.I., and Agami, R. (2010). Major role for mRNA stability in shaping the kinetics of gene induction. BMC Genomics *11*, 259.

Eulalio, A., Behm-Ansmant, I., Schweizer, D., and Izaurralde, E. (2007). P-body formation is a consequence, not the cause, of RNA-mediated gene silencing. Mol. Cell. Biol. *27*, 3970–3981.

Franks, T.M., and Lykke-Andersen, J. (2007). TTP and BRF proteins nucleate processing body formation to silence mRNAs with AU-rich elements. Genes Dev. *21*, 719–735.

Friedel, C.C., Dölken, L., Ruzsics, Z., Koszinowski, U.H., and Zimmer, R. (2009). Conserved principles of mammalian transcriptional regulation revealed by RNA half-life. Nucleic Acids Res. *37*, e115.

Funakoshi, Y., Doi, Y., Hosoda, N., Uchida, N., Osawa, M., Shimada, I., Tsujimoto, M., Suzuki, T., Katada, T., and Hoshino, S. (2007). Mechanism of mRNA deadenylation: evidence for a molecular interplay between translation termination factor eRF3 and mRNA deadenylases. Genes Dev. *21*, 3135–3148.

Gagnon, K.T., Li, L., Chu, Y., Janowski, B.A., and Corey, D.R. (2014). RNAi factors are present and active in human cell nuclei. Cell Rep. *6*, 211–221.

Garcia, J.F., and Parker, R. (2015). MS2 coat proteins bound to yeast mRNAs block 5′ to 3′ degradation and trap mRNA decay products: implications for the localization of mRNAs by MS2-MCP system. RNA *21*, 1393–1395.

Garneau, N.L., Wilusz, J., and Wilusz, C.J. (2007). The highways and byways of mRNA decay. Nat. Rev. Mol. Cell Biol. *8*, 113–126.

Gillespie, D.T. (1977). Exact Stochastic Simulation of Coupled Chemical Reactions. J. Phys. Chem. *81*, 2340–2361.

Gowrishankar, G., Winzen, R., Dittrich-Breiholz, O., Redich, N., Kracht, M., and Holtmann, H. (2006). Inhibition of mRNA deadenylation and degradation by different types of cell stress. Biol. Chem. *387*, 323–327.

Grimm, J.B., English, B.P., Chen, J., Slaughter, J.P., Zhang, Z., Revyakin, A., Patel, R., Macklin, J.J., Normanno, D., Singer, R.H., et al. (2015). A general method to improve fluorophores for live-cell and single-molecule microscopy. Nat. Methods *12*, 244–250, 3, 250.

Halstead, J.M., Lionnet, T., Wilbertz, J.H., Wippich, F., Ephrussi, A., Singer, R.H., and Chao, J.A. (2015). Translation. An RNA biosensor for imaging the first round of translation from single cells to living animals. Science *347*, 1367–1671.

Hao, S., and Baltimore, D. (2009). The stability of mRNA influences the temporal order of the induction of genes encoding inflammatory molecules. Nat. Immunol. *10*, 281–288.

Heinrich, S., Sidler, C.L., Azzalin, C.M., and Weis, K. (2017). Stem-loop RNA labeling can affect nuclear and cytoplasmic mRNA processing. RNA *23*, 134–141.

Hilgers, V., Teixeira, D., and Parker, R. (2006). Translation-independent inhibition of mRNA deadenylation during stress in Saccharomyces cerevisiae. RNA *12*, 1835–1845.

Hocine, S., Raymond, P., Zenklusen, D., Chao, J.A., and Singer, R.H. (2013). Single-molecule analysis of gene expression using two-color RNA labeling in live yeast. Nat. Methods *10*, 119–121.

Isken, O., and Maquat, L.E. (2007). Quality control of eukaryotic mRNA: safeguarding cells from abnormal mRNA function. Genes Dev. *21*, 1833–1856.

Jain, S., and Parker, R. (2013). The discovery and analysis of P Bodies. Adv. Exp. Med. Biol. *768*, 23–43.

Kedersha, N., and Anderson, P. (2007). Mammalian stress granules and processing bodies. Methods Enzymol. *431*, 61–81.

Kieft, J.S., Rabe, J.L., and Chapman, E.G. (2015). New hypotheses derived from the structure of a flaviviral Xrn1-resistant RNA: Conservation, folding, and host adaptation. RNA Biol. *12*, 1169–1177.

Kramer, S. (2017). Simultaneous detection of mRNA transcription and decay intermediates by dual colour single mRNA FISH on subcellular resolution. Nucleic Acids Res. *45*, e49.

Leung, A.K., Calabrese, J.M., and Sharp, P.A. (2006). Quantitative analysis of Argonaute protein reveals microRNA-dependent localization to stress granules. Proc. Natl. Acad. Sci. USA *103*, 18125–18130.

Lionnet, T., Czaplinski, K., Darzacq, X., Shav-Tal, Y., Wells, A.L., Chao, J.A., Park, H.Y., de Turris, V., Lopez-Jones, M., and Singer, R.H. (2011). A transgenic mouse for in vivo detection of endogenous labeled mRNA. Nat. Methods *8*, 165–170.

Lykke-Andersen, J. (2002). Identification of a human decapping complex associated with hUpf proteins in nonsense-mediated decay. Mol. Cell. Biol. *22*, 8114–8121.

Miller, C., Schwalb, B., Maier, K., Schulz, D., Dümcke, S., Zacher, B., Mayer, A., Sydow, J., Marcinowski, L., Dölken, L., et al. (2011). Dynamic transcriptome analysis measures rates of mRNA synthesis and decay in yeast. Mol. Syst. Biol. *7*, 458.

Moon, S.L., Anderson, J.R., Kumagai, Y., Wilusz, C.J., Akira, S., Khromykh, A.A., and Wilusz, J. (2012). A noncoding RNA produced by arthropod-borne flaviviruses inhibits the cellular exoribonuclease XRN1 and alters host mRNA stability. RNA *18*, 2029–2040.

Morisaki, T., Lyon, K., DeLuca, K.F., DeLuca, J.G., English, B.P., Zhang, Z., Lavis, L.D., Grimm, J.B., Viswanathan, S., Looger, L.L., et al. (2016). Real-time quantification of single RNA translation dynamics in living cells. Science *352*, 1425–1429.

Otsu, N. (1979). A Threshold Selection Method from Grey-Level Histograms. IEEE Trans. Syst. Man Cybern. *9*, 62–66.

Pichon, X., Bastide, A., Safieddine, A., Chouaib, R., Samacoits, A., Basyuk, E., Peter, M., Mueller, F., and Bertrand, E. (2016). Visualization of single endogenous polysomes reveals the dynamics of translation in live human cells. J. Cell Biol. *214*, 769–781.

Rabani, M., Levin, J.Z., Fan, L., Adiconis, X., Raychowdhury, R., Garber, M., Gnirke, A., Nusbaum, C., Hacohen, N., Friedman, N., et al. (2011). Metabolic labeling of RNA uncovers principles of RNA production and degradation dynamics in mammalian cells. Nat. Biotechnol. *29*, 436–442.

Raj, A., and van Oudenaarden, A. (2008). Nature, nurture, or chance: stochastic gene expression and its consequences. Cell *135*, 216–226.

Schindelin, J., Arganda-Carreras, I., Frise, E., Kaynig, V., Longair, M., Pietzsch, T., Preibisch, S., Rueden, C., Saalfeld, S., Schmid, B., et al. (2012). Fiji: an open-source platform for biological-image analysis. Nat. Methods *9*, 676–682.

Schoenberg, D.R., and Maquat, L.E. (2012). Regulation of cytoplasmic mRNA decay. Nat. Rev. Genet. *13*, 246–259.

Sheth, U., and Parker, R. (2003). Decapping and decay of messenger RNA occur in cytoplasmic processing bodies. Science *300*, 805–808.

Stoecklin, G., Mayo, T., and Anderson, P. (2006). ARE-mRNA degradation requires the 5′-3′ decay pathway. EMBO Rep. *7*, 72–77.

Tinevez, J.Y., Perry, N., Schindelin, J., Hoopes, G.M., Reynolds, G.D., Laplantine, E., Bednarek, S.Y., Shorte, S.L., and Eliceiri, K.W. (2017). TrackMate: An open and extensible platform for single-particle tracking. Methods *115*, 80–90.

Trcek, T., Larson, D.R., Moldón, A., Query, C.C., and Singer, R.H. (2011). Single-molecule mRNA decay measurements reveal promoter- regulated mRNA stability in yeast. Cell *147*, 1484–1497.

Trcek, T., Sato, H., Singer, R.H., and Maquat, L.E. (2013). Temporal and spatial characterization of nonsense-mediated mRNA decay. Genes Dev. *27*, 541–551.

van Dijk, E., Cougot, N., Meyer, S., Babajko, S., Wahle, E., and Séraphin, B. (2002). Human Dcp2: a catalytically active mRNA decapping enzyme located in specific cytoplasmic structures. EMBO J. *21*, 6915–6924.

Voigt, F., Eglinger, J., and Chao, J.A. (in press). Detection of the first round of translation: the TRICK assay. In RNA Detection, I. Gaspar, ed. (Springer).

Wang, C., Han, B., Zhou, R., and Zhuang, X. (2016). Real-Time Imaging of Translation on Single mRNA Transcripts in Live Cells. Cell *165*, 990–1001.

Weidenfeld, I., Gossen, M., Löw, R., Kentner, D., Berger, S., Görlich, D., Bartsch, D., Bujard, H., and Schönig, K. (2009). Inducible expression of coding and inhibitory RNAs from retargetable genomic loci. Nucleic Acids Res. *37*, e50.

Wu, B., Miskolci, V., Sato, H., Tutucci, E., Kenworthy, C.A., Donnelly, S.K., Yoon, Y.J., Cox, D., Singer, R.H., and Hodgson, L. (2015). Synonymous modification results in high-fidelity gene expression of repetitive protein and nucleotide sequences. Genes Dev. *29*, 876–886.

Wu, B., Eliscovich, C., Yoon, Y.J., and Singer, R.H. (2016). Translation dynamics of single mRNAs in live cells and neurons. Science *352*, 1430–1435.

Yamagishi, R., Hosoda, N., and Hoshino, S. (2014). Arsenite inhibits mRNA deadenylation through proteolytic degradation of Tob and Pan3. Biochem. Biophys. Res. Commun. *455*, 323–331.

Yamashita, A., Chang, T.C., Yamashita, Y., Zhu, W., Zhong, Z., Chen, C.Y., and Shyu, A.B. (2005). Concerted action of poly(A) nucleases and decapping enzyme in mammalian mRNA turnover. Nat. Struct. Mol. Biol. *12*, 1054–1063.

Yan, X., Hoek, T.A., Vale, R.D., and Tanenbaum, M.E. (2016). Dynamics of Translation of Single mRNA Molecules In Vivo. Cell *165*, 976–989.

Yen, J.C., Chang, F.J., and Chang, S. (1995). A new criterion for automatic multilevel thresholding. IEEE transactions on image processing: a publication of the IEEE Signal Processing Society *4*, 370–378.

Zeng, Y., and Cullen, B.R. (2002). RNA interference in human cells is restricted to the cytoplasm. RNA *8*, 855–860.

STAR★METHODS

KEY RESOURCES TABLE

REAGENT or RESOURCE	SOURCE	IDENTIFIER
Antibodies		
Mouse anti-Rrp40	Abcam	ab67661; RRID: AB_1140293
Rabbit anti-α-Tubulin	Abcam	ab18251; RRID: AB_2210057
Rabbit anti-Xrn1	Abcam	ab70259; RRID: AB_1271494
Mouse anti-Actin-pan	ThermoFisher Scientific	MA5-11869; RRID: AB_11004139
Anti-rabbit IRDye 800 CW	LI-COR	926-68071; RRID: AB_10956166
Anti-mouse IRDye 680 RD	LI-COR	926-32210; RRID: AB_621842
Goat anti-rabbit secondary antibody coupled to Alexa Fluor 647	Molecular Probes, Thermo Fisher Scientific	A27040; RRID: AB_2536101
Chemicals, Peptides, and Recombinant Proteins		
JF549 HaloTag Ligand	Grimm et al., 2015	N/A
JF549 SNAP-tag Ligand	Grimm et al., 2015	N/A
FluoroBrite DMEM	Life Technologies	A1896702
Lipofectamine 2000	ThermoFisher Scientific	11668027
Lipofectamine RNAiMAX	ThermoFisher Scientific	13778030
Doxycycline	Sigma	D9891-1G
Hygromycin	ThermoFisher Scientific	10687010
Ganciclovir	BioCat GmbH (TargetMol)	T0688-6-TM
Sodium Arsenite solution	Sigma	35000-1L-R
Harringtonine	LKT Laboratories	H0169-5mg
Cycloheximide	Sigma	C4859-1ML
Puromycin 10 mg/ml	Invivogen	ant-pr-1
TRIzol	Ambion/Life Technologies	15596-026
20% Paraformaldehyde (aqueous, 10×10 mL)	Electron Microscopy Sciences	15713
Amersham Hybond-N+ membrane	GE Healthcare	45-000-763
UltraPure 20x SSC Buffer	Life Technologies	15557036
Methylene Blue Hydrate	Sigma	28514-100G
FastStart Universal SYBR Green Master mix	Roche	4913850001
Actinomycin D	Sigma	A1410-2MG
Bovine Serum Albumin	Sigma	A2153-50G
Dextran sulfate	Sigma	D6001-50G
Formamide (deionized)	Ambion, Life Technologies	AM9342
ProLong Gold Antifade Mountant	Molecular Probes, Life Technologies	P36934
Critical Commercial Assays		
Bradford Protein Assay	BioRad	5000006
DIG-Starter Northern Blot Kit	Roche	000000012039672910
TURBO DNA-free Kit	Ambion, Thermo Fisher Scientific	AM1907
SuperScript Reverse Transcriptase III	Thermo Fisher Scientific	18080093
Renilla Luciferase Assay System	Promega	E2810
Deposited Data		
Unprocessed Image Data	This paper	https://doi.org/10.17632/52wjrtnz2r.1

(*Continued on next page*)

Continued

REAGENT or RESOURCE	SOURCE	IDENTIFIER
Experimental Models: Cell Lines		
HeLa 11ht	Weidenfeld et al., 2009	N/A
HeLa-11ht-TREAT + NLS-stdMCP-Halo + NLS-stdPCP-stdGFP (+ SNAP-Dcp1a)	This paper	N/A
HeLa-11ht-TREAT-siRNA + NLS-stdMCP-Halo + NLS-stdPCP-stdGFP (+ SNAP-Dcp1a)	This paper	N/A
HeLa-11ht-TREAT-ARE + NLS-stdMCP-Halo + NLS-stdPCP-stdGFP (+ SNAP-Dcp1a)	This paper	N/A
Oligonucleotides		
MISSION pLKO.1-puro firefly luciferase shRNA Control: CCGG **CGCTGAGTACTTCGAAATGTC**CTCGAG**GACATTTCGAAGT ACTCAGCG**TTTTT	Sigma Aldrich	SHC007
Renilla FISH probes: TCGTACACCTTGGAAGCCAT AGTGATCATGCGTTTGCGTT GTTCATTTGCTTGCAGCGAG AGTTGATGAAGGAGTCCAGC GCGTGCTTCTCGGAATCATA CAGCGTTACCATGCAGAAAA TCGATGTGAGGCACGACGTG GATGATGCATCTAGCCACGG TTACCCATTCCGATCAGATC GATCCAGGAGGCGATATGAG CAAGCGGTGAGGTACTTGTA TTTGGAAGGTTCAGCAGCTC GTGGCCCACAAAGATGATTT GAGTAGTGAAAGGCCAGACA TTGATCTTGTCTTGGTGCTC CACTCTCAGCATGGACGATG CAGGACTCGATCACGTCCAC ATATCCTCCTCGATGTCAGG CTCTTCGCTCTTGATCAGGG ATTCTCAAGCACCATTTTCT GCATGGTCTCGACGAAGAAG TTTCCGCATGATCTTGCTTG CTTGAATGGCTCCAGGTAGG GAGAGGGTAGGCCGTCTAAC TTAACGAGAGGGATCTCGCG GACAATCTGGACGACGTCGG GAAGGTAGGCGTTGTAGTTG GAACATCTTAGGCAGATCGT TGGAAAAGAACCCAGGGTCG CTTAGCTCCCTCGACAATAG TTCACGAACTCGGTGTTAGG CTTACCCATTTCATCTGGAG GCTCCACGAAGCTCTTGATG TACTGCTCGTTCTTCAGCAC	Biosearch Technologies	N/A

(*Continued on next page*)

Continued

REAGENT or RESOURCE	SOURCE	IDENTIFIER
MS2v4 FISH probes: TGCCGTTTGTAGGTAGGATC CGCTTGAAGATTGGACAGTG GACTGTAATGACAGTGGAGC CTGATGCTGCTGGAGTTTGA ATGTCCTGATGTAGTCGGAG ATCGTCGAGCGTTGAATGAT ATAGTGTCTGAGGCATGCTG GTGATCGTGCAGCCGTTTGA CGATAACGTAGAGGCAGTAG CTGATGCTCGTCGCAGAAGA ATCTGGTATGTCCGATGTTG	Biosearch Technologies	N/A
3′-probe for Northern blot: CTTCAATCGATTTCGCGCGGGATCCAGACCACCTCCCC TGCGAGCTAAGCTGGACAGCCAATGACGGGTAAGAGA GTGACATTTTTCACTAACCTAAGACAGGAGGGCCGTCA GAGCTACTGCCTAATCCAAAGACGGGTAAAAGTGATAA AAATGTATCACTCCAACCTAAGACAGGCGCAGCTTCCG AGGGATTTGAGAT	This paper	N/A
Renilla forward qPCR primer: ATGGCTTCCAAGGTGTAC	This paper	N/A
Renilla reverse qPCR primer: TAGTTGATGAAGGAGTCCA	This paper	N/A
GAPDH forward qPCR primer: CGCTCTCTGCTCCTCCTGTT	This paper	N/A
GAPDH reverse qPCR primer: CCATGGTGTCTGAGCGATGT	This paper	N/A
c-Myc forward qPCR primer: CAGCTGCTTAGACGCTGGATT	This paper	N/A
c-Myc reverse qPCR primer: GTAGAAATACGGCTGCACCGA	This paper	N/A
ON-TARGETplus Human Exosc3 siRNA – SMARTpool: CCUGAAUGCUAGAGCGUGC GUAUUAUUAGAGUCCGAAA ACUCUCAGCAGAAGCGGUA GUGAACACAUGACGUCAGA	Dharmacon	L-031955-01-0005
ON-TARGETplus Non-targeting Pool: UGGUUUACAUGUCGACUAA UGGUUUACAUGUUGUGUGA UGGUUUACAUGUUUUCUGA UGGUUUACAUGUUUUCCUA	Dharmacon	D-001810-10-05
ON-TARGETplus Human Xrn1 siRNA – SMARTpool: CUUCAUAGUUGGUCGGUAU GAACAUAUUACAUGACGAA AAUAAGAAGGUGCGAGUAA AAUAAUUACCUCAGCGUUA	Dharmacon	L-013754-01-0005
Recombinant DNA		
pCAGGS-FLPe-IRESpuro plasmid	Beard et al., 2006	Addgene ID 20733
TNF-α AU-rich element: GATTATTTATTATTTATTTATTATTTATTTATTTAC	Franks and Lykke-Andersen, 2007	N/A
5′-TOP of RPL32: TCCTCTCTTCCTCGGCGCTGCCTACGGAGGTGGCAGCCATC-TCCTTCTCGGC	Damgaard and Lykke-Andersen, 2011	N/A
Software and Algorithms		
Graphpad Prism 7.0a	https://www.graphpad.com	N/A
Fiji including the TrackMate plugin	Schindelin et al., 2012; Tinevez et al., 2017	N/A
KNIME Analytics Platform version 3.2.1	Berthold et al., 2009	N/A
Data File S1 (Track-basedColocalizationAnalysis.knwf)	Voigt et al., in press	N/A

(*Continued on next page*)

Continued

REAGENT or RESOURCE	SOURCE	IDENTIFIER
Other		
Ibidi 35mm glass bottom dishes	ibidi	NOVS81158-IBI
Mini-PROTEAN 4-20% SDS gels	BioRad	4561096
Trans-Blot Turbo Mini PVDF Transfer Packs	BioRad	170-4156
Methods S1	This paper	N/A

CONTACT FOR REAGENT AND RESOURCE SHARING

All plasmids generated in this study are available from Addgene. For any other reagents or questions, please contact the corresponding author, Jeffrey A. Chao (jeffrey.chao@fmi.ch).

EXPERIMENTAL MODEL AND SUBJECT DETAILS

Cell lines and tissue culture

All cell lines are derivatives of a HeLa cell line (HeLa-11ht) constitutively expressing the reverse tetracycline controlled transactivator (rtTA2-M2) for inducible expression that also contains a single FLP recombinase-mediated cassette exchange (RCME) site (Weidenfeld et al., 2009). Cells were grown at 37°C and 5% CO_2 in DMEM containing 4.5 g L^{-1} glucose, 4 mM L-Glutamine, 100 U mL^{-1} Penicillin, 100 μg mL^{-1} Streptomycin and 10% FBS (Sigma Aldrich). To creat stable cell lines, RMCE was performed by replacement of the hygromycin-thymidine kinase (positive/negative) selection cassette with the individual TREAT reporter constructs.

METHOD DETAILS

Plasmid construction

To generate the TREAT reporter, the sequence of the tandem West Nile Virus Kunjin (WNV_{KUN}) pseudoknots (PKs) from the 3′ UTR of the genomic viral RNA was inserted between either 12 or 24 copies of PP7 stem loops and 24 copies of MS2 stem loops. This cassette was placed in the 3′ UTR of a *Renilla* luciferase transcript whose expression is driven by a doxycycline-inducible promoter. The TREAT reporter is composed of a doxycycline-inducible promoter – chimeric β-globin/IgG intron – *Renilla* luciferase coding sequence– stop codon –12x (24x) PP7 stem loops – 2x PKs – 24x MS2 stem loops – constitutive transport element – SV40 poly(A). In order to enable single genomic integration in HeLa cells, the TREAT construct was flanked by recognition sites for the FLP recombinase.

A control dual-color reporter was generated by removal of the PKs from the TREAT construct and was used to benchmark co-localization experiments in fixed and live cells and determine detection efficiencies. To generate a TREAT siRNA reporter that can be cleaved by Ago2, a 21nt long sequence from the firefly luciferase ORF was placed between the PP7 stem loops and the PKs of the TREAT construct. The firefly siRNA target sequence (CGCTGAGTACTTCGAA ATGTC) corresponds to the MISSION pLKO.1-puro firefly luciferase shRNA control (SHC007, Sigma Aldrich). Lentiviral transduction was used to stably integrate the cognate shRNA into HeLa cells. To enhance interaction of TREAT mRNAs with P-bodies, the AU-rich elements from TNF-α (Franks and Lykke-Andersen, 2007) were cloned in front of the PKs or the 5′-TOP sequence from RPL32 (Damgaard and Lykke-Andersen, 2011) was inserted into the 5′ UTR of the TREAT reporter.

HeLa stable cell line construction

A day before transfection, 3×10^5 HeLa cells were seeded into a 6-well plate. The targeting plasmid that contained a TREAT reporter (2 μg) and pCAGGS-FLPe-IRESpuro plasmid (2 μg) were transfected using Lipofectamine 2000 (Invitrogen) according to the manufacturer's protocol (Beard et al., 2006). Transfected cells were selected for two days with 5 μg mL^{-1} puromycin (Invivogen) followed by 10-14 days of negative selection with 50 μM ganciclovir (BioCat GmbH (TargetMol)) in order to obtain single resistant colonies that had undergone RCME. Individual colonies were then tested for expression of TREAT reporters using the *Renilla* Luciferase Assay System (Promega) according to the manufacturer's instructions. Total protein concentration in the lysates was measured using the Bradford Protein Assay (BioRad Laboratories) and used for normalization of luciferase activity.

Northern Blot

HeLa cells (1.5×10^6) with and without expression of the fluorescent coat proteins were seeded in a 10-cm plate. The following day, cells were transiently transfected with 20 μg of plasmid DNA that expressed either the TREAT reporter or a control reporter lacking the viral PKs by Lipofectamine 2000 (Invitrogen) according to the manufacturer's instructions. The next day, expression of the reporters was induced by addition of doxycycline (1 μg mL^{-1}) for 16 hr. Total RNA was extracted from these cells using TRIzol (Ambion). The

concentration of isolated RNAs was measured using a Nanodrop (Thermo Scientific) and 5 μg of total RNA for each condition was loaded on a 1.2% denaturing agarose gel containing 2% formaldehyde. The resolved RNA was transferred onto an Amersham Hybond-N+ membrane (GE Healthcare) by capillary transfer overnight in UltraPure 20 x SSC (Invitrogen) at room temperature. After the RNA was UV-cross-linked to the membrane, methylene blue staining (0.04% (w/v) Methylene Blue (Sigma) in 500 mM NaOAc pH 5.1) was used to assess loading and transfer of the RNA.

An anti-sense RNA probe was designed to detect the 3′ end of the transcript. The RNA probes were synthesized using the DIG-Starter Northern Blot Kit (Roche), and detection of transcripts was performed using the same kit according to the manufacturer's instructions. In brief, the concentration of *in vitro* transcribed DIG-labeled RNA probe was estimated based on an evaluation of labeling efficiency. The membrane was incubated with ~50 ng mL^{-1} RNA probes for 16 hr at 68°C. Upon detection with an anti-DIG antibody, the chemiluminiscent signal of the membrane was detected using an Azure c300 (Axonlab).

RT-qPCR

HeLa cells (6×10^5) stably expressing the TREAT reporter were seeded the day before in a 15-cm tissue culture plates. Induction of reporter transcription was done as described for the smFISH half-life experiment for time points 0, 2, 4 and 8 hr. Total RNA was isolated using TRIzol (Ambion). Total RNA (5 μg) was DNase-treated (TURBO DNA-free Kit, Ambion) and reverse transcribed (SuperScript Reverse Transcriptase III, Thermo Fisher Scientific) using oligo-dT primers to generate cDNA. The abundance of TREAT reporter transcripts was determined by real-time qPCR using FastStart Universal SYBR Green Master mix (Roche) and normalized to an endogenous reference gene GAPDH using the ΔΔCt method. The data were fit to one phase exponential decay using Prism 7.0a (https://www.graphpad.com) in order to calculate the half-life of the TREAT mRNA.

The same procedure was performed when actinomycin D (10 μg mL^{-1}) (Sigma) was added to inhibit transcription of endogenous mRNA. In this experiment, 1 μg of total RNA was used to measure the half-life of c-Myc mRNA.

Renilla luciferase assay

One day in advance, HeLa cells (2.5×10^4) stably expressing the TREAT reporters were seeded into a 24-well plate. Expression of the reporter was induced the next day for 2 hr by addition of doxycycline followed by lysis with 100 μL Passive Lysis Buffer from the *Renilla* Luciferase Assay System (Promega). The lysate (5 μL) was used to measure *Renilla* activity according to the manufacturer's protocol, and 30 μL of the lysate was used for total protein measurement using the Bio-Rad Protein Assay (Bio-Rad) to normalize the data.

siRNA transfection

HeLa cells (2×10^6) stably expressing the TREAT reporter were seeded onto 10-cm dish one day before siRNA transfection. Using Lipofectamine RNAiMAX (Invitrogen) either siXrn1 (ON-TARGETplus Human Xrn1 siRNA – SMARTpool, Dharmacon), siRrp40 (ON-TARGETplus Human Exosc3 siRNA – SMARTpool, Dharmacon), or siCtrl (ON-TARGETplus Non-targeting Pool, Dharmacon) were transfected at a final concentration of 50nM. The transfected cells were re-plated 8 hr later as follows: 0.5×10^6 cells onto a 6-cm dish for subsequent western blot quantification of the knock down efficiency; 2.5×10^4 cells onto a glass coverslip placed in a 12-well plate for smFISH analysis. Both western blot and FISH procedures were started 48 hr after siRNA transfection.

Western Blotting

Cells were washed with 1x PBS and lysed in 200 μL Passive Lysis Buffer (Promega). After a 15 min incubation on ice, cells were collected by scraping and centrifuged at 12,000 rpm for 20 min at 4°C. The supernatant was mixed with Laemmli buffer (Bio-Rad) and boiled for 5 min at 95°C. The protein samples were resolved by SDS-PAGE on a 4%–20% gel (Bio-Rad) followed by transfer to a PVDF membrane. The membrane was blocked with 5% BSA (Sigma) in PBST (1x PBS with 0.1% (v/v) Tween) for 1 hr at room temperature and subsequently probed with antibodies diluted in the same blocking buffer supplemented for 4 hr at room temperature: mouse derived anti-Rrp40 (Abcam, ab67661, 1:500) and rabbit derived anti-α-Tubulin (Abcam, ab18251, 1:1,000); rabbit derived anti-Xrn1 (Abcam, ab70259, 1:1,000) and mouse derived anti-Actin-pan (ThermoFisher Scientific, MA5-11869, 1:2,500). The membrane was washed four times in PBST for 5 min. Secondary antibodies were diluted in the blocking buffer supplemented with 0.01% (v/v) SDS and applied to the membrane for 1 hr at room temperature: anti-rabbit IRDye 800 CW (LI-COR, 1:15,000) and anti-mouse IRDye 680 RD (LI-COR, 1:15,000). After washing the membrane four times in PBST for 5 min, the membrane was imaged using an Odyssey infrared imaging system (LI-COR) and quantitative densitometry was performed using Fiji (Schindelin et al., 2012).

Single-molecule FISH

HeLa cells (2×10^4) were seeded on glass coverslips placed in a 12-well tissue culture plate two days before smFISH was performed. To induce transcription, the medium was replaced by complete DMEM containing doxycycline (1 μg mL^{-1}) for 1.5 hr. Cells were washed extensively with 1x PBS to remove doxycycline in order to stop transcription of TREAT reporter mRNAs. Fresh DMEM was then added to the cells and they were returned to the incubator for an additional 30 min to enable nascent transcription of TREAT reporters to finish. Afterward, cells were fixed at successive time points using 4% paraformaldehyde (Electron Microscopy Sciences) in 1x PBS for 10 min. Following fixation cells were washed twice with 1x PBS before storage in 70% ethanol at 4°C.

Single-molecule RNA detection was performed using Stellaris FISH probes (Biosearch Technologies). Briefly, cells on coverslips were prehybridized in wash buffer (2x SSC (Invitrogen), 10% (v/v) formamide (Ambion)) twice for 5 min. Two sets of FISH probes were designed to detect the *Renilla* ORF (Quasar670) or MS2 stem loops in the 3′ UTR (Quasar570). Cells were then hybridized with a solution that contained 150nM of each FISH probes, 2x SSC, 10% (v/v) formamide, 10% (w/v) dextran sulfate (Sigma) for 4 hr at 37°C. Cells were washed twice with wash buffer for 30 min before counterstaining DNA with DAPI solution (500 μg L^{-1} in 1 x PBS) and mounted on slides using ProLong Gold Antifade Mountant (Molecular Probes).

In order to investigate the effect of oxidative stress and of translational inhibitors on mRNA stability, prior to smFISH, cells were induced for 2 hr by doxycycline followed by either a 2 or 4 hr incubation with: 500 μM arsenite (Sigma), 5 μM harringtonine (LKT Laboratories), 100 μg mL^{-1} cycloheximide (Sigma), 100 μg mL^{-1} puromycin (Invivogen).

Images were acquired using a wide-field microscope (Zeiss) with a Plan-APOCHROMAT 100x 1.4 NA oil objective equipped with an AxioCam 506 mono camera and an X-Cite 120 EXFO metal halide light source. Cells were optically sectioned using a 240 nm z-step, spanning a 5 μm z-depth. Exposure times of 1600 ms were used to acquire images of each plane in the channel for Quasar670, 800 ms in the channel for Quasar570, and 10 ms in the DAPI channel.

Detection of mRNA spots from smFISH and co-localization analysis

Single mRNAs were detected in maximum projections of images using the spot detection algorithm AIRLOCALIZE (Lionnet et al., 2011) written in MATLAB (MathWorks) providing sub-pixel positions of the spots as described previously (Halstead et al., 2015). To detect the diffraction-limited fluorescent spots, thresholding was adjusted for each set of images depending on the signal-to-noise ratio. Either a custom MATLAB script or a KNIME Analytics Platform (Berthold et al., 2009) workflow (allowing segmentation for nuclear and cytoplasmic fraction based on DAPI staining using the Otsu thresholding method [Otsu, 1979]) were used to evaluate pairwise spot co-localization from both FISH channels. *Renilla* and MS2 spots that were within a maximum distance of 5 pixels (225 nm) were considered to be co-localized and were classified as intact mRNAs. Orphan MS2 spots were defined as stabilized 3′ ends.

Correction of co-localization data for detection efficiency

As a result of imperfect detection of single particle fluorescent labels, the observed fraction of co-localized particles underestimates the true fraction. For example, a missed magenta label from a double-labeled particle causes it to be wrongly classified as a single-labeled green particle. In order to correct for this type of error, we assumed that particles and color channels are independent and that there is a fixed rate of detection for each color label (detection efficiency, $e_{magenta}$ and e_{green}).

The detection efficiencies are estimated from a control experiment in which all particles are known to be double-labeled, using the following equations: $e_{magenta} = (n_{magenta}+n_{white})/N$ and $e_{green} = (n_{green}+n_{white})/N$, where $n_{magenta}$, n_{green}, and n_{white} are the normalized numbers of magenta, green, and double-labeled particles, and N is the total number of particles. In practice, N is estimated from $N = n_{magenta}+n_{green}+n_{white}$, which underestimates its true value by the number of particles for which both labels have been missed (n_{black}). For relatively large detection efficiencies as the ones obtained here ($e > 0.85$), $n_{black} > 0.0225$ and using $n_{black} = 0$ is an acceptable approximation.

In an experiment where we do not know the number of double-labeled particles, we can now express the observed numbers of particles (n_x, where x is $_{magenta,\ green}$ or $_{white}$) in terms of the true underlying number of particles (m_x) and the above detection efficiencies. For example, assuming that labels are never detected if they are truly absent, magenta particles can be observed from truly magenta particles (if the magenta label was detected) and from truly white particles (if the magenta label was detected and the green label was not detected): $n_{magenta} = m_{magenta}\cdot e_{magenta}+m_{white}\cdot e_{magenta}\cdot(1-e_{green})$. Double labeled particles can only be detected from truly double labeled ones if both labels were detected: $n_{white} = m_{white}\cdot e_{magenta}\cdot e_{green}$. Solving these equations for the true particle numbers yields:

$$m_{white} = n_{white} / \left(e_{magenta}\cdot e_{green}\right),$$

$$m_{magenta} = n_{magenta} / e_{magenta} - m_{white}\cdot\left(1 - e_{green}\right),$$

$$m_{green} = n_{green} / e_{green} - m_{white}\cdot\left(1 - e_{magenta}\right).$$

Finally, the fraction of co-localized particles is obtained from the estimated true numbers using $f_{white} = m_{white}/(m_{magenta}+m_{green}+m_{white})$.

Means and 95%-confidence intervals (CI) of means for detection efficiencies ($e_{magenta}$ and e_{green}) and normalized counts (n_x) were estimated using data from multiple experiments (cells) by $\bar{x} \mp t* \cdot s/\sqrt{n}$, where $\bar{x}$ is the arithmetic mean over the measurements x_i from individual cells, t^* is the critical value corresponding to the 97.5% quantile for a t distribution with n-1 degrees of freedom, s is the standard deviation estimated from the x_i, and n is the number of cells. These confidence intervals were then propagated to the derived entities calculated using the formulas described above using the R package *propagate* (version 1.0-4) calculated based on first-order Taylor expansion.

Modeling of mRNA half-lives from smFISH measurements

In the absence of transcription, we assumed that the turnover of intact mRNAs and stabilized 3′ ends is described by the following three rate equations, which account for the degradation of these RNA species in terms of three single-step Poisson processes:

$$\frac{d[\mathrm{Nuc}]}{dt} = -\alpha[\mathrm{Nuc}]$$

$$\frac{d[\mathrm{Cyt}]}{dt} = \alpha[\mathrm{Nuc}] - \beta[\mathrm{Cyt}]$$

$$\frac{d[\mathrm{Deg}]}{dt} = \beta[\mathrm{Cyt}] - \gamma[\mathrm{Deg}]$$

where *Nuc* is the number of nuclear mRNAs, *Cyt* is the number of cytoplasmic mRNAs, and *Deg* is the number of stabilized 3′ ends, respectively, and α, β and γ are their decay rates.

We fitted the solutions of this model to the population-averaged intact mRNA and stabilized 3′ end numbers, and obtained $\alpha = 0.94 \pm 0.07\ \mathrm{hr}^{-1}$, and $\beta = 0.43 \pm 0.06\ \mathrm{hr}^{-1}$. $\gamma = 0.16 \pm 0.02\ \mathrm{hr}^{-1}$. The goodness of fit with adjusted R^2 for the rates was $\alpha = 0.99$, $\beta = 0.97$, and $\gamma = 0.98$.

For the TREAT siRNA reporter, we added an additional rate to model the cytoplasmic degradation of the 5′ end generated by slicing:

$$\frac{d[5'\mathrm{Deg}]}{dt} = \beta[\mathrm{Cyt}] - \delta[5'\mathrm{Deg}]$$

We obtained rates of $\alpha = 0.99 \pm 0.25\ \mathrm{hr}^{-1}$, $\beta = 5.45 \pm 0.52\ \mathrm{hr}^{-1}$, $\gamma = 0.17 \pm 0.04\ \mathrm{hr}^{-1}$, and $\delta = 4.27 \pm 0.70\ \mathrm{hr}^{-1}$. The goodness of fit with adjusted R^2 for the rates were $\alpha = 0.94$, $\beta = 0.97$, $\gamma = 0.96$, and $\delta = 0.89$.

Stochastic simulation of mRNA decay

To evaluate to what extent the experimental cell-to-cell variability in mRNA numbers can be predicted by a simple model, we assumed that degradation of intact mRNA and stabilized 3′ end are single-step Poisson processes. To this end, we performed kinetic Monte Carlo simulations using the Gillespie algorithm to solve the master equation associated to the refined model described above, using the same export and decay rates (Gillespie, 1977). To simulate the time evolution of the probability distributions of intact mRNA and stabilized 3′ end after induction was stopped, we took the experimental distributions of all mRNA species after removal of doxycycline as the initial condition (t = 0).

We performed the simulations using the calculated rate constants α, β, γ, and δ that were extracted from fitting the rate equations (thick red lines in Figure S5, 6). We generated confidence intervals by running the simulation with $\alpha \pm \varepsilon_\alpha,\ \beta \pm \varepsilon_\beta,\ \gamma \pm \varepsilon_\gamma\ ,\ \delta \pm \varepsilon_\delta$ where ε are the fitting errors on each parameter returned by the NonLinearModelFit function in Mathematica (red shaded areas in Figure S5, 6).

Immunofluorescence

The HeLa cells (2×10^5) expressing SNAP-Dcp1a fusion were seeded onto glass coverslips placed in 12-well plate 2 days prior the immunostaining. After pre-staining the cells with SNAP dye Janelia Fluor 549 (JF549) (Grimm et al., 2015), the cells were treated with arsenite (500 μM) for 1.5 hr to stress cells and increase P-body levels. All the downstream steps were carried out at room temperature while coverslips were protected from light. Cells were washed with 1x PBS and fixed with 4% paraformaldehyde (Electron Microscopy Sciences) in 1x PBS for 10 min, washed once in 100mM glycine in 1x PBS and twice in 1x PBS, and subsequently permeabilized by methanol for 5 min. Following permeabilization, cells were washed twice with 1x PBS and then blocked for 1 hr in 0.5% BSA in 1x PBS. Cells were then incubated with Xrn1 antibody (Abcam, ab70259; 1:500) diluted in 0.5% BSA in 1x PBS for 1 hr. Cells were washed three times in 0.5% BSA in 1x PBS for 5 min. Cells were then incubated with goat anti-rabbit secondary antibody coupled to Alexa Fluor 647 (Molecular Probes; 1:5,000) diluted in 0.5% BSA in 1x PBS for 30 min. Cells were washed twice with 0.5% BSA in 1x PBS and once only with 1x PBS for 5 min each time. Nucleus was quickly counterstained by DAPI (500 ng mL^{-1} in 1x PBS), washed twice with 1 x PBS and coverslips were mounted onto glass slides with ProLong Gold Antifade Mountant (Molecular Probes).

Image acquisition was performed using a wide-field microscope (Zeiss) with a Plan-APOCHROMAT 63x 1.4 NA oil objective equipped with an AxioCam 506 mono camera and an X-Cite 120 EXFO metal halide light source. Cells were optically sectioned using a 240 nm z-step, spanning a 5 μm z-depth. Exposure times of 800 ms were used to acquire images of each plane in the channel for SNAP(JF549)-Dcp1a, 800 ms in the channel for Xrn1-Alexa647 and 10 ms in the DAPI channel. The co-localization analysis between P-body markers, SNAP-Dcp1a fusion and Xrn1, was done using the Fiji (Schindelin et al., 2012) plugin Coloc2 to calculate the Pearson's correlation coefficient.

Live-cell imaging of TREAT mRNAs

In order to label TREAT reporter mRNAs for live-cell imaging, chimeric fusions of the bacteriophage coat proteins (PCP and MCP) with spectrally distinct fluorescent proteins were used. Synonymous tandem PP7 coat protein (stdPCP) was fused to synonymous tandem green fluorescent protein (stdGFP) and synonymous tandem MS2 coat protein (stdMCP) was fused to Halo protein (Wu et al., 2015). Both fluorescent proteins contain N-terminal nuclear localization signals (NLS) to concentrate the unbound proteins in the nucleus. NLS-stdMCP-Halo was labeled with an organic Halo dye (JF549) (Grimm et al., 2015). Fusion proteins were expressed from a constitutive ubiquitin C promoter and stably integrated into the HeLa cell line by lentiviral transduction using standard protocols. Several rounds of fluorescence activated cell sorting (FACS) were used to derive a cell population expressing the fluorescent fusion proteins at levels appropriate for single-molecule RNA imaging.

In order to visualize P-bodies in live cells, a SNAP-Dcp1a fusion protein was introduced by lentiviruses for constitutive expression. SNAP dye (JF646) (Grimm et al., 2015) was used to label the SNAP-Dcp1a fusion protein. Triple positive cells, expressing NLS-stdPCP-stdGFP, NLS-stdMCP-Halo and SNAP-Dcp1a were isolated by FACS.

Cells were imaged on a spinning-disk confocal microscope based on an Olympus IX81 inverted microscope equipped with a Yokogawa CSU-X1 scanhead with Borealis modification (Andor) using a 100x 1.45 NA PlanApo TIRFM oil immersion objective (Olympus). Images were collected on two precisely aligned back-illuminated EMCCD cameras (EvolveDelta, Photometrics). Solid-state lasers (491 nm, 561 nm, 633 nm; Cobolt) were used as excitation sources. Cells were maintained at a constant temperature of 37°C and 5% CO_2 within an incubation box. Images were acquired using Visiview (Visitron) as single planes at frame rates of 20 Hz (50 ms exposure).

QUANTIFICATION AND STATISTICAL ANALYSIS

Single particle tracking of mRNAs in live cells and track co-localization

Single particle tracking (SPT) and analysis of mRNA molecules was performed on 5 frames of 50 ms exposure time for each of the two registered channels individually. SPT was performed using the Fiji plugin TrackMate (Tinevez et al., 2017) for the nucleus and cytoplasm separately as described before (Voigt et al., in press). For spot detection, we used "LoG detector" with an "Estimated blob diameter" of 0.38-40 μm and defined the "Threshold" based on individual images. We used the "Simple LAP tracker" particle-linking algorithm and applied linking distances that were optimized for particle density. The resulting list of coordinates served as input for a custom-made track co-localization pipeline running in KNIME (Berthold et al., 2009).

Here, we performed a nearest neighbor spot analysis that classifies two spots as co-localizing if their distance is below the user defined threshold of 0.3μm. Tracks co-localized if they contained at least 2 co-localizing spot pairs. Tracks shorter than 3 frames were excluded from the analysis. All other unpaired tracks containing only the MS2 signal were classified as stabilized 3′ ends.

Live-cell slicing analysis

TREAT siRNA and control data were collected as described above and including at least 100 frames of 50 ms exposure time per acquisition. SPT and co-localization analysis of the TREAT siRNA and control live-cell data was performed via automated tracking and track pairing analysis in KNIME.

Automated Tracking and Track Pairing

To this aim, we generated a workflow that enables KNIME to run the Fiji plugin TrackMate (Tinevez et al., 2017) in batch mode and via a custom-made ImageJ2 plugin (KNIME Image Processing → ImageJ2 → FMI → Track Spots). All tracking parameters are chosen as described above. The ROI is generated from an inverted segmentation of the nucleus that results after blurring of the raw image (Gaussian Blur, $\sigma = 5.5$) and global thresholding. Spot co-localization and classification is performed as described above. However, to improve track statistics over long time course experiments (> 100 frames) and avoid redundant counting of co-localizing tracks that cannot always be tracked without violation of gap criteria, we implemented a track pairing algorithm that pairs all tracks into the same pair ID if they spatially co-localize ($\geq$2 spot co-localizations) at some point throughout the experiment. This method stitches co-localizing tracks together that have been interrupted at different time points due to detection errors.

Identification of Slicing Events

For identification of slicing events, we selected for intact tracks that cease to co-localize without one of their labels vanishing. To this aim, we determined the length of both tracks after the last co-localization frame and selected candidate tracks that are detectable for at least three frames after their last co-localization. To more easily identify false-positive track co-localizations, we generated a measure for track inter-label mobility. Specifically, we quantified relative spot movement by assessing the distances between co-localizing spots of both channels (GFP and Halo+JF_{549}). We then calculated squared displacements and instantaneous diffusion coefficients (Berg, 1993) that measure the relative mobility of spots belonging to both labels for each co-localizing track. We applied the empirically determined threshold of 0.1 $\mu m^2\ s^{-1}$ to filter out high inter-label mobility tracks and then manually inspected and verified the candidate slicing events.

Nuclear Segmentation and Distance Analysis

In order to assess the subcellular localization of the slicing events, we determined their distance from the nucleus. To this aim, we segmented the nucleus via Gaussian Blur ($\sigma = 5.5$) and global thresholding (Huang method) and determined the average distance

(of all co-localizing frames per track) from the closest nuclear boundary via a distance map. As control, we used all co-localizing tracks (6,244 particles, 125 cells) of the non-sliced control population reporters.

Bleach Correction and 5′ end Decay Analysis

To generate a bleach curve and determine fluorophore decay rates, we acquired a test dataset under identical experimental conditions using the non-sliced control cell line. We manually tracked and co-localized particles as described above but only included tracks longer than 50 frames in the analysis. To determine the bleach rate of each fluorophore, we described bleaching as exponential decay according to

$$I_0 = \frac{I}{e^{-\lambda t}}$$

where I_0 is the intensity at the beginning of the experiment and λ is the fluorophore decay rate.

In order to experimentally determine λ, we took the natural logarithm of the intensities ($\ln(e^{-\lambda t}) = -\lambda t$), fit linear regressions and extracted λ as the slope of the linear fit:

$$I = \lambda t + I_0$$

To look for evidence of rapid loss of the 5′ end signal from a dual-labeled transcript, we only looked at tracks with more than five co-localizations. We normalized their bleach-corrected NLS-PCP-GFP intensity in each frame against the averaged intensity of the first five frames of each track. To search for putative 5′ end decay candidates, we identified tracks where the NLS-PCP-GFP signal was lost at least two frames before the NLS-MCP-Halo signal due to either differences in the bleach rate of GFP compared to Halo or degradation of the 5′ end after slicing but before the 5′ and 3′ ends separated. We then fit a linear regression to the last five frames of the NLS-PCP-GFP track and determined its slope (*m*). Slopes were determined for both non-sliced control and the TREAT siRNA transcripts to identify possible 5′ end decay events that would have large negative values.

Quantification and co-localization of mRNAs in P-bodies in living cells

Intact and degraded mRNAs were identified by measuring the co-localization of NLS-PCP-GFP and NLS-MCP-Halo tracks as described previously. P-bodies were identified based upon segmentation of the SNAP-Dcp1a fluorescent signal (using the Yen thresholding method (Yen et al., 1995) in KNIME (Berthold et al., 2009) workflow) and used to generate distance maps that measured the number of pixels inside and outside of P-bodies. By overlaying the mRNA tracks with the distance map, we defined pixel positions within P-bodies as positive and positions outside of P-bodies as negative. The position of intact and stabilized 3′ ends with respect to P-bodies was then measured at each frame and the cumulative P-body localization index was then calculated for RNA particles in three consecutive frames.

The RNA content per P-body was determined by quantification of the NLS-PCP-GFP and NLS-MCP-Halo fluorescence intensities per frame of all dual labeled particles using TrackMate (Tinevez et al., 2017) + KNIME (Berthold et al., 2009). The ratio of the two channels was then calculated for all co-localizing spots and compared with the intensity ratio determined for intact mRNAs in the cytosol.

Statistical Analysis

Statistical parameters are shown in the figures and listed in the figure legends. Statistical significance is claimed when $p < 0.05$ in a Student's t test. In figures, asterisks mark statistical significance as following *, $p < 0.05$; **, $p < 0.01$; ***, $p < 0.001$; ****, $p < 0.0001$.

DATA AND SOFTWARE AVAILABILITY

All KNIME workflows are available from the Chao lab upon request. The ImageJ2 plugin that enables TrackMate to run in KNIME has been uploaded into the KNIME Image Processing library. The track-based co-localization workflow Data S1 ("Track-basedColocalizationAnalysis.knwf") used to identify intact and stabilized 3′ end TREAT reporter mRNAs is available as a supplemental item to this manuscript.

The unprocessed image files used to prepare the figures in this manuscript have been deposited at Mendeley Data (https://doi.org/10.17632/52wjrtnz2r.1)

Molecular Cell, Volume *68*

Supplemental Information

The Dynamics of mRNA Turnover Revealed by Single-Molecule Imaging in Single Cells

Ivana Horvathova, Franka Voigt, Anna V. Kotrys, Yinxiu Zhan, Caroline G. Artus-Revel, Jan Eglinger, Michael B. Stadler, Luca Giorgetti, and Jeffrey A. Chao

Figure S1

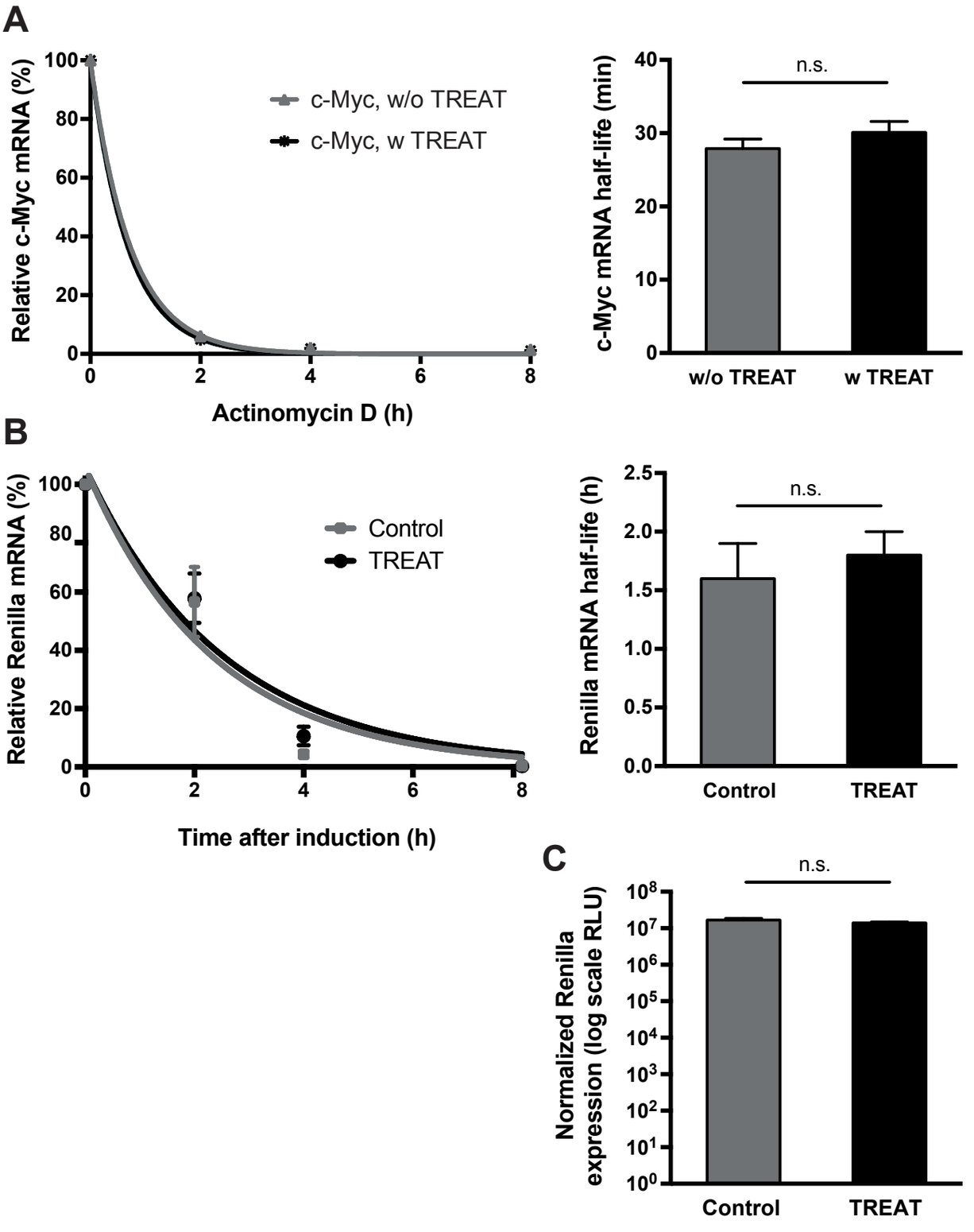

Figure S1. Viral pseudo-knots in TREAT reporter do not alter mRNA degradation or translation. Related to Figure 1. A, Quantitative RT-PCR analysis of endogenous c-Myc mRNA half-life in HeLa cells in the presence or absence of the TREAT reporter. HeLa cells were induced for 2 hours with doxycycline (1 µg ml^{-1}) to express the TREAT reporter followed by addition of actinomycin D (10 µg ml^{-1}) to stop transcription. RNA was isolated at the indicated time points. **B**, Quantitative RT-PCR analysis of control and TREAT reporter half-lives in HeLa cells, which were induced for 2 hours with doxycycline. Samples were collected at the indicated time points. The average of three independent experiments ± SEM is shown. **C**, Measurement of Renilla luciferase activity in HeLa cells induced for 4 hours to express control or TREAT transcripts. Graphs show mean ± SEM (n.s. = not significant; unpaired t-test).

Figure S2

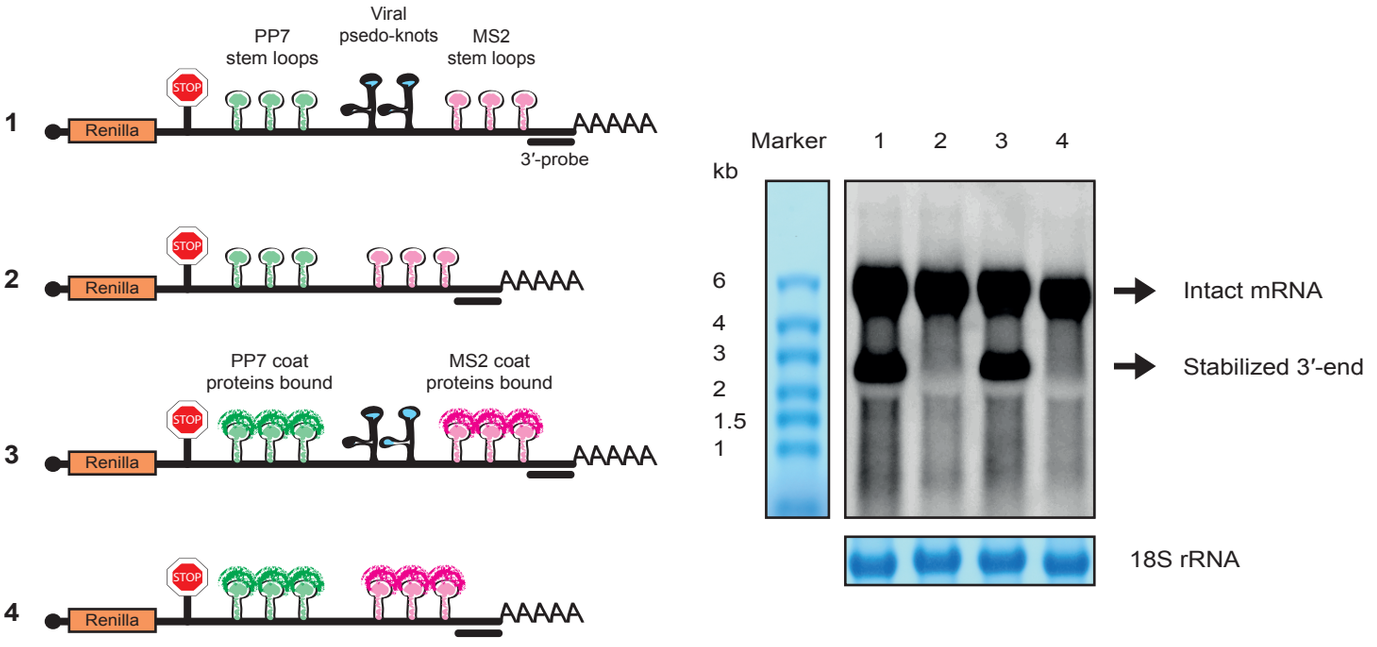

Figure S2. Viral pseudo-knots are required to stabilize the 3′-end of TREAT reporter. Related to Figure 1. Northern blot analysis of total RNA from HeLa cells transiently expressing the TREAT reporter (lane 1) and a control lacking the tandem PKs in-between PP7 and MS2 stem-loops (lane 2). The same constructs were also expressed in Hela cells expressing NLS-PCP-GFP and NLS-MCP-Halo (lane 3 and 4). Expression was induced by addition of doxycycline (1 µg ml^{-1}) for 16 hours and the isolated RNA was resolved on a denaturing agarose gel and probed with an oligo that recognizes both intact mRNA (4,604bp including PKs, 4,368bp without PKs) and stabilized 3′-end (1,873bp). Before hybridization, the membrane was stained with methylene blue to visualize the RNA size ladder and ribosomal RNAs that serve as a loading control.

Figure S3

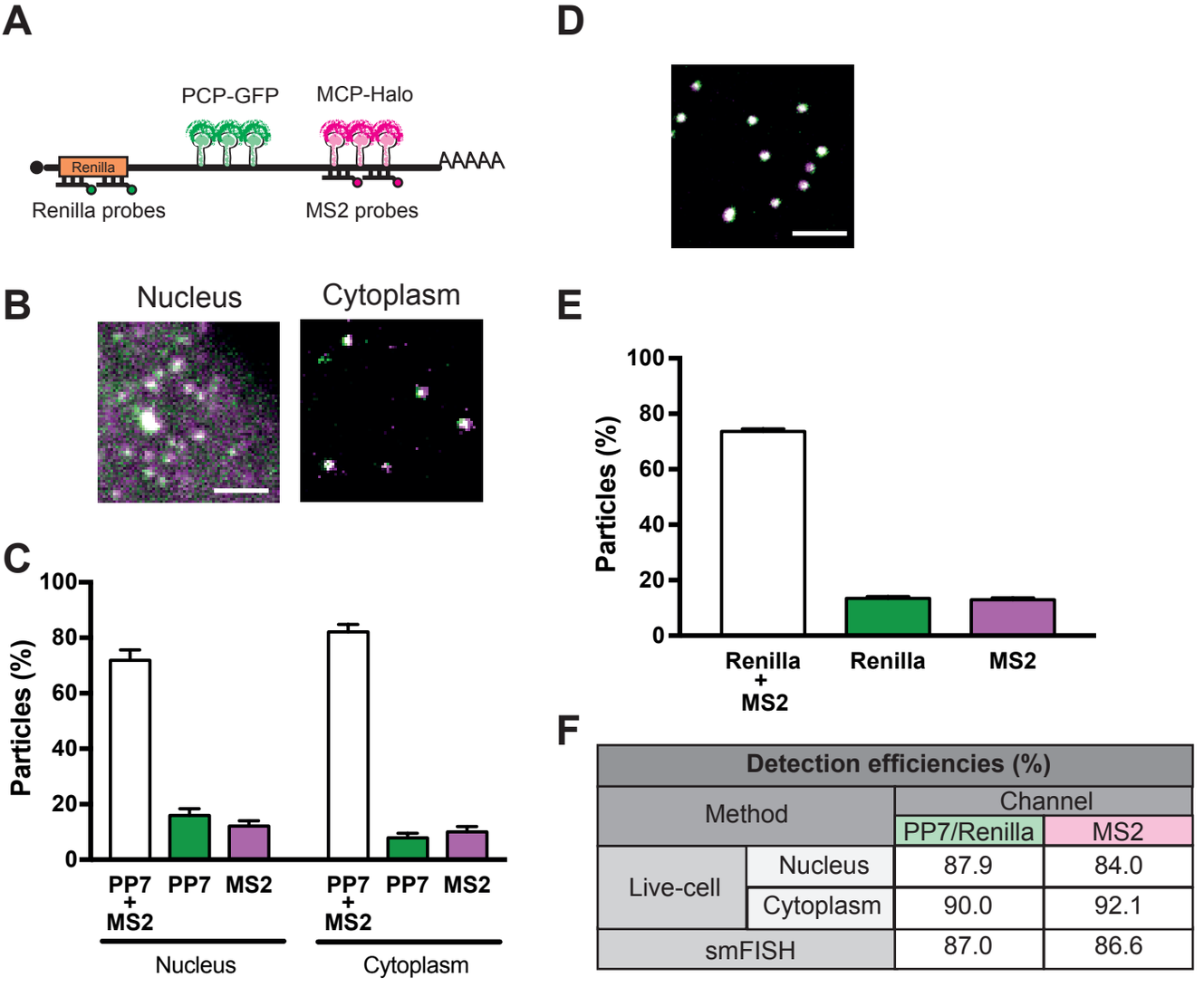

Detection efficiencies (%)			
Method		Channel	
		PP7/Renilla	MS2
Live-cell	Nucleus	87.9	84.0
	Cytoplasm	90.0	92.1
smFISH		87.0	86.6

Figure S3. Determination of detection efficiencies based on imaging of control transcripts without pseudo-knots. Related to Figure 1. A, Schematic of control reporters lacking PKs. **B**, Representative live-cell images of nucleus and cytoplasm of a HeLa cell expressing control transcripts labeled with NLS-PCP-GFP and NLS-MCP-Halo. Intact mRNAs are dual labeled with NLS-MCP-Halo (magenta) and NLS-PCP-GFP (green) and appear as white spots. **C**, Quantification of co-localization of SPT of NLS-PCP-GFP and NLS-MCP-Halo in the nucleus (443 particles, 10 cells) and cytoplasm (531 particles, 10 cells). **D**, Representative smFISH images of a HeLa cell expressing control reporter hybridized with Renilla (green) and MS2 (magenta) probes. **E**, Quantification of co-localization of Renilla and MS2 probes in smFISH images (particles = 17,186, cells = 139). **F**, Table showing calculated detection efficiencies. Graphs show mean ± SEM. Scale bar = 2 μm.

Figure S4

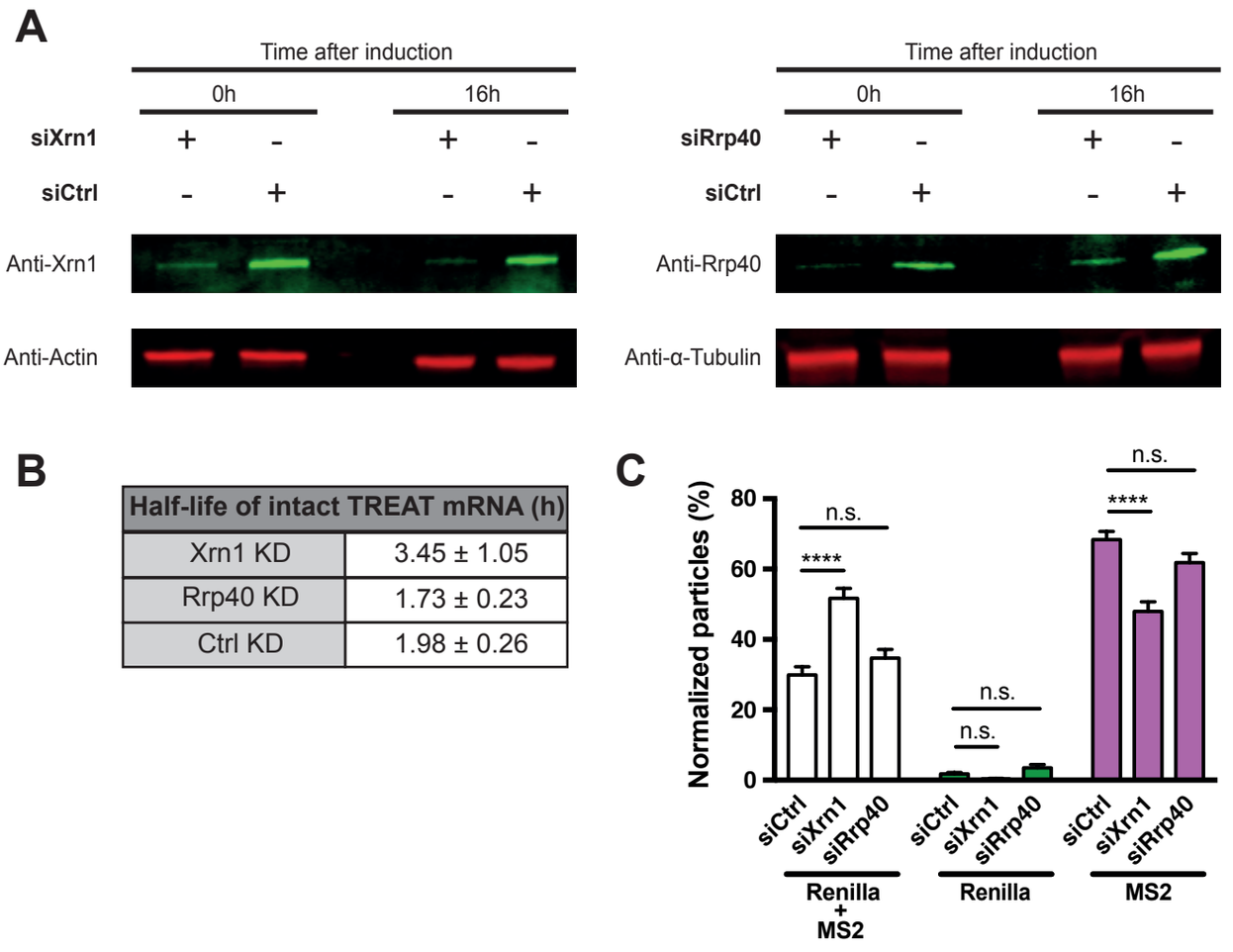

Figure S4. Xrn1 knock-down affects TREAT mRNA stability. Related to Figure 2. A, Western blot analysis of Xrn1 and Rrp40 knock-down. Protein lysates from HeLa cells transfected with siXrn1, siRrp40 or siCtrl for 48 hours. Transcription of TREAT reporter was induced with doxycycline for 2 hours. Lysates were collected after induction and 16 hours later. Xrn1 and Rrp40 were efficiently knocked-down at both time points (0h: Xrn1 84%, Rrp40 86%; 16h: Xrn1 81%, Rrp40 84%). Actin and α-tubulin serve as loading controls. **B**, Calculation of half-lives of intact mRNAs based on smFISH time course. The half-life of intact TREAT mRNA upon Xrn1 knock-down significantly increased whereas half-life upon Rrp40 knock-down was similar when compared to control siRNA (> 65 cells per time point). **C,** Quantification of co-localization analysis of smFISH data. Xrn1 knockdown alters the stability of the TREAT reporter while Rrp40 knockdown does not. Neither Xrn1 nor Rrp40 knock-down alters the number of Renilla particles detected. (n.s. = not significant; ANOVA). Graph shows mean ± SEM.

Figure S5

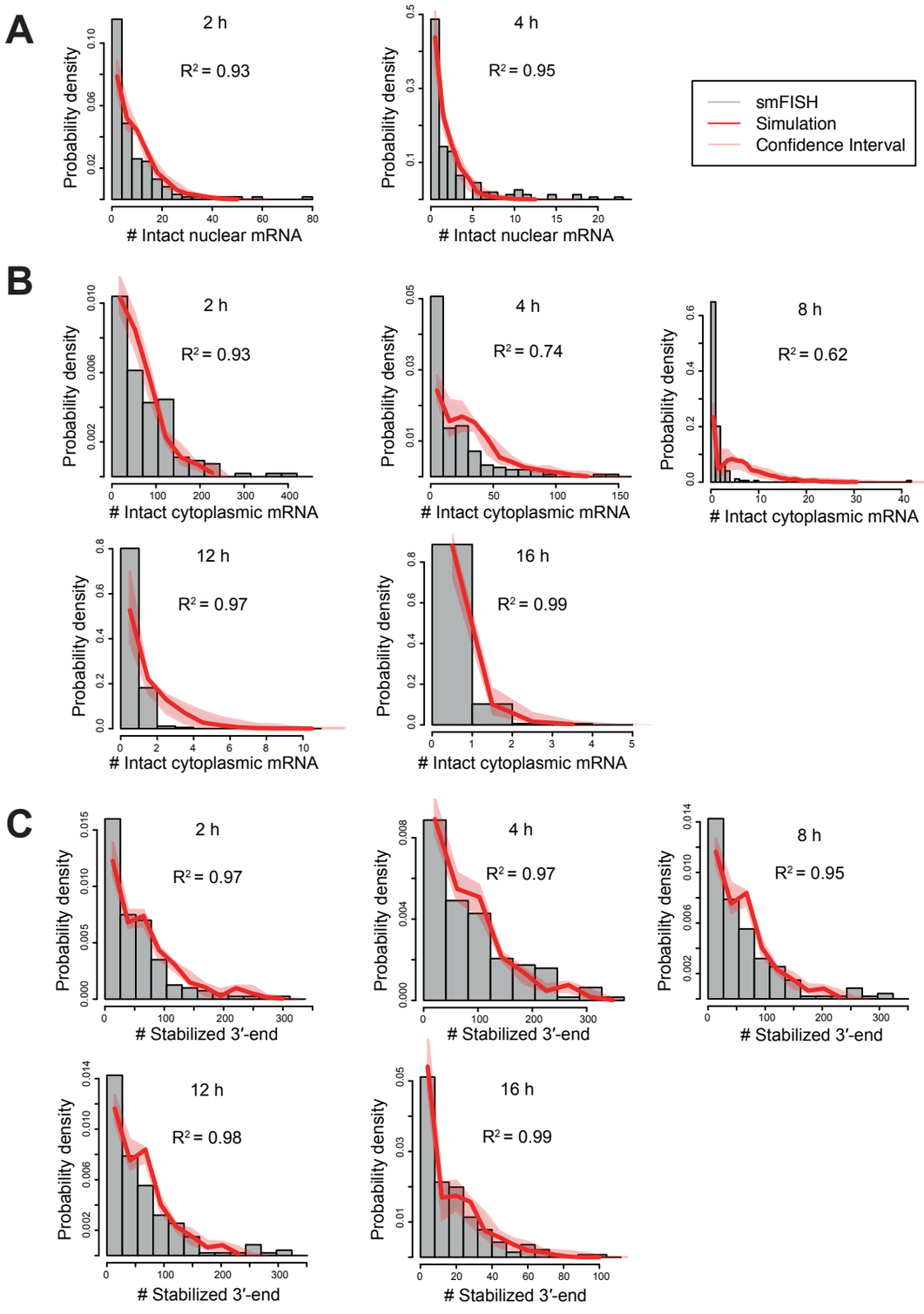

Figure S5. Degradation of TREAT mRNA is a Poisson process. Related to Figure 2. Probability density function (shown as histogram with grey bars) of the number of intact nuclear mRNA (**A**), cytoplasmic mRNA (**B**) and stabilized 3′-end (**C**) at different time points measured with smFISH. The area of every bar corresponds to the fraction of cells where the number of mRNAs lies in the corresponding interval (bin) on the horizontal axis. The bin size of the histograms is determined by the Freedman-Diaconis rule. Predictions of stochastic RNA decay simulations (shown as red lines) assuming that mRNA degradation occurs as a simple Poisson process. The probability density function of the number of mRNAs at the initial time point, representing the cell-to-cell variability in mRNA species after induction was used as an input for the simulation. Decay rates used in the simulation are those calculated in Figure 2C. Shaded red areas correspond to confidence intervals.

Figure S6

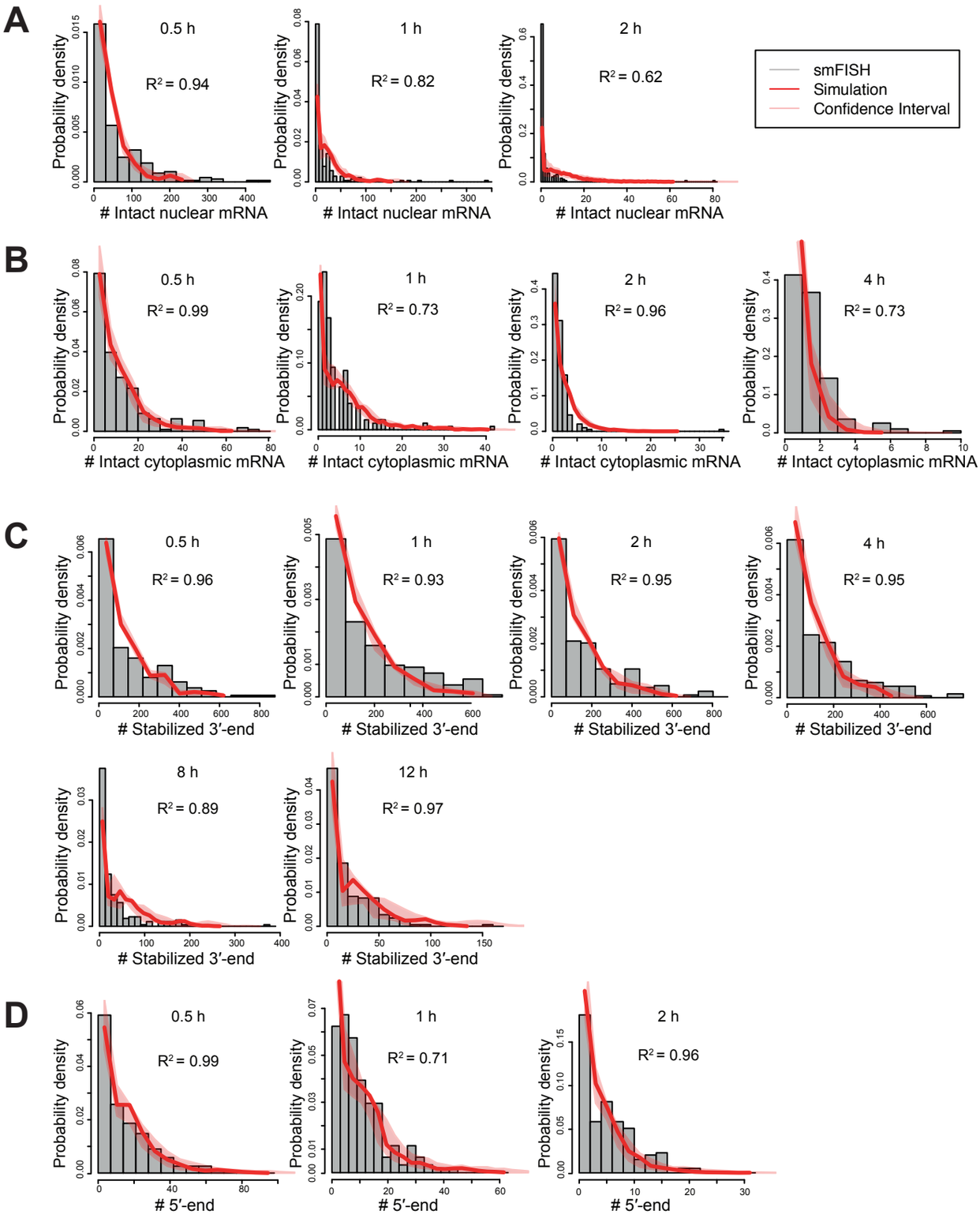

Figure S6. Degradation of TREAT siRNA mRNA is a Poisson process. Related to Figure 3. Probability density function (shown as histogram with grey bars) of the number of intact nuclear mRNA (**A**), cytoplasmic mRNA (**B**), stabilized 3′-end (**C**) and 5′-end (**D**) at different time points measured with smFISH. The area of every bar corresponds to the fraction of cells where the number of mRNAs lies in the corresponding interval (bin) on the horizontal axis. The bin size of the histograms is determined by the Freedman-Diaconis rule. Predictions of stochastic RNA decay simulations (shown as red lines) assuming that mRNA degradation occurs as a simple Poisson process. The probability density function of the number of mRNAs at the initial time point, representing the cell-to-cell variability in mRNA species after induction was used as an input for the simulation. Decay rates used in the simulation are those calculated in Figure 3B with addition of 5′-end decay. Shaded red areas correspond to confidence intervals.

Figure S7

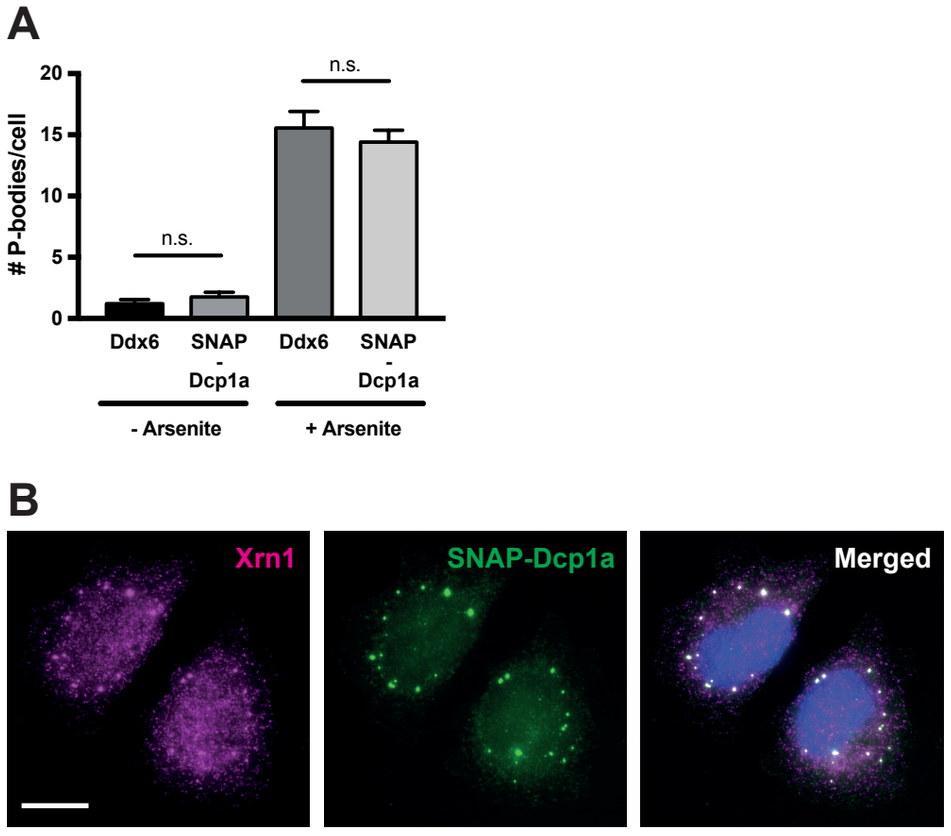

Figure S7. SNAP-Dcp1a labeled P-Bodies co-localize with Xrn1. Related to Figure 5. A, SNAP-Dcp1a labels P-bodies in HeLa cells. The number of endogenous P-bodies in unstressed and arsenite (500μM) stressed cells (25 cells, immunofluorescence with Ddx6 antibody) are similar to the numbers of P-bodies identified in living cells by SNAP-Dcp1a (20 cells). Graph shows the mean ± SEM. (n.s. = not significant; unpaired t-test). **B**, Representative immunofluorescence images of HeLa cells stably expressing SNAP-Dcp1a and co-stained with Xrn1 antibody to visualize their subcellular localization. Co-localization was measured by Pearson's correlation coefficient in Fiji (Schindelin et al., 2012) resulting in 0.79 ± 0.01 (mean ± SEM, 19 cells).

Figure S8

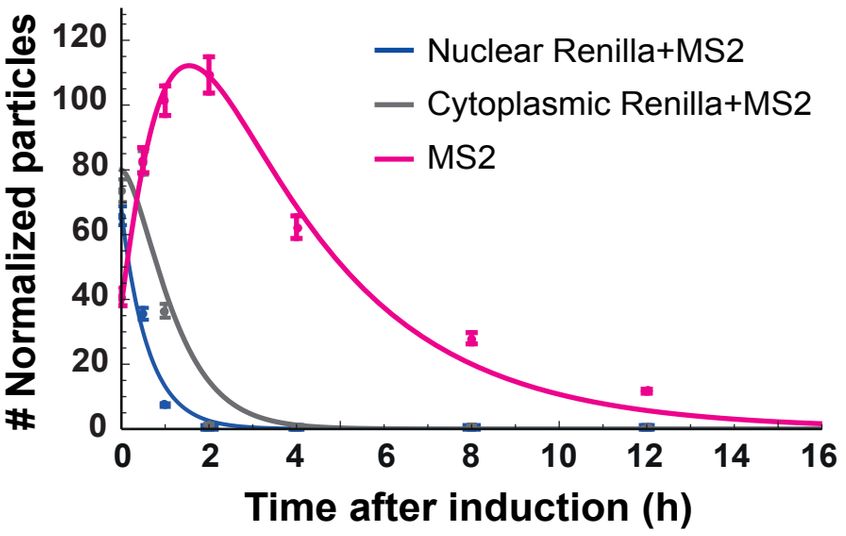

Figure S8. smFISH measurement of TREAT TNF-α ARE half-life. Related to Figure 5. Counts of intact mRNAs (nuclear or cytoplasmic) and stabilized 3′-ends were obtained from the quantitative analysis of smFISH data at fixation time points (> 130 cells per time point in two biological replicates). Data were fit to the model to calculate the experimental rate constants ($\alpha = 1.63 \pm 0.21\ h^{-1}$, $\beta = 1.44 \pm 0.26\ h^{-1}$, $\gamma = 0.31 \pm 0.02\ h^{-1}$). All error bars indicate SEM.

5. MY CONTRIBUTION

The attached publication presented in my thesis is a result of a highly collaborative work of all indicated authors. I significantly contributed to the enclosed publication under the supervision of J.A.C. by designing and cloning of all the TREAT reporters and the derived control reporter lacking PKs. Furthermore, I established the HeLa stable cell lines bearing one of the reporters in a single genomic locus. Additionally, I transduced cell lines intended for live-cell imaging by lentiviruses bearing the tagged MS2 and PP7 coat proteins and the PB marker. Likewise, for the TREAT slicing reporter, I introduced a specific siRNA coding sequence into the HeLa genome by lentiviruses. To validate the imaging system in fixed and living cells, I detected, tracked and quantified the fraction of dual- and single-labeled RNA particles in single cells (Figure 1). Furthermore, I carried out qPCR and luciferase assay experiments from cell populations (Figure S1). Together with C.G.A.-R., we transiently transfected HeLa cells to overexpress the reporters and we subjected the extracted RNA samples to a northern blotting (Figure S2). To obtain the detection efficiencies in the used imaging experimental set-ups, I imaged and analyzed fixed cells bearing the control reporter and F.V. imaged and analyzed living cells bearing the control reporter. Subsequently, the detection efficiencies were calculated using a tool developed by M.B.S. (Figure S3). The rest of the imaging data were normalized to the calculated detection efficiencies throughout the publication. In order to obtain the half-life measurements, I personally performed smFISH time-course experiments where RNA particles were detected and quantified with the help of A.V.K., and the degradation rate constants were calculated by Y.Z. under supervision of L.G. (Figure 2, 3B, S4B, S8). The data obtained from these time-course experiments were also used by Y.Z. and L.G. to computationally simulate the stochastic RNA degradation (Figure S5 and S6). To investigate which exonucleases are involved in degradation of the reporter, I performed the knock-down experiments followed by western blotting and smFISH quantification (Figure S4). Next, I applied SPT to compare the nuclear RNA particles of the reporter targeted and not targeted for endonucleolytic cleavage in living cells (Figure 3C, D). The imaging and analysis of cytoplasmic slicing events were performed by F.V. (Figure 4). Supported by J.E., F.V. developed workflows for semi-automated image analysis in KNIME. I specifically looked at the co-localization of RNA particles with stained PBs within living-cells and quantified the fraction of PB-associated RNA

particles with the help of J.A.C. (Figure 5 and 6). In order to validate the PB-labeling method, I monitored the number of PBs under physiological and stress conditions with help of J.A.C. (Figure S7). Moreover, I conducted smFISH quantification of RNAs in cells treated with arsenite or translational inhibitors with the help of A.V.K. (Figure 7).

Finally, I was extensively involved in writing of the first version of the manuscript and in the preparation of the figures. The final version of the manuscript was created with a significant contribution of all the authors.

6. CONCLUSION AND DISCUSSION

In my work, I established a dual-color single-mRNA microscopy tool, called TREAT, that can expose molecular aspects of the RNA decay dynamics and kinetics that have remained unresolved in ensemble experiments. The innovative use of viral Xrn1-resistant PKs within the TREAT enables the unambiguous discrimination of mRNA decay from other causes of a signal loss such as photobleaching. The TREAT system relies on a direct monitoring of the intact mRNA and its decay intermediate that can be distinguished from each other. Advantages of the established TREAT system are: (i) temporal control over the expression of a reporter from a single genomic locus in HeLa cells, (ii) no apparent interference with other cellular processes, (iii) versatility of its applications (e.g. various *cis*-regulatory sequences), (iv) compatibility with antibody staining and experimental manipulation of proteins. Moreover, the TREAT system offers also possibilities for future improvements.

I used the TREAT method to tackle biological questions regarding mRNA turnover and found that: (i) TREAT mRNA export and decay rates can be measured by smFISH, (ii) degradation of TREAT mRNAs does not burst, (iii) real-time observation of Ago2-mediated cleavage of a shortly-lived TREAT mRNAs reveals spatial separation of cleavage fragments from each other *in vivo*, (iv) TREAT mRNAs are degraded in the cytoplasm without a spatial preference, (v) PBs are not sites of active TREAT mRNA degradation under physiological or stress conditions, (vi) *cis*-elements such as ARE or 5′-TOP within TREAT do not trigger its degradation in PBs, (vii) degradation of TREAT mRNAs is repressed by inhibition of translation in various steps.

Altogether, the developed TREAT technique enables to resolve spatio-temporal information and cell-to-cell heterogeneity of mRNA degradation on the level of individual molecules. My observations lay a foundation for determining how are degradation steps modulated within a cell at the single-molecule level and serves as a base for further sophisticated imaging experiments to unravel the complexity of mRNA regulation in time and space.

6.1. ADVANTAGES AND ADAPTATION OF THE TREAT

6.1.1. Use of viral PKs to resist 5′-to-3′ decay

Sequence folding pattern plays a fundamental role in RNA functionality. Certain RNA structures within RNAs have been found to slow down or resist degradation in the past (Alifano et al., 1994; reviewed in Brierley et al., 2008; reviewed in Conrad, 2014; Emory et al., 1992). While poly(G)-tracts and related elements have been used successfully to stall the 5′-to-3′exoribonuclease in yeast and trypanosomes and thus study RNA degradation, these types of structures have not consistently worked in mammalian cells (Decker and Parker, 1993; Li et al., 2006; Muhlrad et al., 1994; Poole and Stevens, 1997; Sheth and Parker, 2003). The recently solved crystal structure of a part of the flaviviral 3′-UTR has shown that a specific three-dimensional fold provides a readily protection from the complete Xrn1-mediated degradation of the flaviviral genomic RNA in mammalian host cells (Chapman et al., 2014a; Chapman et al., 2014b; Moon et al., 2012). For construction of the single-mRNA reporter, I took advantage of these flaviviral PKs in order to stabilize mRNA degradation intermediates in mammalian cells. The accumulation of these intermediates can be used as a proxy for the mRNA degradation in context of the cellular environment. To interrogate RNA degradation, researchers from the Gehring laboratory have chosen a similar strategy. They primarily studied mRNA degradation of a transcript bearing a PTC upstream from the flaviviral PKs, an NMD reporter, employing semi-quantitative bulk measurements. Their conclusions relied on the ratio of whole transcripts to stabilized degradation intermediates seen as distinct bands of particular intensities on northern blots (Boehm et al., 2016). I also used northern blot method to distinguish intact TREAT mRNAs from its degradation intermediates and to confirm that the used flaviviral PKs have the ability to cause accumulation of stabilized 3′-ends in bulk (Figure S2 lane 1 and 2 in Horvathova et al., 2017). Thus, besides single-molecule studies, the TREAT system is suitable for bulk measurements as well.

The degree of stabilization of degradation intermediates could be modulated by the number of PKs inserted within a reporter. In the case of the TREAT reporter, I inserted West Nile virus (WNV)-derived tandem PKs with their natural linker to preserve the integrity of their structures. Tandem PKs have been shown to be more potent in blocking Xrn1 activity than a single one of them (Chapman et al., 2014b). In addition, inclusion of more than two PKs within the 3′-UTR of the TREAT reporter

would further increase the half-life of the stabilized intermediates and would help to investigate the directionality of degradation of stabilized intermediates as these do not resist ribonucleases infinitely. This strategy, though, was used to observe a step-wise yet continuous degradation of stabilized intermediates via 5′-to-3′ decay due to multiple repeats of tandem Murray Valley Encephalitis (MVE)-derived PKs included within the 3′-UTR of the NMD reporter (Boehm et al., 2016). This result suggests that indeed Xrn1 has the capacity to eventually surpass the PKs and degrade the reporter remainders. Most likely, Xrn1 is the enzyme that is responsible for degradation of stabilized 3′-ends in the TREAT system as well. I showed that siRNA-mediated inactivation of the exosome complex does not significantly reflect on stability of the decay intermediates, whereas the knockdown of Xrn1 may have stabilized the degradation intermediates. However, this increase in number of stabilized 3′-ends would be masked by a decreased rate at which the stabilized 3′-ends are formed by the residual Xrn1 activity (Figure S4 in Horvathova et al., 2017). To confirm my assumption that Xrn1 is responsible for turnover of stabilized degradation intermediates, additional repeats of tandem PKs derived from WNV could be placed into 3′-UTR of the TREAT reporter and the degradation pattern could be resolved by a northern blot.

6.1.1.1. Sequestration of Xrn1 and RNAi factors

It has been proposed that Xrn1 gets sequestered after stalling on the refractory flaviviral structures. The accumulation of subgenomic flaviviral RNAs (sfRNAs) has been shown to be directly responsible for a stabilization of cellular mRNAs (Moon et al., 2012). In this study, they generated sfRNAs in mammalian cells in two ways. Either a reporter gene forming sfRNAs due to Xrn1 activity was transiently transfected or cells were infected by flaviviruses. This led to an overexpression of reporter mRNA or flaviviral genomic RNA, respectively. The high number of resultant sfRNAs may have diminished the pool of Xrn1 enzyme otherwise available for degradation of other transcripts. Importantly, I did not observe decreased Xrn1 activity while the TREAT reporter was expressed in HeLa cells. To test whether formation of TREAT stabilized 3′-end affects Xrn1 activity, I measured and compared half-lives of inherently transient *c*-Myc mRNA in cells expressing and cells not expressing the TREAT reporter. This comparison showed almost identical degradation rates indicating no dysregulation of

Xrn1 decay pathways (Figure S1 in Horvathova et al., 2017). Even if the flaviviral PKs have the ability to sequester Xrn1 after its stalling, it would not most probably affect degradation rates of other RNAs since TREAT reporter is expressed from a single genomic locus at relatively low levels. My observation is further supported by the work of Boehm and colleagues who also did not find evidence about impairment of Xrn1-mediated decay in their system (Boehm et al., 2016).

Xrn1 was shown to bind to sfRNAs in Dengue virus and WNV infected cells as revealed by immunoprecipitation after crosslinking followed by RT-PCR or qRT-PCR analysis of bound RNA (Moon et al., 2012). Nevertheless, Chapman and colleague were unable to obtain evidence of formation of a stable complex between the resistant RNA and Xrn1 in a purified system arguing against the Xrn1 sequestration model (Chapman et al., 2014b). Altogether, PKs may act as reversible inhibitors of Xrn1, perhaps changing its activity in infected cells with high level of accumulated sfRNA. It is necessary to bear this in mind when using the TREAT system in different models (different types of cells, different organisms); the method always has to be validated in order to prove the full capacity of Xrn1 to degrade cellular transcripts.

In another study, co-immunoprecipitation of sfRNAs with RNAi mediators Dicer and Ago2 in human cells has pointed towards an ability of flaviviruses to serve as a decoy for these dsRNA-binding proteins and thereby to suppress RNAi. It has been concluded that RNAi is mildly but significantly suppressed during Dengue virus or WNV infection of human cells (Moon et al., 2015b). One possible explanation for only mild repression of RNAi despite the binding of two important RNAi mediators is that the RNA-protein interaction may have relatively quick dissociation rate. As, in addition to low expressed amounts, the TREAT reporter contains only a fraction of the WNV sfRNA, I therefore reason that its expression does not interfere with the RNAi pathway in our experimental system.

6.1.2. Use of other refractory elements to study different RNA decay steps

Besides the flaviviral Xrn1-resistant RNAs blocking 5′-to-3′ exonuclease activity, other structured elements protect RNAs against degradation from the 3′-end. Two non-coding RNAs with exceptionally long half-lives and significant sequence homology, both with direct importance to human health, share similar strategy to resist

the 3′-to-5′ degradation. Firstly, Kaposi's sarcoma-associated herpesvirus (KSHV) produces a noncoding polyadenylated nuclear (PAN) RNA. This viral transcript contains expression and nuclear retention element (ENE) and is expressed abundantly in the nucleus during the lytic phase of KSHV infection. The ENE element base pairs with the poly(A)-tail of the transcript forming an inhibitory structure for exoribonucleases (Conrad and Steitz, 2005; Mitton-Fry et al., 2010; Sun et al., 1996). Secondly, the long non-coding RNA MALAT1 was identified as a highly stable nuclear marker in different lung cancers (Ji et al., 2003). The 3′-stem-loop structure of processed MALAT1 confers stability by engaging a downstream A-rich tract in a triple-helix thus sequestering the 3′-end from the helicase and exonuclease activities of the exosome (Brown et al., 2014). Hence, by engaging the A-rich 3′-tail in stable RNA structure, efficient loading and progression of exosome is prevented, which normally requires ~30 nt of single stranded RNA as a landing pad (Bonneau et al., 2009; Makino et al., 2013). Unlike mature MALAT1 with blunt ended 3′-end, PAN ENE features a poly(A)-overhang at the 3′-end. As a result, PAN RNA exhibits biphasic decay kinetics with rapid degradation of the overhanging tail followed by slow decay of remaining RNA (Brown et al., 2014).

To study the deadenylation-dependent degradation, a reporter with the 3′-sequence of MALAT1 has been already applied, which forms a terminal stable triple-helix upon cellular processing without additional polyadenylation (Wilusz et al., 2012). An NMD reporter with the Xrn1-resistant PKs within 3′-UTR contained either MALAT1 triple-helix or poly(A)-tail at the 3′-end and was tethered to Smg7. Here, Smg7 preferentially triggered degradation of the polyadenylated reporter, however, it also induced deadenylation-independent degradation of the reporter terminating in the triple-helix. This suggested that Smg7 elicits both 3′-to-5′ and 5′-to-3′ decay pathways (Boehm et al., 2016). A similar assay tethering degradation factors to polyadenylated and triple-helix terminated mRNA reporters helped to investigate the miRNA-mediated silencing (Kuzuoglu-Ozturk et al., 2016). Hence, one could design a new version of TREAT reporter where the exosome-resistant structure would be placed instead of the poly(A)-tail. If any of single-colored 3′-ends arising from the reporter accumulates, it would mean that deadenylation-independent degradation by Xrn1 operates in the cells.

Moreover, to fluorescently distinguish intact mRNAs from 5′-end degradation intermediates, the 3′-to-5′ decay preceded by deadenylation needs to be blocked. This could be achieved by design of a reporter similar to TREAT where flaviviral PKs are

replaced by an exosome-resistant structure. However, this exosome-resistant structure has to be able to stop the exosome progression once it is engaged in degradation. Since placing MALAT1 or PAN ENE structures into 3′-UTR of a reporter would provide a landing pad for the exosome downstream of one of the structures, these structures may not resist the helicase and nuclease activity of the exosome long enough to trap the degradation intermediates. Despite of that, it would be valuable to test whether embedding of the triple-helix structure within 3′-UTR of the TREAT reporter causes stabilization of the 5′-end degradation intermediates. If a firm block for the exosome exonuclease activity existed, a set of reporters with elements blocking either the 3′-to-5′ or 5′-to-3′ degradation could be designed. Such reporters could, for example, be applied to a scenario of a PTC-evoked NMD. The modes of degradation could be thus distinguished, as NMD is proposed to involve endonucleolytic cleavage by Smg6 or recruitment of both 3′-to-5′ or 5′-to-3′ degradation machineries by Smg5-Smg7 (reviewed in Boehm et al., 2016; Nicholson and Muhlemann, 2010).

Altogether, these refractory RNA elements reveal different mechanisms to evade exonucleases and suggest that structure-based ribonuclease resistance may be a widespread mechanism of regulation of RNA decay. More of natural ribonuclease refractory elements are expected to be discovered and their potential folding may be determined by sensitive structure-solving methods. Alternatively, a rational structure design promises engineering of synthetic forms of refractory elements to come. In combination with structural features of a particular ribonuclease and its mechanistic function, new RNA elements can be designed based on their predicted folding pattern, perhaps inspired by the refractory structures that are already known. Then, an ability to block the selected nucleases can be experimentally tested.

6.1.3. Contribution of deadenylation, Xrn1, exosome and Dis3l2 to the overall cytoplasmic mRNA decay

The activation of cytoplasmic decay machineries has been most extensively studied in yeast as the most commonly utilized eukaryotic model organism in research related to mRNA metabolism. Deadenylation has been long considered as the rate-limiting step in the processes of mRNA degradation. It seems now that uridylation can stimulate decapping without prior poly(A)-tail shortening in mammalian cells (Morgan et al., 2017; Song and Kiledjian, 2007). Noteworthy, uridylyl-transferases are absent in *S.cerevisiae* (uridylyl-transferase Cid1 exists in *S.pombe*) and shortening of a

poly(A)-tail beyond a certain limit is the predominant event activating degradation of mRNA. Therefore, rates of deadenylation, uridylation, decapping or exoribonucleolytic digestion can each be limiting to the overall transcript degradation rate depending on the organism.

What is the contribution of different exoribonucleases to the overall mRNA degradation? According to the current model, Xrn1, as the sole 5′-to-3′ nuclease, plays a major role in the mRNA decay (Stoecklin et al., 2006). Although, it is clear that 3′-to-5′ degradation pathways also make a significant contribution (Murray and Schoenberg, 2007). It is well documented that mRNA surveillance pathways exploit exosome to a high extent (reviewed in Houseley et al., 2006). Illustrated by exosome and Dis3l2 that are able to catalyze degradation in the same direction, different levels of functional redundancy in RNA decay processes exist. Moreover, the opposite directionality of decay does not necessarily have to be mutually exclusive, but can be also functionally linked (Murray and Schoenberg, 2007). To dissect the contribution of Xrn1 and exosome to the overall degradation of the TREAT mRNA, I measured half-life of the reporter upon knockdown of Xrn1 or a core component of the exosome Rrp40 and compared the results to a control. The calculated half-life upon exosome knockdown was in agreement with the control, whereas Xrn1 knockdown resulted in increased stability of the mRNA. In conclusion, the Xrn1-mediated degradation is indeed the dominant decay pathway for the TREAT transcripts (Figure S4 in Horvathova et al., 2017). It would be worth determining the range of poly(A)-tail lengths of TREAT intact mRNA and its degradation intermediates. However, measuring the poly(A)-tail length on single transcripts in cells by fluorescent tags is challenging owing to the ubiquitous presence of adenylated transcripts in the cytoplasm as well as in the nucleus. To estimate the length of poly(A)-tails, bulk biochemical methods such as RNaseH-oligo(dT) digestion coupled to northern blot analysis, or PAT assay can be employed (Murray and Schoenberg, 2008). Alternatively, a single transcript resolution can be achieved by sequencing the 3′-extremities by TAIL-seq method, albeit the spatial information would be lost. But the advantage of this method is that additional modifications can be detected at the 3′-ends of transcripts (Chang et al., 2014b). Additionally, siRNA-mediated depletion of other factors such as Dis3l2 and TUTases would provide a deeper insight into the regulation of stability of TREAT reporters.

6.1.4. TREAT for imaging endogenous mRNAs

In my work, I used engineered reporter mRNAs to study their degradation within whole cells. Using a reporter system has its advantages, however, an exogenous mRNA reporter may not recapitulate the full behavior of endogenous mRNAs. In general, an mRNA reporter may lack some of the *cis*-regulatory elements and thus *trans*-acting binding proteins that are otherwise important in context of an endogenous mRNA. Also, a reporter may not undergo proper processing (e.g., properly regulated splicing) to be bound by essential adaptors. Therefore, a question is: Can the TREAT system be also applied to endogenous genes? With the current availability of various gene-editing tools based on CRISPR/Cas9, transcription activator-like effector nucleases (TALENs) or zinc-finger nucleases (ZFNs), I foresee the TREAT system to be applied for inspection of endogenous mRNAs degradation (reviewed in Gaj et al., 2013). Genome-editing tools could be used to insert the TREAT components, sequences coding PP7 and MS2 stem-loops as well as flaviviral PKs, into 3′-UTR of a carefully selected protein-coding gene. In a favor of this, a transgenic mouse has been generated that bears a cassette containing repeats of MS2 stem-loops in the 3′-UTR of the essential β-actin gene. Importantly, born homozygous knock-in mice were viable and fertile and, furthermore, the endogenous β-actin gene could be visualized by smFISH or live-cell imaging (Lionnet et al., 2011). Moreover, transgenic zebrafish carrying MS2-labeled β-actin gene was used to study dynamics of transcription and subcellular localization of an mRNA *in vivo* (Campbell et al., 2015). This indicates that the presence of the MS2 stem-loops in the genome is not deleterious for the cells and predicts feasibility of simultaneous insertion of multiple elements.

Since the emergence of CRISPR/Cas9, many techniques have been developed that utilize this adaptive immune system originating from bacteria and archaea. Redesigning the CRISPR/Cas9 system to bind RNA instead of DNA was a key step to develop an RNA imaging tool that is programmable for virtually any endogenous RNA (O'Connell et al., 2014). Catalytically inactive nuclease Cas9 fused with GFP forms a complex with a guide RNA and a PAM-presenting oligonucleotide. This complex specifically binds and tracks localization of mRNAs in live single-cells, without a need to modify the mRNA (Nelles et al., 2016). However, the method's resolution is not yet at the level of single-molecule detection pointing towards benefits of the TREAT system.

Analogous to our TREAT approach in fixed cells, dual-color smFISH has been used recently for simultaneous detection of an endogenous extraordinary long mRNA and its decay intermediate in *Trypanosoma brucei*. This approach is based on fluorescently distinguishable probes hybridizing to the extreme 5′- and 3′-ends of a very long transcript allowing for both decay directionalities to be investigated. No artificial stabilization of decay intermediates was needed because the extensive length of the questioned transcript allowed observing them for sufficient time. The activity of nucleases from either site results in a switch from a dual-labeled intact transcript to a single-labeled decay intermediate. These data confirmed that 5′-to-3′ decay pathway is the major cytoplasmic mRNA degradation mechanism. The suitability of this system was successfully tested for mouse fibroblast cells, however, only for very long endogenous transcripts that are generally rare. So, the question arises as to whether these very long mRNAs are representative enough for reporting on mRNA metabolism, particularly as these long mRNAs are expressed as only a few copies per cell (Kramer, 2017). Although TREAT reporter yields information especially about 5′-to-3′ decay pathway, it is predicted to be mostly independent of mRNA length. Therefore, it would be worth to generate a cell line with integrated TREAT components into an endogenous gene and acquire insightful data that would help to understand the turnover of particular intrinsic mRNAs of interest.

6.1.5. Different applications of TREAT

Can TREAT be extrapolated to image mRNAs with different *cis*-regulatory elements? I have studied the effect of several *cis*-elements by the TREAT method. First, a single siRNA-binding site was placed just upstream of the PKs, which provided an insight into the spatio-temporal regulation of the Ago2-mediated cleavage. Second, AU-rich elements of TNF-α were also placed within the TREAT's 3′-UTR to study how these elements affect recruitment and degradation of the reporter in PBs. Third, a 5′-TOP sequence was placed within the 5′-UTR of the TREAT reporter to examine the role of PBs in storage and degradation of mRNAs. To yield more biological insights into specific roles of the multitude of existing *cis*-elements in mRNA metabolism, the particular sequences can be inserted in virtually any position within the TREAT reporter depending on the question asked. For instance, specific sequences recognizable by multiple endonucleases are known. In particular, cleavage sites for the endonuclease

Regnase1 within TNF-α and IL6 mRNAs were mapped recently, however, spatial and temporal information about its activity within the cell is missing (Boehm et al., 2016). Furthermore, single or multiple miRNA sites can be introduced within the 3′-UTR of TREAT. Given the proposed cooperative mode of miRNAs, different combinations of miRNA-binding sites and their spacing can be examined with respect to their efficacy to trigger degradation (Saetrom et al., 2007). Finally, the *Renilla* luciferase ORF within the TREAT reporters I used can be exchanged for sequence encoding a gene of interest. In conclusion, TREAT system has a modular character, which can be exploited to address a functionality of various sequences.

Can TREAT be extrapolated to image different types of RNAs than mRNAs? Besides mRNA, the eukaryotic genome encodes many non-coding RNAs (ncRNAs). The function of some classes is well defined (e.g. tRNA, rRNA). But we have little knowledge about the biological role of long non-coding RNAs (lncRNA) or their degradation. The class of lncRNAs comprises transcripts that are at least ~200 nt in length. Firstly, transcripts arising from pervasive transcription in yeast, e.g. cryptic unstable transcripts (CUTs), and their related form in vertebrates (promoter upstream transcripts (PROMPTs)) belong among lncRNAs. These transcripts are quickly degraded in the nucleus and only became detected after depletion of key components of the RNA exosome (Preker et al., 2008; Wyers et al., 2005). On the other hand, depleting Xrn1 in yeast results in cytoplasmic accumulation of normally unstable lncRNAs called Xrn1-sensitive unstable transcripts (XUTs) (van Dijk et al., 2011). Next subclass of lncRNAs is circular RNAs (circRNAs). CircRNAs do not have free ends, which explains their increased stability. Thus, their degradation can be only initiated by endonucleolytic cleavage. Indeed, miR-671 directs cleavage of a circular antisense transcript of the cerebellar degeneration-related protein 1 (CDR1-AS) locus in Ago2-dependent manner in the nucleus of human cells. Concomitantly with downregulation of CDR1-AS, the CDR1 mRNA levels decrease suggesting a novel gene regulatory mechanism (Hansen et al., 2011). Finally, X-chromosome inactivation is induced by coverage by multiple copies of long non-coding RNA called Xist. MS2-tagging of Xist has been successfully used to visualize transgenically expressed Xist in mouse embryonic stem cells. This tool helped to investigate the dynamics of Xist spreading over the inactivated X-chromosome (Ng et al., 2011). The majority of enzymes involved in the decay are shared between mRNA and ncRNA, however, specific mechanisms ensuring that these non-coding transcripts are degraded properly are largely unknown (reviewed in Labno et al., 2016a). Using TREAT system in a

context of lncRNA may significantly help to shed light on their spatial and temporal regulation of degradation within cells.

Can TREAT be extrapolated to image RNAs in different biological models? Local translation of mRNAs, which has an important role in synaptic plasticity, has been extensively studied in cell culture of primary hippocampal neurons (Wang et al., 2016; Wu et al., 2016). It would be of particular interest to understand if mRNAs that are specifically localized for their translation in neuronal dendrites also get degraded in response to synaptic activity, and if specialized degradation machineries concentrate in synapses. There are several reasons why TREAT system could be broadly used not only in cultured cells but also in various model organisms. First, the endogenous MS2-tagged mRNA was not harmful for the generated transgenic mouse or zebrafish (Campbell et al., 2015; Lionnet et al., 2011). Second, the observation of activated translation of *oskar* mRNA TRICK reporter, dually-labeled with PP7 and MS2 system, during *Drosophila* oogenesis was enabled by immunofluorescence (Halstead et al., 2015). Third, RNA degradation systems are ubiquitous and present in all living organisms. Among others, Xrn1 and its homologues play a crucial role in all eukaryotic experimental systems. Although it may be challenging to express different transgenes in the same primary cell or organism for live-cell imaging (TREAT reporter, MCP and PCP), one of the strength of the TREAT system is that intact mRNAs and degradation products can initially be distinguished simply by smFISH. By the expression of only the TREAT reporter and its visualization by smFISH probes in fixed cells can still yield a lot of information about spatio-temporal regulation and serve as pilot experiments for designing live-cell imaging approaches. Therefore, I anticipate a usage of TREAT reporter system in experimental models such as neuronal cells, mouse, zebrafish, flies, and perhaps nematodes. For instance, Xlhbox2 (also known as HoxB7) mRNA has been found to possess a specific short sequence prone to endonucleolytic cleavage in Drosophila embryo and *Xenopus* oocyte. Moreover, the responsible endonuclease was suggested to be in competition with an inhibitor of the endonuclease activity. This inhibitor-regulated cleavage mechanism may play an important role during embryogenesis and precise timing of the cleavage activation may ensure a proper development (Brown et al., 1993). By investigating a TREAT reporter bearing the cleavage site from Xlhbox2 mRNA, information about cellular position of this cleavage and its temporal activation during MZT could be obtained.

6.2. BIOLOGICAL QUESTIONS ADDRESSED BY TREAT

6.2.1. Temporal regulation of mRNA decay

Initially, a simplified model of gene expression assumed the transcription rate as well as RNA degradation rate to be constant. This interpretation of gene expression would ensure maintenance of the same steady-state levels of mRNAs in genetically identical cells. However, more recently, it has been evidenced that genetically identical cells in a population may be different at the molecular level. How the variability among cells is generated and controlled remains a major challenge in the field. Moreover, the reasons why the cells in a population can be different await to be answered. Researchers have been trying to decompose and understand the multiple factors of the inherent stochasticity in gene expression that leads to variability in mRNA and protein levels among cells. This noise has been shown to depend on the rates of transcription and translation across species (reviewed in Raj and van Oudenaarden, 2008). While some house-keeping genes occurred to be transcribed rather constitutively in yeast, other genes can randomly switch back and forth between transcriptionally active and inactive states and display "transcriptional bursting" reflecting on high fluctuation of mRNA levels within particular cells (Raj et al., 2006; Zenklusen et al., 2008). Nevertheless, whether mRNA degradation may contribute to the stochasticity in gene expression by "bursting" has been poorly addressed yet. The single-molecule measurement by TREAT system is able to address this. While measuring export and decay rates of TREAT reporters, I observed a significant variability in counts of both the intact mRNAs and stabilized 3′-ends per cell over the time-course of smFISH experiments. This pointed towards possible existence of degradational bursting that would cause increased degradation rate in some of the cells in the population. The experimental data, however, were in agreement with a computer simulation assuming degradation as a single-step Poisson process. Thus, I conclude that degradation of TREAT mRNA does not happen in bursts and that the observed cell-to-cell variability in 3′-ends could be explained by variability in the amounts of intact transcripts at the initial time-point of the experiment (Figure S5 and S6 in Horvathova et al., 2017). However, I speculate that the decay burst of specific mRNAs may occur under different biological conditions. Recently, a heat-stress was shown to lead to dynamics changes in epitranscriptome (Zhou et al., 2015). To control a heat-shock response, it has been proposed that Hsp70 mRNA is co-transcriptionally methylated in order to be timely degraded in mES cells (Knuckles et al., 2017).

Perhaps, methylation marks deposited on mRNAs in response to a heat-stress regulate subsequent degradation burst of particular mRNAs during the cell recovery from heat-stress. In general, whether environmental stimuli, various *cis*- or *trans*-acting factors, or their combination may trigger degradational burst may be investigated by the TREAT system in the future.

The best approach how to address the hypothesized phenomenon of degradational bursting would be to revisit particular living cells and observe changes over time in amounts of dual-labeled intact transcripts and single-labeled stabilized 3′-ends. This approach has been technically challenging so far, because the high-intensity illumination of the same cell over long time periods can lead to production of reactive oxygen species and thus compromise the entire cell. In addition, observing a cell under high magnification over several hours may result in the cell moving out from the field of view. Nevertheless, technical advances can soon overcome the phototoxic effect and enable this type of experiment. Altogether, TREAT provides a means how to measure temporal control of mRNA decay with preserved information on cell-to-cell variability.

Since TREAT reporter mRNAs are not degraded in the nucleus, their nuclear export rate could be calculated and the time it takes for an mRNA to be degraded once it enters the cytoplasm was measured. As expected, I demonstrated that the half-lives of TREAT reporters regulated by siRNA molecules or AU-rich binding proteins significantly decreased compared to TREAT without inserted regulatory sequences. Intriguingly, the nuclear export rate of the TREAT-ARE reporter as well as the degradation rate of its stabilized 3′-end was enhanced by these *cis*-elements as compared to other reporters investigated. I hypothesize that HuR, an AU-rich binding factor, may accompany TREAT-ARE and accelerate its export from the nucleus (Doller et al., 2008; Doller et al., 2007; Lafarga et al., 2009). By overexpression or knockdown of HuR levels, the role of HuR in the export of ARE-containing transcripts can be elucidated. It is also probable that other than Xrn1 decay pathways contribute to the degradation of the TREAT-ARE reporter, which may explain the accelerated degradation of intact mRNAs and stabilized 3′-ends. Also, the fact that TREAT visualizes the nascent transcripts at the transcription site reveals a possibility to investigate the feedback loop between degradation and transcription (Haimovich et al., 2013; Sun et al., 2013). Further investigation of nuclear export rates and cytoplasmic

mRNA degradation rates by TREAT may reveal contribution of these steps to the overall abundance of transcripts within the cell.

6.2.2. Spatial regulation of mRNA decay

6.2.2.1. The role of processing bodies

What is the role of subcellular compartments in mRNA degradation? This is one of the key questions that still remains open. Two functions have been assigned to PBs - the degradation and storage of mRNA. PBs may serve as a storage site especially for translationally repressed mRNAs (Halstead et al., 2015). But there has been a lot of controversy about the role of PBs in RNA degradation processes. Certainly, PBs concentrate multiple degradation enzymes, however, direct evidence for active engagement of these enzymes in RNA degradation within these foci is missing. By concentrating mRNA decay enzymes in PBs, the mRNA decay could be enhanced only for the pathways with otherwise limiting cytoplasmic concentrations. However, this scenario seems unlikely as most of the decay enzymes also occur diffused in the cytoplasm.

Without staining for PBs, I found the vast majority of intact TREAT mRNA and stabilized 3′-ends dispersed throughout cytoplasm with no obvious clustering in fixed and living cells. Co-staining for PBs in live-cell experiments did not show accumulation of intact TREAT mRNA or presence of stabilized 3′-ends in PBs. Only a small fraction of intact mRNA of TREAT-ARE accumulated in PBs, suggesting a partial recruitment of this reporter to PBs via AU-rich elements (Franks and Lykke-Andersen, 2007). Similarly, a small amount of intact mRNAs was found in PBs in case of TREAT and 5′-TOP-TREAT reporter under arsenite stress (Figure 5 and 6 in Horvathova et al., 2017). However, as evidenced by smFISH, general degradation is attenuated under arsenite stress (Figure 7 in Horvathova et al., 2017). Therefore, it is plausible that arsenite stress inactivates one or more mRNA decay pathways resulting in a recruitment of mRNAs to PBs. I conclude that PBs may occasionally serve as a storage site for TREAT mRNAs, but do not serve as an active mRNA degradation hub. Instead, PBs may fulfill a buffering function for the decay factors in order to maintain their appropriate levels in the cytosol and thus regulate the decay rates of cytosolic mRNAs. It remains to be elucidated whether PBs may serve as degradation foci for specialized mRNA

decay mechanisms. I speculate that the extent to which PBs contribute to mRNA decay may also differ between species as experiments in yeast have suggested the active mRNA degradation within these foci (Sheth and Parker, 2003). It would be interesting to revisit these findings from yeast with a two-color biosensor similar to TREAT where poly(G)-tract is in place instead of viral PKs.

Based on a recent technique, which sorted PB-associated RNAs from those assembled in other RNPs, it has been also concluded that mRNAs accumulated in PBs are repressed, but not decayed (Hubstenberger et al., 2017). The potential role of PBs as degradation sites is further challenged by the observation that transcripts can be degraded co-translationally while associated with polysomes (Hu et al., 2009; Pelechano et al., 2015). In line with my observations, this indicates that the degradation processes do not require the movement of mRNAs into distinct cellular compartments.

The RNA granules in somatic cells, PBs and SGs, are compositionally similar to other mRNP granules such as maternal mRNA storage granules and neuronal RNA granules (Anderson and Kedersha, 2006). This similarity suggests shared function in mRNA metabolism. Thus, the usage of TREAT can be possibly extended to understand mRNA storage and degradational activities of other PB-like granules found in specialized cells such as germline cells or neurons.

6.2.2.2. The role of endoplasmic reticulum

The involvement of the ER in assembly of the RISC complex and subsequent steps of the sRNA-mediated silencing was proposed (Barman and Bhattacharyya, 2015; Li et al., 2013a; Sahoo et al., 2017; Stalder et al., 2013). So far, I have not stained for ER compartment to correlate the occurrence of slicing events of TREAT-siRNA reporter with the network of ER. However, the distance measurement of observed slicing events from the nuclear boundary agrees with the measured distances of a control reporter (Figure 4 in Horvathova et al., 2017). This indicates that the slicing reporter is not differentially recruited to any specific subcytoplasmic location to get degraded. As a few intact mRNAs can diffuse further from the nuclear boundary and some of the slicing events occurred towards the cell periphery, this shows that a small fraction of exported TREAT-siRNA mRNAs can escape the programmed RISC

temporarily. I have not measured the expression level of mature TREAT-specific siRNA in the respective experimental cell line. Nevertheless, it would be worth to alter the cognate shRNA expression level and observe how the kinetics of the cleavage changes.

There were two possible scenarios for how the degradation upon slicing can happen. Either the responsible 3′-to-5′ exonuclease degrades the unprotected 5′-fragment right after the cleavage, viewed as a color change from white (dual-labeled intact mRNA) to magenta (single-labeled stabilized 3′-fragment) particle, or the two fragments separate from each other after the cleavage but before they are recruited to the responsible decay machineries. For the time being, imaging of the TREAT-siRNA reporter in live cells has enabled detection of 17 slicing events, where the fragments were severed from each other. The 5′-fragment is not immediately degraded by a 3′-to-5′ exonuclease after the cleavage, however, I cannot exclude the possible coupling of Xrn1 (5′-to-3′ exonuclease) to Ago2-mediated cleavage due to presence of Xrn1-resistant PKs. Alternatively, reporter lacking the PKs albeit still susceptible to the specific siRNA-mediated cleavage, would resolve if this scenario is possible. Altogether, capturing more slicing events would be needed for an extensive analysis to conclude that the spatial separation of cleaved fragments is general feature for the Ago2-mediated degradation. Also, more data acquisition would be needed to conclude on the importance of the ER in the sRNA-mediated silencing.

Given the expansive character of the ER throughout the cytoplasm, it would be interesting to stain the ER while observing the mRNA undergoing Ago2-mediated cleavage. Furthermore, to investigate if the microenvironment on the ER membrane may provide a kinetic advantage for the Ago2-mediated cleavage, the TREAT-siRNA can be specifically tethered to the ER by localizing its translation. To do so, a specific signal sequence can be included at the 5′-site of the TREAT's ORF (reviewed in Nyathi et al., 2013; Wu et al., 2016). Translation of the N-terminal positioned nascent peptides encoded by the signal sequence would therefore allow for a recruitment of the mRNA-ribosome-peptide complex to the ER surface. The tethered reporter may undergo altered mode of degradation. Perhaps, the degradation rate increases and the downstream decay of fragments by exonucleases would be directly coupled to the Ago2-endonucleolytic cleavage.

To study another degradation mechanism associated with ER, a TREAT reporter susceptible for regulated Ire1-dependent decay (RIDD) on the ER surface

could be studied in response to ER-stress. The susceptibility for RIDD in mammalian cells can be acquired by including a cleavage site with a consensus sequence (CTGCAG) within a SL structure into the reporter (Oikawa et al., 2010). In addition, simultaneous tethering of the reporter to labeled ER would be required to increase the likelihood for observation of the cleavage events. To experimentally induce the ER-stress, treatment with thapsigargin can be used to inhibit Ca^{2+} ATPase and thus to dysregulate calcium homeostasis in the cell leading to an activation of UPR. The questions addressed by this strategy could be: What fraction of reporter mRNAs undergoes the Ire-mediated cleavage at the ER within a given time? Do the cleaved fragments dissociate from ER before their degradation or they are degraded on the surface of ER? Since Ire1 has been reported to form temporal microscopically visible foci upon stress-induced oligomerization, it would be of interest to visualize these clusters simultaneously with the TREAT reporter (Li et al., 2010). By additional expression of a fluorescently labeled Ire1 in the studied cells, the spatial and temporal information gained from TREAT reporter prone to RIDD could be correlated with the occurrence of Ire1 clusters. Under these conditions, if the TREAT reporter degrades faster when co-localized with Ire1 foci, it would suggest that clustering of Ire1 enhances its endonucleolytic activity and provides a kinetic advantage for local mRNA degradation. Interestingly, in *Drosophila* S2 cells, the ER-associated mRNA of plexin A (protein functioning in axon guidance in neuronal cells) was shown to be protected from RIDD via continued translation during stress. This protection was shown to be mediated by upstream ORFs (uORFs) in the 5′-UTR (Gaddam et al., 2013). Hence, TREAT reporters with various uORFs could be evaluated with respect to their ability to protect certain mRNAs from Ire1-mediated degradation during ER stress.

Taken together, coupling of particular steps in mRNA metabolism in space and time could provide a kinetic boost to a series of processes. This may be reflected in the interdependence of localization, translation, storage, and mRNA decay. The biological significance of PBs and ER in coupling mRNA degradation steps with translation is only partially resolved and further investigations by TREAT would help to provide more insights into the dynamic steps happening within these subcellular locations.

6.2.3. The effect of translational inhibition on mRNA stability

The link between translation and mRNA degradation can be seen either as a competition or cooperation. If the model of circular mRNA is correct and allows a rapid ribosome recycling, ongoing translation competes with the degradation initiation by protecting the mRNA ends in a closed loop (reviewed in Gallie, 1998). The cooperative model of translation and degradation is proposed by mRNA quality control mechanisms and by observed co-translational degradation (reviewed in Garneau et al., 2007; Pelechano et al., 2015). So, how an inhibition of translation affects the mRNA stability?

I showed that arsenite-induced stabilization of TREAT transcripts occurred in the entire cytoplasm and was not restricted only to the mRNAs occasionally stored within PBs (Figure 7 in Horvathova et al., 2017). Since arsenite leads indirectly to general translational inhibition via the eIF2α phosphorylation and to polysome disassembly, I tested the effect of three translational inhibitors on stability of the TREAT mRNA to find out to what extent translational is required for continuous mRNA degradation. Interestingly, each of the tested drugs (harringtonine, cycloheximide, puromycin), inhibiting different translational step, dramatically stabilized the reporter mRNA (Figure 7 in Horvathova et al., 2017). This result shows that the TREAT mRNA degradation is dependent on active translation in mammalian cells. Consistently, a treatment of HeLa cells with either cycloheximide or puromycin strongly impaired degradation of an NMD reporter and reporters containing 3′-UTR of cytokines (Boehm et al., 2016). In another recent study, the same two drugs were used to impair translation in cells of *Trypanosoma brucei* and the effect on mRNA degradation was assessed by smFISH. Here, consistently with my results, cycloheximide treatment showed increase of intact mRNA fraction when compared to untreated cells, whereas puromycin treatment did not show significant difference (Kramer, 2017). In contrast to cycloheximide, puromycin does not stabilize polysomes, and thus an mRNA may be better accessible for nucleases in some organisms. The discrepancy between observations from puromycin treated mammalian cells and *Trypanosoma* cells may point to inter-species regulatory differences. In addition to that, by smFISH, I have observed that cycloheximide treatment of the cell line expressing TREAT-siRNA reporter allowed for Ago2-mediated cleavage but was deficient in degrading the separated fragments (data not shown). This observation is in line with previous study in *Drosophila* cells, where the degradation of 5′-fragments was blocked by CHX

treatment (Orban and Izaurralde, 2005). Hence, the majority of the degradation pathways in mammalian cells seem to involve translation-coupled mechanisms. Although, the stabilization of mRNAs upon cycloheximide-mediated translational inhibition is a long known effect (reviewed in Jacobson and Peltz, 1996), mechanistically, it still remains an open question as to how the degradation machinery senses the translational inhibition.

The global regulation of degradation can be achieved by controlling the expression of factors that mediate the interaction between mRNAs and deadenylase complexes. For instance, the family of Tob proteins directly recruits the deadenylation complex Ccr4-Not to the PAPB-bound poly(A)-tail via their ability to simultaneously interact with PAPB and Caf1 (Ezzeddine et al., 2007; Mauxion et al., 2008). In addition, arsenite inhibits mRNA deadenylation through proteolytic degradation of Tob and Pan3, the latter being a cofactor of deadenylase Pan2 (Yamagishi et al., 2014). Besides that, eukaryotic release factor 3 (eRF3) has been shown to couple deadenylation with translation termination by catalyzing deadenylation (Funakoshi et al., 2007). It would be interesting to find out whether Tob or eRF3 can be the general regulator implicated in the link between translational and degradational inhibition. To assess whether Tob or eRF3 are limiting for efficient TREAT mRNA degradation, these two proteins could be knocked-down and direct levels of TREAT mRNA could be measured. Conversely, in a rescue experiment, an overexpression of these proteins in translationally blocked cells could reflect in derepressing the mRNA degradation inhibition. Furthermore, investigation of the poly(A)-length (by methods described in 5.1.3. section) of the TREAT reporter treated with the translational inhibitors can shed light on the importance of deadenylation in coupling translation to degradation.

6.2.4. Further combination of TREAT with other tools

To expand the variety of biological questions that can be addressed by the TREAT system, this method can be combined with other tools. A careful selection of a set of fluorophores and RNA labeling methods would allow simultaneous three-color imaging of single particles (Shaner et al., 2005; reviewed in Weil et al., 2010). There is a constant improvement in brightness and photostability of fluorophores allowing for a longer illumination time (Grimm et al., 2015; Grimm et al., 2017). Among others, ƛN-derived RNA-labeling method exists that can be used within an RNA reporter next to

PP7 and MS2 systems due to their orthogonality (Daigle and Ellenberg, 2007). With the use of three independent RNA labeling systems at the same time, TREAT can be combined with TRICK methodology to investigate the interrelation of mRNA turnover and the pioneer round of translation (Halstead et al., 2015). This approach could be very informative when studying turnover of an NMD target since this surveillance pathway was suggested to be triggered during the pioneer round of translation (Ishigaki et al., 2001). To further illuminate the relationship between translation and mRNA turnover, TREAT can be used together with the recently developed method for labeling of nascent polypeptides, as they emerge from a ribosome translating the TREAT mRNA (Morisaki et al., 2016; Wang et al., 2016; Wu et al., 2016; Yan et al., 2016). This approach could be used to study the miRNA-mediated gene silencing since this post-transcriptional regulation is proposed both to initiate mRNA degradation and to repress translation. Recently, miRNAs were suggested to play a role in regulation of protein expression noise (Schmiedel et al., 2015). This would be of particular interest to be studied by a next generation of TREAT reporter due to its ability to address variability and sense fluctuations at single mRNA level. Finally, for certain applications, one of the RNA labeling systems can be exploited for tethering of mRNA molecules to subcellular structures allowing for its immobilization. This helps to keep an observed mRNA molecule in the same focal plane for a longer period of time in contrast to freely moving molecules that impede longer particle tracking (Yan et al., 2016). The continued evolution of multicolored RNA biosensors will enable to resolve events during the lifecycle of mRNAs in a greater detail.

6.3. OVERCOMING LIMITATIONS OF TREAT SYSTEM

The TREAT imaging method is a novel tool that provides significant advantages over current methods to study mRNA degradation. However, it has its own limitations. One limitation is the time scale of real-time observations in my experimental setup, usually about 5-10 sec. While the specific siRNA induces rapid siRNA-TREAT mRNA decay ($t_{1/2}$ = ~7 min) seen as a particle color change in living-cells, I found the real-time observation of a degradation moment of TREAT without presence of the siRNA challenging. Although, the half-life of this TREAT reporter in HeLa cells is still relatively short ($t_{1/2}$ = ~1.6 h), compared to median half-life measured by a genome-wide sequencing after pulse-labeling of endogenous mRNAs in HeLa cells ($t_{1/2}$ = ~3.4

h) or in mouse NIH3T3 fibroblasts ($t_{1/2}$ = ~9 h), this system is limited for real-time imaging of transcripts with higher stability than few minutes (Schwanhausser et al., 2011; Tani et al., 2012). Nevertheless, the pulse-labeling methods can be limited in the yield of recovered labeled mRNAs by several steps after cell lysis including immunoprecipitation, therefore the accuracy of these measurements can be questioned. On the other hand, TREAT has the advantage of counting mRNAs within the whole cells with detection efficiencies ~90% (Figure S7 in Horvathova et al., 2017). The advancement of photostable fluorophores and/or a tethering of the reporter to a cellular structure will facilitate real-time imaging of slower decaying mRNAs in the future.

In yeast and human cells, NMD pathway has been proposed to degrade mRNAs with long 3′-UTRs (Hogg and Goff, 2010; Kebaara and Atkin, 2009). A recent genome-wide study has shown only a slight correlation between extensive 3′-UTRs and mRNA instability in murine cells (Spies et al., 2013). Due to multiple RNA stem-loops within 3′-UTR of the TREAT reporter, this region is artificially extended. This may raise the question as to whether the length of the 3′-UTR influences the stability of the reporter. Since the NMD has been found to function early after nuclear export of an mRNA, the TREAT reporter is most probably not a target of NMD as I could observe many intact mRNAs in the cytoplasm for rather long periods (Trcek et al., 2013). However, a closer investigation is needed to exclude that NMD does not impact stability of TREAT mRNA.

Recently, it has been suggested that the interpretation of data from live-cell imaging using arrays of MS2 and PP7 stem-loops can be complicated by potential defects in RNA processing, including inhibition of 5′-to-3′ degradation by bound coat proteins in yeast (Garcia and Parker, 2015, 2016; Heinrich et al., 2017). In a response to these findings, evidence against this phenomenon was gathered (Haimovich et al., 2016). To validate that the MS2 and PP7 stem-loops do not interfere with TREAT mRNA decay in HeLa cells, I demonstrated that no 3′-degradation intermediates were accumulated from a control reporter lacking the viral PKs expressed within cells expressing MCPs and PCPs (Figure S2 lane 3 and 4 in Horvathova et al., 2017). The fact that MS2 and PP7 system components do not stabilize TREAT degradation intermediates may indicate that higher eukaryotes feature more robust molecular machineries, and thus process the stem-loop arrays differently than yeast. Moreover, the HeLa cell lines synthetizing fluorescent MCPs and PCPs were FACS sorted for low

levels of fluorescence in order to decrease background for imaging. The low level of coat proteins may also reduce the potential negative impact on the RNA reporter processing.

A potential negative impact of the stem-loop arrays and viral PKs on the RNA stability and localization has to be evaluated on a case-to-case basis in order to reduce the likelihood of processing perturbations of the tagged mRNA. Notably, the addition of only the viral PKs without the MS2 and PP7 stem-loops within a reporter's 3′-UTR would be sufficient for blocking Xrn1 and would allow for FISH experiments in fixed cells. Therefore, the impact of MS2 and PP7 stem-loops on mRNA processing could be uncoupled. In addition to the removal of the MS2 and PP7 components, the overall length of 3′-UTR would in such case shorten, which would in turn decrease the possibility of triggering the NMD pathway.

7. LIST OF USED ABBREVIATIONS

4sU – 4-thiouridine
actD – actinomycin D
Ago – argonaute
AMD – ARE-mediated decay
AMPK – AMP-activated kinase
Ape – apurinic/apyrimidinic endonuclease
ARE – AU-rich element
AUF – AU-rich binding factor
BP – binding protein
BRF – butyrate response factor
Cas – CRISPR-associated
CBP – cap binding protein
Cdk – cyclin-dependent kinase
cDNA – complementary DNA
CDR – cerebellar degeneration-related protein
CDR-AS – cerebellar degeneration-related protein antisense
circRNA – circular RNA
CPEB – cytoplasmic polyadenylation element- binding protein
CRISPR – Clustered regularly-interspaced short palindromic repeats
CUGBP – CUG-binding protein
CUT – cryptic unstable transcript
Dcp – decapping enzyme
DcpS – scavenger decapping enzyme
DGCR8 – DiGeorge syndrome critical region 8
Dis3 – Dis3-like
DNA – deoxynucleic acid
dsRNA – double-stranded RNA
eIF – eukaryotic initiation factor
EJC – exon junction complex
endo-siRNA – endogenous siRNA
ER – endoplasmic reticulum
ERK – extracellular signal-regulated kinase
FISH – fluorescence in situ hybridization
G3BP – Ras-GTPase activating protein SH3 domain-binding protein
GCN – general control nonderepressible
GMCSF – granulocyte macrophage colony-stimulating factor
GRE – GU-rich elements
HCV – hepatitits C virus
hnRNP – heterogeneous nuclear ribonucleoprotein
HRI – heme-regulated initiation factor 2α kinase
Hsp – heat-shock protein
HuR – human antigen R
IL – interleukin

Ire – inositol-requiring enzyme
IRE – iron-responsive element
IRES – internal ribosome entry site
IRP – iron regulatory protein
JNK – c-Jun N-terminal kinase
KSRP – KH-type splicing regulatory protein
lncRNA – long non-coding RNA
lncRNA – long non-coding RNA
m^{6}A – *N*^{6}-methyladenosine
MALAT – metastasis-associated lung adenocarcinoma transcript
MAPK – mitogen-activated protein kinase
MCP – MS2 coat protein
miRNA – micro RNA
mRNA – messenger RNA
mRNP – mRNA nucleoprotein
mTOR – mammalian target of rapamycin
MVE – Murray Valley Encephalitis
ncRNA – non-coding RNA
NGD – no-go decay
NMD – nonsense-mediated decay
NSD – non-stop decay
nt – nucleotide
ORF – open reading frame
PABP – poly(A)-binding protein
PACT – protein activator of the interferon-induced protein kinase
PBs – processing bodies
PCP – PP7 coat protein
PCR – polymerase chain reaction
PERK – PKR-like ER kinase
piRNA – piwi-interacting RNAs
PK – pseudo-knot
PKR – protein kinase R
Pmr – polysomal ribonuclease
Pol II – polymerase II
pre-miRNA – precursor miRNA
pri-miRNA – primary miRNA
PROMPT – promoter upstream transcripts
PTC – pre-mature termination codon
PTGS – post-transcriptional gene silencing
PTM – post-translational modification
qPCR – quantitative PCR
RdRP – RNA-dependent RNA polymerase
rER – rough ER
RIDD – regulated Ire1-dependent decay
RISC – RNA-induced silencing complex
RNA – ribonucleic acid

RNA-seq – RNA sequencing
RNAi – RNA interference
RT-PCR – reverse-transcription-PCR
RT-qPCR – reverse-transcription-quantitative PCR
scRNA-seq – single-cell RNA-seq
sfRNA – subgenomic flaviviral RNA
SGs – stress granules
siRNA – small interfering RNA
SL – stem-loop
SLBP – SL-binding protein
SMD – Stau-mediated decay
smFISH – single-molecule FISH
Smg – suppressor with a morphogenetic effect on genitalia
SPT – single particle tracking
sRNA – small RNA
ssRNA – single-stranded RNA
Stau – Staufen
Tet – teracycline
TGA – transcriptional gene activation
TGS – transcriptional gene silencing
TIA – T-cell internal antigen
TIAR – TIA-related
TNF – tumor necrosis factor
TOP – terminal oligopyrimidine
TRBP – TAR RNA binding protein
TREAT – three-RNA end accumulation during turnover
TRICK – translation coat protein knock-off
tRNA – transfer RNA
TTP – tristetraprolin
TUTase – terminal uridyl-transferase
Upf – up-frameshift
UPR – unfolded protein response
UTR – untranslated region
UV – ultra-violet
VACV – vaccinia virus
VEGFA – vascular endothelial growth factor A
WNV – West Nile virus
Xrn – exoribonuclease
xrRNA – Xrn1-resistant RNA
XUT – Xrn1-sensitive unstable transcript

8. REFERENCES

Abernathy, E., Gilbertson, S., Alla, R., and Glaunsinger, B. (2015). Viral Nucleases Induce an mRNA Degradation-Transcription Feedback Loop in Mammalian Cells. Cell host & microbe *18*, 243-253.

Aizer, A., Brody, Y., Ler, L.W., Sonenberg, N., Singer, R.H., and Shav-Tal, Y. (2008). The dynamics of mammalian P body transport, assembly, and disassembly in vivo. Molecular biology of the cell *19*, 4154-4166.

Aizer, A., Kalo, A., Kafri, P., Shraga, A., Ben-Yishay, R., Jacob, A., Kinor, N., and Shav-Tal, Y. (2014). Quantifying mRNA targeting to P-bodies in living human cells reveals their dual role in mRNA decay and storage. Journal of cell science *127*, 4443-4456.

Alifano, P., Bruni, C.B., and Carlomagno, M.S. (1994). Control of mRNA processing and decay in prokaryotes. Genetica *94*, 157-172.

Anderson, P., and Kedersha, N. (2006). RNA granules. The Journal of cell biology *172*, 803-808.

Anderson, P., and Kedersha, N. (2008). Stress granules: the Tao of RNA triage. Trends in biochemical sciences *33*, 141-150.

Arthur, L., Pavlovic-Djuranovic, S., Smith-Koutmou, K., Green, R., Szczesny, P., and Djuranovic, S. (2015). Translational control by lysine-encoding A-rich sequences. Science advances *1*.

Astuti, D., Morris, M.R., Cooper, W.N., Staals, R.H., Wake, N.C., Fews, G.A., Gill, H., Gentle, D., Shuib, S., Ricketts, C.J.*, et al.* (2012). Germline mutations in DIS3L2 cause the Perlman syndrome of overgrowth and Wilms tumor susceptibility. Nature genetics *44*, 277-284.

Banani, S.F., Lee, H.O., Hyman, A.A., and Rosen, M.K. (2017). Biomolecular condensates: organizers of cellular biochemistry. Nature reviews Molecular cell biology *18*, 285-298.

Barber, G.N. (2005). The dsRNA-dependent protein kinase, PKR and cell death. Cell death and differentiation *12*, 563-570.

Barman, B., and Bhattacharyya, S.N. (2015). mRNA Targeting to Endoplasmic Reticulum Precedes Ago Protein Interaction and MicroRNA (miRNA)-mediated Translation Repression in Mammalian Cells. The Journal of biological chemistry *290*, 24650-24656.

Barnes, T., Kim, W.C., Mantha, A.K., Kim, S.E., Izumi, T., Mitra, S., and Lee, C.H. (2009). Identification of Apurinic/apyrimidinic endonuclease 1 (APE1) as the endoribonuclease that cleaves c-myc mRNA. Nucleic acids research *37*, 3946-3958.

Bashkirov, V.I., Scherthan, H., Solinger, J.A., Buerstedde, J.M., and Heyer, W.D. (1997). A mouse cytoplasmic exoribonuclease (mXRN1p) with preference for G4 tetraplex substrates. The Journal of cell biology *136*, 761-773.

Bengtsson, M., Hemberg, M., Rorsman, P., and Stahlberg, A. (2008). Quantification of mRNA in single cells and modelling of RT-qPCR induced noise. BMC molecular biology *9*, 63.

Berezikov, E., Chung, W.J., Willis, J., Cuppen, E., and Lai, E.C. (2007). Mammalian mirtron genes. Molecular cell *28*, 328-336.

Bertrand, E., Chartrand, P., Schaefer, M., Shenoy, S.M., Singer, R.H., and Long, R.M. (1998). Localization of ASH1 mRNA particles in living yeast. Molecular cell *2*, 437-445.

Bhattacharyya, S.N., Habermacher, R., Martine, U., Closs, E.I., and Filipowicz, W. (2006). Relief of microRNA-mediated translational repression in human cells subjected to stress. Cell *125*, 1111-1124.

Bhowmick, R., Mukherjee, A., Patra, U., and Chawla-Sarkar, M. (2015). Rotavirus disrupts cytoplasmic P bodies during infection. Virus research *210*, 344-354.

Bidet, K., Dadlani, D., and Garcia-Blanco, M.A. (2014). G3BP1, G3BP2 and CAPRIN1 are required for translation of interferon stimulated mRNAs and are targeted by a dengue virus non-coding RNA. PLoS pathogens *10*, e1004242.

Bisbal, C., and Silverman, R.H. (2007). Diverse functions of RNase L and implications in pathology. Biochimie *89*, 789-798.

Boehm, V., Gerbracht, J.V., Marx, M.C., and Gehring, N.H. (2016). Interrogating the degradation pathways of unstable mRNAs with XRN1-resistant sequences. Nature communications *7*, 13691.

Bonneau, F., Basquin, J., Ebert, J., Lorentzen, E., and Conti, E. (2009). The yeast exosome functions as a macromolecular cage to channel RNA substrates for degradation. Cell *139*, 547-559.

Bravo, R., Parra, V., Gatica, D., Rodriguez, A.E., Torrealba, N., Paredes, F., Wang, Z.V., Zorzano, A., Hill, J.A., Jaimovich, E.*, et al.* (2013). Endoplasmic reticulum and the unfolded protein response: dynamics and metabolic integration. International review of cell and molecular biology *301*, 215-290.

Bregman, A., Avraham-Kelbert, M., Barkai, O., Duek, L., Guterman, A., and Choder, M. (2011). Promoter elements regulate cytoplasmic mRNA decay. Cell *147*, 1473-1483.

Brengues, M., Teixeira, D., and Parker, R. (2005). Movement of eukaryotic mRNAs between polysomes and cytoplasmic processing bodies. Science *310*, 486-489.

Brennan, C.M., and Steitz, J.A. (2001). HuR and mRNA stability. Cellular and molecular life sciences : CMLS *58*, 266-277.

Briata, P., Forcales, S.V., Ponassi, M., Corte, G., Chen, C.Y., Karin, M., Puri, P.L., and Gherzi, R. (2005). p38-dependent phosphorylation of the mRNA decay-promoting factor KSRP controls the stability of select myogenic transcripts. Molecular cell *20*, 891-903.

Brierley, I., Gilbert, R.J., and Pennell, S. (2008). RNA pseudoknots and the regulation of protein synthesis. Biochemical Society transactions *36*, 684-689.

Brook, M., Tchen, C.R., Santalucia, T., McIlrath, J., Arthur, J.S., Saklatvala, J., and Clark, A.R. (2006). Posttranslational regulation of tristetraprolin subcellular localization and protein stability by p38 mitogen-activated protein kinase and extracellular signal-regulated kinase pathways. Molecular and cellular biology *26*, 2408-2418.

Brown, B.D., Zipkin, I.D., and Harland, R.M. (1993). Sequence-specific endonucleolytic cleavage and protection of mRNA in Xenopus and Drosophila. Genes & development *7*, 1620-1631.

Brown, J.A., Bulkley, D., Wang, J., Valenstein, M.L., Yario, T.A., Steitz, T.A., and Steitz, J.A. (2014). Structural insights into the stabilization of MALAT1 noncoding RNA by a bipartite triple helix. Nature structural & molecular biology *21*, 633-640.

Burgess, H.M., and Mohr, I. (2015). Cellular 5'-3' mRNA exonuclease Xrn1 controls double-stranded RNA accumulation and anti-viral responses. Cell host & microbe *17*, 332-344.

Cacace, F., Paci, P., Cusimano, V., Germani, A., and Farina, L. (2012). Stochastic modeling of expression kinetics identifies messenger half-lives and reveals sequential waves of co-ordinated transcription and decay. PLoS computational biology *8*, e1002772.

Campbell, P.D., Chao, J.A., Singer, R.H., and Marlow, F.L. (2015). Dynamic visualization of transcription and RNA subcellular localization in zebrafish. Development *142*, 1368-1374.

Carthew, R.W., and Sontheimer, E.J. (2009). Origins and Mechanisms of miRNAs and siRNAs. Cell *136*, 642-655.

Catalanotto, C., Cogoni, C., and Zardo, G. (2016). MicroRNA in Control of Gene Expression: An Overview of Nuclear Functions. International journal of molecular sciences *17*.

Chang, C.T., Bercovich, N., Loh, B., Jonas, S., and Izaurralde, E. (2014a). The activation of the decapping enzyme DCP2 by DCP1 occurs on the EDC4 scaffold and involves a conserved loop in DCP1. Nucleic acids research *42*, 5217-5233.

Chang, H., Lim, J., Ha, M., and Kim, V.N. (2014b). TAIL-seq: genome-wide determination of poly(A) tail length and 3' end modifications. Molecular cell *53*, 1044-1052.

Chang, H.M., Triboulet, R., Thornton, J.E., and Gregory, R.I. (2013a). A role for the Perlman syndrome exonuclease Dis3l2 in the Lin28-let-7 pathway. Nature *497*, 244-248.

Chang, J.H., Xiang, S., Xiang, K., Manley, J.L., and Tong, L. (2011). Structural and biochemical studies of the 5'-->3' exoribonuclease Xrn1. Nature structural & molecular biology *18*, 270-276.

Chang, R.Y., Hsu, T.W., Chen, Y.L., Liu, S.F., Tsai, Y.J., Lin, Y.T., Chen, Y.S., and Fan, Y.H. (2013b). Japanese encephalitis virus non-coding RNA inhibits activation of interferon by

blocking nuclear translocation of interferon regulatory factor 3. Veterinary microbiology *166*, 11-21.

Chao, J.A., Patskovsky, Y., Almo, S.C., and Singer, R.H. (2008). Structural basis for the coevolution of a viral RNA-protein complex. Nature structural & molecular biology *15*, 103-105.

Chapman, E.G., Costantino, D.A., Rabe, J.L., Moon, S.L., Wilusz, J., Nix, J.C., and Kieft, J.S. (2014a). The structural basis of pathogenic subgenomic flavivirus RNA (sfRNA) production. Science *344*, 307-310.

Chapman, E.G., Moon, S.L., Wilusz, J., and Kieft, J.S. (2014b). RNA structures that resist degradation by Xrn1 produce a pathogenic Dengue virus RNA. eLife *3*, e01892.

Cheadle, C., Fan, J., Cho-Chung, Y.S., Werner, T., Ray, J., Do, L., Gorospe, M., and Becker, K.G. (2005). Stability regulation of mRNA and the control of gene expression. Annals of the New York Academy of Sciences *1058*, 196-204.

Chekulaeva, M., Mathys, H., Zipprich, J.T., Attig, J., Colic, M., Parker, R., and Filipowicz, W. (2011). miRNA repression involves GW182-mediated recruitment of CCR4-NOT through conserved W-containing motifs. Nature structural & molecular biology *18*, 1218-1226.

Chen, C.Y., and Shyu, A.B. (2011). Mechanisms of deadenylation-dependent decay. Wiley interdisciplinary reviews RNA *2*, 167-183.

Chen, L., Dumelie, J.G., Li, X., Cheng, M.H., Yang, Z., Laver, J.D., Siddiqui, N.U., Westwood, J.T., Morris, Q., Lipshitz, H.D*., et al.* (2014a). Global regulation of mRNA translation and stability in the early Drosophila embryo by the Smaug RNA-binding protein. Genome biology *15*, R4.

Chen, Q., Jagannathan, S., Reid, D.W., Zheng, T., and Nicchitta, C.V. (2011). Hierarchical regulation of mRNA partitioning between the cytoplasm and the endoplasmic reticulum of mammalian cells. Molecular biology of the cell *22*, 2646-2658.

Chen, Y., Boland, A., Kuzuoglu-Ozturk, D., Bawankar, P., Loh, B., Chang, C.T., Weichenrieder, O., and Izaurralde, E. (2014b). A DDX6-CNOT1 complex and W-binding pockets in CNOT9 reveal direct links between miRNA target recognition and silencing. Molecular cell *54*, 737-750.

Chlebowski, A., Lubas, M., Jensen, T.H., and Dziembowski, A. (2013). RNA decay machines: the exosome. Biochimica et biophysica acta *1829*, 552-560.

Chu, C.Y., and Rana, T.M. (2006). Translation repression in human cells by microRNA-induced gene silencing requires RCK/p54. PLoS biology *4*, e210.

Clement, S.L., Scheckel, C., Stoecklin, G., and Lykke-Andersen, J. (2011). Phosphorylation of tristetraprolin by MK2 impairs AU-rich element mRNA decay by preventing deadenylase recruitment. Molecular and cellular biology *31*, 256-266.

Conrad, K.D., Giering, F., Erfurth, C., Neumann, A., Fehr, C., Meister, G., and Niepmann, M. (2013). MicroRNA-122 dependent binding of Ago2 protein to hepatitis C virus RNA is associated with enhanced RNA stability and translation stimulation. PloS one *8*, e56272.

Conrad, N.K. (2014). The emerging role of triple helices in RNA biology. Wiley interdisciplinary reviews RNA *5*, 15-29.

Conrad, N.K., and Steitz, J.A. (2005). A Kaposi's sarcoma virus RNA element that increases the nuclear abundance of intronless transcripts. The EMBO journal *24*, 1831-1841.

Cougot, N., Babajko, S., and Seraphin, B. (2004). Cytoplasmic foci are sites of mRNA decay in human cells. The Journal of cell biology *165*, 31-40.

Coulon, A., Ferguson, M.L., de Turris, V., Palangat, M., Chow, C.C., and Larson, D.R. (2014). Kinetic competition during the transcription cycle results in stochastic RNA processing. eLife *3*.

Cox, E.M., Sagan, S.M., Mortimer, S.A., Doudna, J.A., and Sarnow, P. (2013). Enhancement of hepatitis C viral RNA abundance by precursor miR-122 molecules. Rna *19*, 1825-1832.

Daigle, N., and Ellenberg, J. (2007). LambdaN-GFP: an RNA reporter system for live-cell imaging. Nature methods *4*, 633-636.

Damgaard, C.K., and Lykke-Andersen, J. (2011). Translational coregulation of 5'TOP mRNAs by TIA-1 and TIAR. Genes & development *25*, 2057-2068.

Decker, C.J., and Parker, R. (1993). A turnover pathway for both stable and unstable mRNAs in yeast: evidence for a requirement for deadenylation. Genes & development *7*, 1632-1643.

Decker, C.J., and Parker, R. (2012). P-bodies and stress granules: possible roles in the control of translation and mRNA degradation. Cold Spring Harbor perspectives in biology *4*, a012286.

Decker, C.J., Teixeira, D., and Parker, R. (2007). Edc3p and a glutamine/asparagine-rich domain of Lsm4p function in processing body assembly in Saccharomyces cerevisiae. The Journal of cell biology *179*, 437-449.

Dickson, A.M., and Wilusz, J. (2011). Strategies for viral RNA stability: live long and prosper. Trends in genetics : TIG *27*, 286-293.

Doller, A., Akool el, S., Huwiler, A., Muller, R., Radeke, H.H., Pfeilschifter, J., and Eberhardt, W. (2008). Posttranslational modification of the AU-rich element binding protein HuR by protein kinase Cdelta elicits angiotensin II-induced stabilization and nuclear export of cyclooxygenase 2 mRNA. Molecular and cellular biology *28*, 2608-2625.

Doller, A., Huwiler, A., Muller, R., Radeke, H.H., Pfeilschifter, J., and Eberhardt, W. (2007). Protein kinase C alpha-dependent phosphorylation of the mRNA-stabilizing factor HuR: implications for posttranscriptional regulation of cyclooxygenase-2. Molecular biology of the cell *18*, 2137-2148.

Dominissini, D., Moshitch-Moshkovitz, S., Schwartz, S., Salmon-Divon, M., Ungar, L., Osenberg, S., Cesarkas, K., Jacob-Hirsch, J., Amariglio, N., Kupiec, M.*, et al.* (2012). Topology of the human and mouse m6A RNA methylomes revealed by m6A-seq. Nature *485*, 201-206.

Dunckley, T., and Parker, R. (1999). The DCP2 protein is required for mRNA decapping in Saccharomyces cerevisiae and contains a functional MutT motif. The EMBO journal *18*, 5411-5422.

Eberle, A.B., Lykke-Andersen, S., Muhlemann, O., and Jensen, T.H. (2009). SMG6 promotes endonucleolytic cleavage of nonsense mRNA in human cells. Nature structural & molecular biology *16*, 49-55.

Elbashir, S.M., Martinez, J., Patkaniowska, A., Lendeckel, W., and Tuschl, T. (2001). Functional anatomy of siRNAs for mediating efficient RNAi in Drosophila melanogaster embryo lysate. The EMBO journal *20*, 6877-6888.

Elkon, R., Ugalde, A.P., and Agami, R. (2013). Alternative cleavage and polyadenylation: extent, regulation and function. Nature reviews Genetics *14*, 496-506.

Elkon, R., Zlotorynski, E., Zeller, K.I., and Agami, R. (2010). Major role for mRNA stability in shaping the kinetics of gene induction. BMC genomics *11*, 259.

Emory, S.A., Bouvet, P., and Belasco, J.G. (1992). A 5'-terminal stem-loop structure can stabilize mRNA in Escherichia coli. Genes & development *6*, 135-148.

Eulalio, A., Behm-Ansmant, I., Schweizer, D., and Izaurralde, E. (2007). P-body formation is a consequence, not the cause, of RNA-mediated gene silencing. Molecular and cellular biology *27*, 3970-3981.

Eystathioy, T., Chan, E.K., Tenenbaum, S.A., Keene, J.D., Griffith, K., and Fritzler, M.J. (2002). A phosphorylated cytoplasmic autoantigen, GW182, associates with a unique population of human mRNAs within novel cytoplasmic speckles. Molecular biology of the cell *13*, 1338-1351.

Ezzeddine, N., Chang, T.C., Zhu, W., Yamashita, A., Chen, C.Y., Zhong, Z., Yamashita, Y., Zheng, D., and Shyu, A.B. (2007). Human TOB, an antiproliferative transcription factor, is a poly(A)-binding protein-dependent positive regulator of cytoplasmic mRNA deadenylation. Molecular and cellular biology *27*, 7791-7801.

Fan, Y.H., Nadar, M., Chen, C.C., Weng, C.C., Lin, Y.T., and Chang, R.Y. (2011). Small noncoding RNA modulates Japanese encephalitis virus replication and translation in trans. Virology journal *8*, 492.

Fang, F., Phillips, S., and Butler, J.S. (2005). Rat1p and Rai1p function with the nuclear exosome in the processing and degradation of rRNA precursors. Rna *11*, 1571-1578.

Fernandez-Garcia, M.D., Mazzon, M., Jacobs, M., and Amara, A. (2009). Pathogenesis of flavivirus infections: using and abusing the host cell. Cell host & microbe *5*, 318-328.

Franks, T.M., and Lykke-Andersen, J. (2007). TTP and BRF proteins nucleate processing body formation to silence mRNAs with AU-rich elements. Genes & development *21*, 719-735.

Friedel, C.C., Dolken, L., Ruzsics, Z., Koszinowski, U.H., and Zimmer, R. (2009). Conserved principles of mammalian transcriptional regulation revealed by RNA half-life. Nucleic acids research *37*, e115.

Friedman, R.C., Farh, K.K., Burge, C.B., and Bartel, D.P. (2009). Most mammalian mRNAs are conserved targets of microRNAs. Genome research *19*, 92-105.

Funakoshi, Y., Doi, Y., Hosoda, N., Uchida, N., Osawa, M., Shimada, I., Tsujimoto, M., Suzuki, T., Katada, T., and Hoshino, S. (2007). Mechanism of mRNA deadenylation: evidence for a molecular interplay between translation termination factor eRF3 and mRNA deadenylases. Genes & development *21*, 3135-3148.

Funk, A., Truong, K., Nagasaki, T., Torres, S., Floden, N., Balmori Melian, E., Edmonds, J., Dong, H., Shi, P.Y., and Khromykh, A.A. (2010). RNA structures required for production of subgenomic flavivirus RNA. Journal of virology *84*, 11407-11417.

Gaddam, D., Stevens, N., and Hollien, J. (2013). Comparison of mRNA localization and regulation during endoplasmic reticulum stress in Drosophila cells. Molecular biology of the cell *24*, 14-20.

Gagnon, K.T., Li, L., Chu, Y., Janowski, B.A., and Corey, D.R. (2014). RNAi factors are present and active in human cell nuclei. Cell reports *6*, 211-221.

Gaj, T., Gersbach, C.A., and Barbas, C.F., 3rd (2013). ZFN, TALEN, and CRISPR/Cas-based methods for genome engineering. Trends in biotechnology *31*, 397-405.

Gallie, D.R. (1998). A tale of two termini: a functional interaction between the termini of an mRNA is a prerequisite for efficient translation initiation. Gene *216*, 1-11.

Gallina, M.E., Xu, J., Dertinger, T., Aizer, A., Shav-Tal, Y., and Weiss, S. (2013). Resolving the spatial relationship between intracellular components by dual color super resolution optical fluctuations imaging (SOFI). Optical nanoscopy *2*.

Garcia, J.F., and Parker, R. (2015). MS2 coat proteins bound to yeast mRNAs block 5' to 3' degradation and trap mRNA decay products: implications for the localization of mRNAs by MS2-MCP system. Rna *21*, 1393-1395.

Garcia, J.F., and Parker, R. (2016). Ubiquitous accumulation of 3' mRNA decay fragments in Saccharomyces cerevisiae mRNAs with chromosomally integrated MS2 arrays. Rna *22*, 657-659.

Garcia-Martinez, J., Aranda, A., and Perez-Ortin, J.E. (2004). Genomic run-on evaluates transcription rates for all yeast genes and identifies gene regulatory mechanisms. Molecular cell *15*, 303-313.

Garneau, N.L., Wilusz, J., and Wilusz, C.J. (2007). The highways and byways of mRNA decay. Nature reviews Molecular cell biology *8*, 113-126.

Ghosh, S., and Jacobson, A. (2010). RNA decay modulates gene expression and controls its fidelity. Wiley interdisciplinary reviews RNA *1*, 351-361.

Gilks, N., Kedersha, N., Ayodele, M., Shen, L., Stoecklin, G., Dember, L.M., and Anderson, P. (2004). Stress granule assembly is mediated by prion-like aggregation of TIA-1. Molecular biology of the cell *15*, 5383-5398.

Godwin, A.R., Kojima, S., Green, C.B., and Wilusz, J. (2013). Kiss your tail goodbye: the role of PARN, Nocturnin, and Angel deadenylases in mRNA biology. Biochimica et biophysica acta *1829*, 571-579.

Grimm, J.B., English, B.P., Chen, J., Slaughter, J.P., Zhang, Z., Revyakin, A., Patel, R., Macklin, J.J., Normanno, D., Singer, R.H.*, et al.* (2015). A general method to improve fluorophores for live-cell and single-molecule microscopy. Nature methods *12*, 244-250, 243 p following 250.

Grimm, J.B., Muthusamy, A.K., Liang, Y., Brown, T.A., Lemon, W.C., Patel, R., Lu, R., Macklin, J.J., Keller, P.J., Ji, N.*, et al.* (2017). A general method to fine-tune fluorophores for live-cell and in vivo imaging. Nature methods *14*, 987-994.

Grunwald, D., and Singer, R.H. (2010). In vivo imaging of labelled endogenous beta-actin mRNA during nucleocytoplasmic transport. Nature *467*, 604-607.

Haase, A.D., Jaskiewicz, L., Zhang, H., Laine, S., Sack, R., Gatignol, A., and Filipowicz, W. (2005). TRBP, a regulator of cellular PKR and HIV-1 virus expression, interacts with Dicer and functions in RNA silencing. EMBO reports *6*, 961-967.

Haimovich, G., Medina, D.A., Causse, S.Z., Garber, M., Millan-Zambrano, G., Barkai, O., Chavez, S., Perez-Ortin, J.E., Darzacq, X., and Choder, M. (2013). Gene expression is circular: factors for mRNA degradation also foster mRNA synthesis. Cell *153*, 1000-1011.

Haimovich, G., Zabezhinsky, D., Haas, B., Slobodin, B., Purushothaman, P., Fan, L., Levin, J.Z., Nusbaum, C., and Gerst, J.E. (2016). Use of the MS2 aptamer and coat protein for RNA localization in yeast: A response to "MS2 coat proteins bound to yeast mRNAs block 5' to 3' degradation and trap mRNA decay products: implications for the localization of mRNAs by MS2-MCP system". Rna *22*, 660-666.

Halbach, F., Reichelt, P., Rode, M., and Conti, E. (2013). The yeast ski complex: crystal structure and RNA channeling to the exosome complex. Cell *154*, 814-826.

Halstead, J.M., Lionnet, T., Wilbertz, J.H., Wippich, F., Ephrussi, A., Singer, R.H., and Chao, J.A. (2015). Translation. An RNA biosensor for imaging the first round of translation from single cells to living animals. Science *347*, 1367-1671.

Hamilton, A., Voinnet, O., Chappell, L., and Baulcombe, D. (2002). Two classes of short interfering RNA in RNA silencing. The EMBO journal *21*, 4671-4679.

Hamilton, T.L., Stoneley, M., Spriggs, K.A., and Bushell, M. (2006). TOPs and their regulation. Biochemical Society transactions *34*, 12-16.

Hansen, T.B., Wiklund, E.D., Bramsen, J.B., Villadsen, S.B., Statham, A.L., Clark, S.J., and Kjems, J. (2011). miRNA-dependent gene silencing involving Ago2-mediated cleavage of a circular antisense RNA. The EMBO journal *30*, 4414-4422.

Hao, S., and Baltimore, D. (2009). The stability of mRNA influences the temporal order of the induction of genes encoding inflammatory molecules. Nature immunology *10*, 281-288.

Harding, H.P., Zhang, Y., Bertolotti, A., Zeng, H., and Ron, D. (2000). Perk is essential for translational regulation and cell survival during the unfolded protein response. Molecular cell *5*, 897-904.

Harrold, S., Genovese, C., Kobrin, B., Morrison, S.L., and Milcarek, C. (1991). A comparison of apparent mRNA half-life using kinetic labeling techniques vs decay following administration of transcriptional inhibitors. Analytical biochemistry *198*, 19-29.

Heinrich, S., Sidler, C.L., Azzalin, C.M., and Weis, K. (2017). Stem-loop RNA labeling can affect nuclear and cytoplasmic mRNA processing. Rna *23*, 134-141.

Herzog, V.A., Reichholf, B., Neumann, T., Rescheneder, P., Bhat, P., Burkard, T.R., Wlotzka, W., von Haeseler, A., Zuber, J., and Ameres, S.L. (2017). Thiol-linked alkylation of RNA to assess expression dynamics. Nature methods.

Hocine, S., Raymond, P., Zenklusen, D., Chao, J.A., and Singer, R.H. (2013). Single-molecule analysis of gene expression using two-color RNA labeling in live yeast. Nature methods *10*, 119-121.

Hoefig, K.P., Rath, N., Heinz, G.A., Wolf, C., Dameris, J., Schepers, A., Kremmer, E., Ansel, K.M., and Heissmeyer, V. (2013). Eri1 degrades the stem-loop of oligouridylated histone mRNAs to induce replication-dependent decay. Nature structural & molecular biology *20*, 73-81.

Hogg, J.R., and Goff, S.P. (2010). Upf1 senses 3'UTR length to potentiate mRNA decay. Cell *143*, 379-389.

Horvathova, I., Voigt, F., Kotrys, A.V., Zhan, Y., Artus-Revel, C.G., Eglinger, J., Stadler, M.B., Giorgetti, L., and Chao, J.A. (2017). The Dynamics of mRNA Turnover Revealed by Single-Molecule Imaging in Single Cells. Molecular cell.

Houseley, J., LaCava, J., and Tollervey, D. (2006). RNA-quality control by the exosome. Nature reviews Molecular cell biology *7*, 529-539.

Hu, W., Sweet, T.J., Chamnongpol, S., Baker, K.E., and Coller, J. (2009). Co-translational mRNA decay in Saccharomyces cerevisiae. Nature *461*, 225-229.

Hubstenberger, A., Courel, M., Benard, M., Souquere, S., Ernoult-Lange, M., Chouaib, R., Yi, Z., Morlot, J.B., Munier, A., Fradet, M.*, et al.* (2017). P-Body Purification Reveals the Condensation of Repressed mRNA Regulons. Molecular cell *68*, 144-157 e145.

Huntzinger, E., Kashima, I., Fauser, M., Sauliere, J., and Izaurralde, E. (2008). SMG6 is the catalytic endonuclease that cleaves mRNAs containing nonsense codons in metazoan. Rna *14*, 2609-2617.

Ishigaki, Y., Li, X., Serin, G., and Maquat, L.E. (2001). Evidence for a pioneer round of mRNA translation: mRNAs subject to nonsense-mediated decay in mammalian cells are bound by CBP80 and CBP20. Cell *106*, 607-617.

Ito-Harashima, S., Kuroha, K., Tatematsu, T., and Inada, T. (2007). Translation of the poly(A) tail plays crucial roles in nonstop mRNA surveillance via translation repression and protein destabilization by proteasome in yeast. Genes & development *21*, 519-524.

Jacobson, A., and Peltz, S.W. (1996). Interrelationships of the pathways of mRNA decay and translation in eukaryotic cells. Annual review of biochemistry *65*, 693-739.

Jagannath, A., and Wood, M.J. (2009). Localization of double-stranded small interfering RNA to cytoplasmic processing bodies is Ago2 dependent and results in up-regulation of GW182 and Argonaute-2. Molecular biology of the cell *20*, 521-529.

Jakymiw, A., Lian, S., Eystathioy, T., Li, S., Satoh, M., Hamel, J.C., Fritzler, M.J., and Chan, E.K. (2005). Disruption of GW bodies impairs mammalian RNA interference. Nature cell biology *7*, 1267-1274.

Janowski, B.A., Huffman, K.E., Schwartz, J.C., Ram, R., Nordsell, R., Shames, D.S., Minna, J.D., and Corey, D.R. (2006). Involvement of AGO1 and AGO2 in mammalian transcriptional silencing. Nature structural & molecular biology *13*, 787-792.

Janssen, H.L., Reesink, H.W., Lawitz, E.J., Zeuzem, S., Rodriguez-Torres, M., Patel, K., van der Meer, A.J., Patick, A.K., Chen, A., Zhou, Y.*, et al.* (2013). Treatment of HCV infection by targeting microRNA. The New England journal of medicine *368*, 1685-1694.

Jeffries, C.D., Fried, H.M., and Perkins, D.O. (2011). Nuclear and cytoplasmic localization of neural stem cell microRNAs. Rna *17*, 675-686.

Ji, P., Diederichs, S., Wang, W., Boing, S., Metzger, R., Schneider, P.M., Tidow, N., Brandt, B., Buerger, H., Bulk, E.*, et al.* (2003). MALAT-1, a novel noncoding RNA, and thymosin beta4 predict metastasis and survival in early-stage non-small cell lung cancer. Oncogene *22*, 8031-8041.

Jiao, X., Xiang, S., Oh, C., Martin, C.E., Tong, L., and Kiledjian, M. (2010). Identification of a quality-control mechanism for mRNA 5'-end capping. Nature *467*, 608-611.

Jinek, M., Coyle, S.M., and Doudna, J.A. (2011). Coupled 5' nucleotide recognition and processivity in Xrn1-mediated mRNA decay. Molecular cell *41*, 600-608.

Jones, C.I., Pashler, A.L., Towler, B.P., Robinson, S.R., and Newbury, S.F. (2016). RNA-seq reveals post-transcriptional regulation of Drosophila insulin-like peptide dilp8 and the neuropeptide-like precursor Nplp2 by the exoribonuclease Pacman/XRN1. Nucleic acids research *44*, 267-280.

Jones, C.I., Zabolotskaya, M.V., and Newbury, S.F. (2012). The 5' --> 3' exoribonuclease XRN1/Pacman and its functions in cellular processes and development. Wiley interdisciplinary reviews RNA *3*, 455-468.

Jopling, C.L., Schutz, S., and Sarnow, P. (2008). Position-dependent function for a tandem microRNA miR-122-binding site located in the hepatitis C virus RNA genome. Cell host & microbe *4*, 77-85.

Jopling, C.L., Yi, M., Lancaster, A.M., Lemon, S.M., and Sarnow, P. (2005). Modulation of hepatitis C virus RNA abundance by a liver-specific MicroRNA. Science *309*, 1577-1581.

Kawai, T., Fan, J., Mazan-Mamczarz, K., and Gorospe, M. (2004). Global mRNA stabilization preferentially linked to translational repression during the endoplasmic reticulum stress response. Molecular and cellular biology *24*, 6773-6787.

Kaygun, H., and Marzluff, W.F. (2005). Regulated degradation of replication-dependent histone mRNAs requires both ATR and Upf1. Nature structural & molecular biology *12*, 794-800.

Kebaara, B.W., and Atkin, A.L. (2009). Long 3'-UTRs target wild-type mRNAs for nonsense-mediated mRNA decay in Saccharomyces cerevisiae. Nucleic acids research *37*, 2771-2778.

Kedersha, N., and Anderson, P. (2002). Stress granules: sites of mRNA triage that regulate mRNA stability and translatability. Biochemical Society transactions *30*, 963-969.

Kedersha, N., Stoecklin, G., Ayodele, M., Yacono, P., Lykke-Andersen, J., Fritzler, M.J., Scheuner, D., Kaufman, R.J., Golan, D.E., and Anderson, P. (2005). Stress granules and processing bodies are dynamically linked sites of mRNP remodeling. The Journal of cell biology *169*, 871-884.

Kenzelmann, M., Maertens, S., Hergenhahn, M., Kueffer, S., Hotz-Wagenblatt, A., Li, L., Wang, S., Ittrich, C., Lemberger, T., Arribas, R.*, et al.* (2007). Microarray analysis of newly synthesized RNA in cells and animals. Proceedings of the National Academy of Sciences of the United States of America *104*, 6164-6169.

Khvorova, A., Reynolds, A., and Jayasena, S.D. (2003). Functional siRNAs and miRNAs exhibit strand bias. Cell *115*, 209-216.

Kim, D.H., Villeneuve, L.M., Morris, K.V., and Rossi, J.J. (2006). Argonaute-1 directs siRNA-mediated transcriptional gene silencing in human cells. Nature structural & molecular biology *13*, 793-797.

Kim, H.H., Abdelmohsen, K., Lal, A., Pullmann, R., Jr., Yang, X., Galban, S., Srikantan, S., Martindale, J.L., Blethrow, J., Shokat, K.M.*, et al.* (2008). Nuclear HuR accumulation through phosphorylation by Cdk1. Genes & development *22*, 1804-1815.

Kim, M., Krogan, N.J., Vasiljeva, L., Rando, O.J., Nedea, E., Greenblatt, J.F., and Buratowski, S. (2004). The yeast Rat1 exonuclease promotes transcription termination by RNA polymerase II. Nature *432*, 517-522.

Knuckles, P., Carl, S.H., Musheev, M., Niehrs, C., Wenger, A., and Buhler, M. (2017). RNA fate determination through cotranscriptional adenosine methylation and microprocessor binding. Nature structural & molecular biology *24*, 561-569.

Kok, K.H., Ng, M.H., Ching, Y.P., and Jin, D.Y. (2007). Human TRBP and PACT directly interact with each other and associate with dicer to facilitate the production of small interfering RNA. The Journal of biological chemistry *282*, 17649-17657.

Kolodziejczyk, A.A., Kim, J.K., Svensson, V., Marioni, J.C., and Teichmann, S.A. (2015). The technology and biology of single-cell RNA sequencing. Molecular cell *58*, 610-620.

Kramer, S. (2017). Simultaneous detection of mRNA transcription and decay intermediates by dual colour single mRNA FISH on subcellular resolution. Nucleic acids research *45*, e49.

Kulkarni, M., Ozgur, S., and Stoecklin, G. (2010). On track with P-bodies. Biochemical Society transactions *38*, 242-251.

Kuno, G., Chang, G.J., Tsuchiya, K.R., Karabatsos, N., and Cropp, C.B. (1998). Phylogeny of the genus Flavivirus. Journal of virology *72*, 73-83.

Kuzuoglu-Ozturk, D., Bhandari, D., Huntzinger, E., Fauser, M., Helms, S., and Izaurralde, E. (2016). miRISC and the CCR4-NOT complex silence mRNA targets independently of 43S ribosomal scanning. The EMBO journal *35*, 1186-1203.

Kwon, S.C., Nguyen, T.A., Choi, Y.G., Jo, M.H., Hohng, S., Kim, V.N., and Woo, J.S. (2016). Structure of Human DROSHA. Cell *164*, 81-90.

Labno, A., Tomecki, R., and Dziembowski, A. (2016a). Cytoplasmic RNA decay pathways - Enzymes and mechanisms. Biochimica et biophysica acta *1863*, 3125-3147.

Labno, A., Warkocki, Z., Kulinski, T., Krawczyk, P.S., Bijata, K., Tomecki, R., and Dziembowski, A. (2016b). Perlman syndrome nuclease DIS3L2 controls cytoplasmic non-coding RNAs and provides surveillance pathway for maturing snRNAs. Nucleic acids research *44*, 10437-10453.

Lackey, P.E., Welch, J.D., and Marzluff, W.F. (2016). TUT7 catalyzes the uridylation of the 3' end for rapid degradation of histone mRNA. Rna *22*, 1673-1688.

Lafarga, V., Cuadrado, A., Lopez de Silanes, I., Bengoechea, R., Fernandez-Capetillo, O., and Nebreda, A.R. (2009). p38 Mitogen-activated protein kinase- and HuR-dependent stabilization of p21(Cip1) mRNA mediates the G(1)/S checkpoint. Molecular and cellular biology *29*, 4341-4351.

Lanford, R.E., Hildebrandt-Eriksen, E.S., Petri, A., Persson, R., Lindow, M., Munk, M.E., Kauppinen, S., and Orum, H. (2010). Therapeutic silencing of microRNA-122 in primates with chronic hepatitis C virus infection. Science *327*, 198-201.

Larson, D.R., Fritzsch, C., Sun, L., Meng, X., Lawrence, D.S., and Singer, R.H. (2013). Direct observation of frequency modulated transcription in single cells using light activation. eLife *2*, e00750.

Larson, D.R., Zenklusen, D., Wu, B., Chao, J.A., and Singer, R.H. (2011). Real-time observation of transcription initiation and elongation on an endogenous yeast gene. Science *332*, 475-478.

Le Hir, H., Sauliere, J., and Wang, Z. (2016). The exon junction complex as a node of post-transcriptional networks. Nature reviews Molecular cell biology *17*, 41-54.

Lee, W.H., Lee, H.H., Vo, M.T., Kim, H.J., Ko, M.S., Im, Y.C., Min, Y.J., Lee, B.J., Cho, W.J., and Park, J.W. (2011). Casein kinase 2 regulates the mRNA-destabilizing activity of tristetraprolin. The Journal of biological chemistry *286*, 21577-21587.

Lerner, R.S., Seiser, R.M., Zheng, T., Lager, P.J., Reedy, M.C., Keene, J.D., and Nicchitta, C.V. (2003). Partitioning and translation of mRNAs encoding soluble proteins on membrane-bound ribosomes. Rna *9*, 1123-1137.

Li, C.H., Irmer, H., Gudjonsdottir-Planck, D., Freese, S., Salm, H., Haile, S., Estevez, A.M., and Clayton, C. (2006). Roles of a Trypanosoma brucei 5'->3' exoribonuclease homolog in mRNA degradation. Rna *12*, 2171-2186.

Li, H., Korennykh, A.V., Behrman, S.L., and Walter, P. (2010). Mammalian endoplasmic reticulum stress sensor IRE1 signals by dynamic clustering. Proceedings of the National Academy of Sciences of the United States of America *107*, 16113-16118.

Li, S., Liu, L., Zhuang, X., Yu, Y., Liu, X., Cui, X., Ji, L., Pan, Z., Cao, X., Mo, B.*, et al.* (2013a). MicroRNAs inhibit the translation of target mRNAs on the endoplasmic reticulum in Arabidopsis. Cell *153*, 562-574.

Li, Y., Masaki, T., Yamane, D., McGivern, D.R., and Lemon, S.M. (2013b). Competing and noncompeting activities of miR-122 and the 5' exonuclease Xrn1 in regulation of hepatitis C virus replication. Proceedings of the National Academy of Sciences of the United States of America *110*, 1881-1886.

Li, Y., Yamane, D., Masaki, T., and Lemon, S.M. (2015). The yin and yang of hepatitis C: synthesis and decay of hepatitis C virus RNA. Nature reviews Microbiology *13*, 544-558.

Liao, J.Y., Ma, L.M., Guo, Y.H., Zhang, Y.C., Zhou, H., Shao, P., Chen, Y.Q., and Qu, L.H. (2010). Deep sequencing of human nuclear and cytoplasmic small RNAs reveals an unexpectedly complex subcellular distribution of miRNAs and tRNA 3' trailers. PloS one *5*, e10563.

Lim, L.P., Lau, N.C., Garrett-Engele, P., Grimson, A., Schelter, J.M., Castle, J., Bartel, D.P., Linsley, P.S., and Johnson, J.M. (2005). Microarray analysis shows that some microRNAs downregulate large numbers of target mRNAs. Nature *433*, 769-773.

Lionnet, T., Czaplinski, K., Darzacq, X., Shav-Tal, Y., Wells, A.L., Chao, J.A., Park, H.Y., de Turris, V., Lopez-Jones, M., and Singer, R.H. (2011). A transgenic mouse for in vivo detection of endogenous labeled mRNA. Nature methods *8*, 165-170.

Liu, J., Carmell, M.A., Rivas, F.V., Marsden, C.G., Thomson, J.M., Song, J.J., Hammond, S.M., Joshua-Tor, L., and Hannon, G.J. (2004). Argonaute2 is the catalytic engine of mammalian RNAi. Science *305*, 1437-1441.

Liu, J., Rivas, F.V., Wohlschlegel, J., Yates, J.R., 3rd, Parker, R., and Hannon, G.J. (2005). A role for the P-body component GW182 in microRNA function. Nature cell biology *7*, 1261-1266.

Liu, N., and Pan, T. (2016). N6-methyladenosine-encoded epitranscriptomics. Nature structural & molecular biology *23*, 98-102.

Liu, R., and Moss, B. (2016). Opposing Roles of Double-Stranded RNA Effector Pathways and Viral Defense Proteins Revealed with CRISPR-Cas9 Knockout Cell Lines and Vaccinia Virus Mutants. Journal of virology *90*, 7864-7879.

Loflin, P.T., Chen, C.Y., Xu, N., and Shyu, A.B. (1999). Transcriptional pulsing approaches for analysis of mRNA turnover in mammalian cells. Methods *17*, 11-20.

Loschi, M., Leishman, C.C., Berardone, N., and Boccaccio, G.L. (2009). Dynein and kinesin regulate stress-granule and P-body dynamics. Journal of cell science *122*, 3973-3982.

Lu, J., Kobertz, W.R., and Deutsch, C. (2007). Mapping the electrostatic potential within the ribosomal exit tunnel. Journal of molecular biology *371*, 1378-1391.

Lubas, M., Damgaard, C.K., Tomecki, R., Cysewski, D., Jensen, T.H., and Dziembowski, A. (2013). Exonuclease hDIS3L2 specifies an exosome-independent 3'-5' degradation pathway of human cytoplasmic mRNA. The EMBO journal *32*, 1855-1868.

Lykke-Andersen, J. (2002). Identification of a human decapping complex associated with hUpf proteins in nonsense-mediated decay. Molecular and cellular biology *22*, 8114-8121.

Lykke-Andersen, S., Tomecki, R., Jensen, T.H., and Dziembowski, A. (2011). The eukaryotic RNA exosome: same scaffold but variable catalytic subunits. RNA biology *8*, 61-66.

Machlin, E.S., Sarnow, P., and Sagan, S.M. (2011). Masking the 5' terminal nucleotides of the hepatitis C virus genome by an unconventional microRNA-target RNA complex. Proceedings of the National Academy of Sciences of the United States of America *108*, 3193-3198.

Mahtani, K.R., Brook, M., Dean, J.L., Sully, G., Saklatvala, J., and Clark, A.R. (2001). Mitogen-activated protein kinase p38 controls the expression and posttranslational modification of tristetraprolin, a regulator of tumor necrosis factor alpha mRNA stability. Molecular and cellular biology *21*, 6461-6469.

Makino, D.L., Baumgartner, M., and Conti, E. (2013). Crystal structure of an RNA-bound 11-subunit eukaryotic exosome complex. Nature *495*, 70-75.

Malecki, M., Viegas, S.C., Carneiro, T., Golik, P., Dressaire, C., Ferreira, M.G., and Arraiano, C.M. (2013). The exoribonuclease Dis3L2 defines a novel eukaryotic RNA degradation pathway. The EMBO journal *32*, 1842-1854.

Manokaran, G., Finol, E., Wang, C., Gunaratne, J., Bahl, J., Ong, E.Z., Tan, H.C., Sessions, O.M., Ward, A.M., Gubler, D.J.*, et al.* (2015). Dengue subgenomic RNA binds TRIM25 to inhibit interferon expression for epidemiological fitness. Science *350*, 217-221.

Maquat, L.E., Tarn, W.Y., and Isken, O. (2010). The pioneer round of translation: features and functions. Cell *142*, 368-374.

Martin, R.M., Rino, J., Carvalho, C., Kirchhausen, T., and Carmo-Fonseca, M. (2013). Live-cell visualization of pre-mRNA splicing with single-molecule sensitivity. Cell reports *4*, 1144-1155.

Marzluff, W.F., Wagner, E.J., and Duronio, R.J. (2008). Metabolism and regulation of canonical histone mRNAs: life without a poly(A) tail. Nature reviews Genetics *9*, 843-854.

Mathys, H., Basquin, J., Ozgur, S., Czarnocki-Cieciura, M., Bonneau, F., Aartse, A., Dziembowski, A., Nowotny, M., Conti, E., and Filipowicz, W. (2014). Structural and biochemical insights to the role of the CCR4-NOT complex and DDX6 ATPase in microRNA repression. Molecular cell *54*, 751-765.

Matsushita, K., Takeuchi, O., Standley, D.M., Kumagai, Y., Kawagoe, T., Miyake, T., Satoh, T., Kato, H., Tsujimura, T., Nakamura, H.*, et al.* (2009). Zc3h12a is an RNase essential for controlling immune responses by regulating mRNA decay. Nature *458*, 1185-1190.

Mauxion, F., Faux, C., and Seraphin, B. (2008). The BTG2 protein is a general activator of mRNA deadenylation. The EMBO journal *27*, 1039-1048.

Mazzoni, C., D'Addario, I., and Falcone, C. (2007). The C-terminus of the yeast Lsm4p is required for the association to P-bodies. FEBS letters *581*, 4836-4840.

McEwen, E., Kedersha, N., Song, B., Scheuner, D., Gilks, N., Han, A., Chen, J.J., Anderson, P., and Kaufman, R.J. (2005). Heme-regulated inhibitor kinase-mediated phosphorylation of eukaryotic translation initiation factor 2 inhibits translation, induces stress granule formation, and mediates survival upon arsenite exposure. The Journal of biological chemistry *280*, 16925-16933.

Medina, D.A., Jordan-Pla, A., Millan-Zambrano, G., Chavez, S., Choder, M., and Perez-Ortin, J.E. (2014). Cytoplasmic 5'-3' exonuclease Xrn1p is also a genome-wide transcription factor in yeast. Frontiers in genetics *5*, 1.

Medioni, C., Mowry, K., and Besse, F. (2012). Principles and roles of mRNA localization in animal development. Development *139*, 3263-3276.

Meister, G., Landthaler, M., Patkaniowska, A., Dorsett, Y., Teng, G., and Tuschl, T. (2004). Human Argonaute2 mediates RNA cleavage targeted by miRNAs and siRNAs. Molecular cell *15*, 185-197.

Melvin, W.T., Milne, H.B., Slater, A.A., Allen, H.J., and Keir, H.M. (1978). Incorporation of 6-thioguanosine and 4-thiouridine into RNA. Application to isolation of newly synthesised RNA by affinity chromatography. European journal of biochemistry *92*, 373-379.

Meyer, K.D., and Jaffrey, S.R. (2014). The dynamic epitranscriptome: N6-methyladenosine and gene expression control. Nature reviews Molecular cell biology *15*, 313-326.

Meyer, K.D., Saletore, Y., Zumbo, P., Elemento, O., Mason, C.E., and Jaffrey, S.R. (2012). Comprehensive analysis of mRNA methylation reveals enrichment in 3' UTRs and near stop codons. Cell *149*, 1635-1646.

Miki, T.S., Carl, S.H., and Grosshans, H. (2017). Two distinct transcription termination modes dictated by promoters. Genes & development *31*, 1870-1879.

Milac, A.L., Bojarska, E., and Wypijewska del Nogal, A. (2014). Decapping Scavenger (DcpS) enzyme: advances in its structure, activity and roles in the cap-dependent mRNA metabolism. Biochimica et biophysica acta *1839*, 452-462.

Miller, C., Schwalb, B., Maier, K., Schulz, D., Dumcke, S., Zacher, B., Mayer, A., Sydow, J., Marcinowski, L., Dolken, L.*, et al.* (2011). Dynamic transcriptome analysis measures rates of mRNA synthesis and decay in yeast. Molecular systems biology *7*, 458.

Mino, T., Murakawa, Y., Fukao, A., Vandenbon, A., Wessels, H.H., Ori, D., Uehata, T., Tartey, S., Akira, S., Suzuki, Y.*, et al.* (2015). Regnase-1 and Roquin Regulate a Common Element in Inflammatory mRNAs by Spatiotemporally Distinct Mechanisms. Cell *161*, 1058-1073.

Mitton-Fry, R.M., DeGregorio, S.J., Wang, J., Steitz, T.A., and Steitz, J.A. (2010). Poly(A) tail recognition by a viral RNA element through assembly of a triple helix. Science *330*, 1244-1247.

Moon, S.L., Anderson, J.R., Kumagai, Y., Wilusz, C.J., Akira, S., Khromykh, A.A., and Wilusz, J. (2012). A noncoding RNA produced by arthropod-borne flaviviruses inhibits the cellular exoribonuclease XRN1 and alters host mRNA stability. Rna *18*, 2029-2040.

Moon, S.L., Blackinton, J.G., Anderson, J.R., Dozier, M.K., Dodd, B.J., Keene, J.D., Wilusz, C.J., Bradrick, S.S., and Wilusz, J. (2015a). XRN1 stalling in the 5' UTR of Hepatitis C virus and Bovine Viral Diarrhea virus is associated with dysregulated host mRNA stability. PLoS pathogens *11*, e1004708.

Moon, S.L., Dodd, B.J., Brackney, D.E., Wilusz, C.J., Ebel, G.D., and Wilusz, J. (2015b). Flavivirus sfRNA suppresses antiviral RNA interference in cultured cells and mosquitoes and directly interacts with the RNAi machinery. Virology *485*, 322-329.

Moraes, K.C., Wilusz, C.J., and Wilusz, J. (2006). CUG-BP binds to RNA substrates and recruits PARN deadenylase. Rna *12*, 1084-1091.

Morgan, M., Much, C., DiGiacomo, M., Azzi, C., Ivanova, I., Vitsios, D.M., Pistolic, J., Collier, P., Moreira, P.N., Benes, V.*, et al.* (2017). mRNA 3' uridylation and poly(A) tail length sculpt the mammalian maternal transcriptome. Nature *548*, 347-351.

Morisaki, T., Lyon, K., DeLuca, K.F., DeLuca, J.G., English, B.P., Zhang, Z., Lavis, L.D., Grimm, J.B., Viswanathan, S., Looger, L.L.*, et al.* (2016). Real-time quantification of single RNA translation dynamics in living cells. Science *352*, 1425-1429.

Mortimer, S.A., and Doudna, J.A. (2013). Unconventional miR-122 binding stabilizes the HCV genome by forming a trimolecular RNA structure. Nucleic acids research *41*, 4230-4240.

Muckenthaler, M.U., Rivella, S., Hentze, M.W., and Galy, B. (2017). A Red Carpet for Iron Metabolism. Cell *168*, 344-361.

Muhlrad, D., Decker, C.J., and Parker, R. (1994). Deadenylation of the unstable mRNA encoded by the yeast MFA2 gene leads to decapping followed by 5'-->3' digestion of the transcript. Genes & development *8*, 855-866.

Mullen, T.E., and Marzluff, W.F. (2008). Degradation of histone mRNA requires oligouridylation followed by decapping and simultaneous degradation of the mRNA both 5' to 3' and 3' to 5'. Genes & development *22*, 50-65.

Muller-McNicoll, M., and Neugebauer, K.M. (2013). How cells get the message: dynamic assembly and function of mRNA-protein complexes. Nature reviews Genetics *14*, 275-287.

Murray, E.L., and Schoenberg, D.R. (2007). A+U-rich instability elements differentially activate 5'-3' and 3'-5' mRNA decay. Molecular and cellular biology *27*, 2791-2799.

Murray, E.L., and Schoenberg, D.R. (2008). Assays for determining poly(A) tail length and the polarity of mRNA decay in mammalian cells. Methods in enzymology *448*, 483-504.

Nagarajan, V.K., Jones, C.I., Newbury, S.F., and Green, P.J. (2013). XRN 5'-->3' exoribonucleases: structure, mechanisms and functions. Biochimica et biophysica acta *1829*, 590-603.

Nelles, D.A., Fang, M.Y., O'Connell, M.R., Xu, J.L., Markmiller, S.J., Doudna, J.A., and Yeo, G.W. (2016). Programmable RNA Tracking in Live Cells with CRISPR/Cas9. Cell *165*, 488-496.

Neve, J., Patel, R., Wang, Z., Louey, A., and Furger, A.M. (2017). Cleavage and polyadenylation: Ending the message expands gene regulation. RNA biology *14*, 865-890.

Newbury, S., and Woollard, A. (2004). The 5'-3' exoribonuclease xrn-1 is essential for ventral epithelial enclosure during C. elegans embryogenesis. Rna *10*, 59-65.

Ng, K., Daigle, N., Bancaud, A., Ohhata, T., Humphreys, P., Walker, R., Ellenberg, J., and Wutz, A. (2011). A system for imaging the regulatory noncoding Xist RNA in living mouse embryonic stem cells. Molecular biology of the cell *22*, 2634-2645.

Nicholson, P., and Muhlemann, O. (2010). Cutting the nonsense: the degradation of PTC-containing mRNAs. Biochemical Society transactions *38*, 1615-1620.

Niepmann, M. (2013). Hepatitis C virus RNA translation. Current topics in microbiology and immunology *369*, 143-166.

Nishi, K., Nishi, A., Nagasawa, T., and Ui-Tei, K. (2013). Human TNRC6A is an Argonaute-navigator protein for microRNA-mediated gene silencing in the nucleus. Rna *19*, 17-35.

Nover, L., Scharf, K.D., and Neumann, D. (1989). Cytoplasmic heat shock granules are formed from precursor particles and are associated with a specific set of mRNAs. Molecular and cellular biology *9*, 1298-1308.

Nyathi, Y., Wilkinson, B.M., and Pool, M.R. (2013). Co-translational targeting and translocation of proteins to the endoplasmic reticulum. Biochimica et biophysica acta *1833*, 2392-2402.

O'Connell, M.R., Oakes, B.L., Sternberg, S.H., East-Seletsky, A., Kaplan, M., and Doudna, J.A. (2014). Programmable RNA recognition and cleavage by CRISPR/Cas9. Nature *516*, 263-266.

Ohrt, T., Mutze, J., Staroske, W., Weinmann, L., Hock, J., Crell, K., Meister, G., and Schwille, P. (2008). Fluorescence correlation spectroscopy and fluorescence cross-correlation spectroscopy reveal the cytoplasmic origination of loaded nuclear RISC in vivo in human cells. Nucleic acids research *36*, 6439-6449.

Oikawa, D., Tokuda, M., Hosoda, A., and Iwawaki, T. (2010). Identification of a consensus element recognized and cleaved by IRE1 alpha. Nucleic acids research *38*, 6265-6273.

Okamura, K., Hagen, J.W., Duan, H., Tyler, D.M., and Lai, E.C. (2007). The mirtron pathway generates microRNA-class regulatory RNAs in Drosophila. Cell *130*, 89-100.

Orban, T.I., and Izaurralde, E. (2005). Decay of mRNAs targeted by RISC requires XRN1, the Ski complex, and the exosome. Rna *11*, 459-469.

Ozgur, S., Basquin, J., Kamenska, A., Filipowicz, W., Standart, N., and Conti, E. (2015). Structure of a Human 4E-T/DDX6/CNOT1 Complex Reveals the Different Interplay of DDX6-Binding Proteins with the CCR4-NOT Complex. Cell reports *13*, 703-711.

Palusa, S., Ndaluka, C., Bowen, R.A., Wilusz, C.J., and Wilusz, J. (2012). The 3' untranslated region of the rabies virus glycoprotein mRNA specifically interacts with cellular PCBP2 protein and promotes transcript stability. PloS one *7*, e33561.

Park, E., and Maquat, L.E. (2013). Staufen-mediated mRNA decay. Wiley interdisciplinary reviews RNA *4*, 423-435.

Pelechano, V., Wei, W., and Steinmetz, L.M. (2015). Widespread Co-translational RNA Decay Reveals Ribosome Dynamics. Cell *161*, 1400-1412.

Pijlman, G.P., Funk, A., Kondratieva, N., Leung, J., Torres, S., van der Aa, L., Liu, W.J., Palmenberg, A.C., Shi, P.Y., Hall, R.A.*, et al.* (2008). A highly structured, nuclease-resistant, noncoding RNA produced by flaviviruses is required for pathogenicity. Cell host & microbe *4*, 579-591.

Pilkington, G.R., and Parker, R. (2008). Pat1 contains distinct functional domains that promote P-body assembly and activation of decapping. Molecular and cellular biology *28*, 1298-1312.

Pillai, R.S., Bhattacharyya, S.N., Artus, C.G., Zoller, T., Cougot, N., Basyuk, E., Bertrand, E., and Filipowicz, W. (2005). Inhibition of translational initiation by Let-7 MicroRNA in human cells. Science *309*, 1573-1576.

Poole, T.L., and Stevens, A. (1997). Structural modifications of RNA influence the 5' exoribonucleolytic hydrolysis by XRN1 and HKE1 of Saccharomyces cerevisiae. Biochemical and biophysical research communications *235*, 799-805.

Preker, P., Nielsen, J., Kammler, S., Lykke-Andersen, S., Christensen, M.S., Mapendano, C.K., Schierup, M.H., and Jensen, T.H. (2008). RNA exosome depletion reveals transcription upstream of active human promoters. Science *322*, 1851-1854.

Presnyak, V., Alhusaini, N., Chen, Y.H., Martin, S., Morris, N., Kline, N., Olson, S., Weinberg, D., Baker, K.E., Graveley, B.R.*, et al.* (2015). Codon optimality is a major determinant of mRNA stability. Cell *160*, 1111-1124.

Pyhtila, B., Zheng, T., Lager, P.J., Keene, J.D., Reedy, M.C., and Nicchitta, C.V. (2008). Signal sequence- and translation-independent mRNA localization to the endoplasmic reticulum. Rna *14*, 445-453.

Rabani, M., Levin, J.Z., Fan, L., Adiconis, X., Raychowdhury, R., Garber, M., Gnirke, A., Nusbaum, C., Hacohen, N., Friedman, N.*, et al.* (2011). Metabolic labeling of RNA uncovers principles of RNA production and degradation dynamics in mammalian cells. Nature biotechnology *29*, 436-442.

Radhakrishnan, A., Chen, Y.H., Martin, S., Alhusaini, N., Green, R., and Coller, J. (2016). The DEAD-Box Protein Dhh1p Couples mRNA Decay and Translation by Monitoring Codon Optimality. Cell *167*, 122-132 e129.

Raj, A., Peskin, C.S., Tranchina, D., Vargas, D.Y., and Tyagi, S. (2006). Stochastic mRNA synthesis in mammalian cells. PLoS biology *4*, e309.

Raj, A., van den Bogaard, P., Rifkin, S.A., van Oudenaarden, A., and Tyagi, S. (2008). Imaging individual mRNA molecules using multiple singly labeled probes. Nature methods *5*, 877-879.

Raj, A., and van Oudenaarden, A. (2008). Nature, nurture, or chance: stochastic gene expression and its consequences. Cell *135*, 216-226.

Reid, D.W., and Nicchitta, C.V. (2012). Primary role for endoplasmic reticulum-bound ribosomes in cellular translation identified by ribosome profiling. The Journal of biological chemistry *287*, 5518-5527.

Reijns, M.A., Alexander, R.D., Spiller, M.P., and Beggs, J.D. (2008). A role for Q/N-rich aggregation-prone regions in P-body localization. Journal of cell science *121*, 2463-2472.

Rissland, O.S., and Norbury, C.J. (2009). Decapping is preceded by 3' uridylation in a novel pathway of bulk mRNA turnover. Nature structural & molecular biology *16*, 616-623.

Ruby, J.G., Jan, C.H., and Bartel, D.P. (2007). Intronic microRNA precursors that bypass Drosha processing. Nature *448*, 83-86.

Rudel, S., Flatley, A., Weinmann, L., Kremmer, E., and Meister, G. (2008). A multifunctional human Argonaute2-specific monoclonal antibody. Rna *14*, 1244-1253.

Saetrom, P., Heale, B.S., Snove, O., Jr., Aagaard, L., Alluin, J., and Rossi, J.J. (2007). Distance constraints between microRNA target sites dictate efficacy and cooperativity. Nucleic acids research *35*, 2333-2342.

Sahoo, M.R., Gaikwad, S., Khuperkar, D., Ashok, M., Helen, M., Yadav, S.K., Singh, A., Magre, I., Deshmukh, P., Dhanvijay, S.*, et al.* (2017). Nup358 binds to AGO proteins through its SUMO-interacting motifs and promotes the association of target mRNA with miRISC. EMBO reports *18*, 241-263.

Schmidlin, M., Lu, M., Leuenberger, S.A., Stoecklin, G., Mallaun, M., Gross, B., Gherzi, R., Hess, D., Hemmings, B.A., and Moroni, C. (2004). The ARE-dependent mRNA-destabilizing activity of BRF1 is regulated by protein kinase B. The EMBO journal *23*, 4760-4769.

Schmidt, M.J., West, S., and Norbury, C.J. (2011). The human cytoplasmic RNA terminal U-transferase ZCCHC11 targets histone mRNAs for degradation. Rna *17*, 39-44.

Schmiedel, J.M., Klemm, S.L., Zheng, Y., Sahay, A., Bluthgen, N., Marks, D.S., and van Oudenaarden, A. (2015). Gene expression. MicroRNA control of protein expression noise. Science *348*, 128-132.

Schnettler, E., Sterken, M.G., Leung, J.Y., Metz, S.W., Geertsema, C., Goldbach, R.W., Vlak, J.M., Kohl, A., Khromykh, A.A., and Pijlman, G.P. (2012). Noncoding flavivirus RNA displays RNA interference suppressor activity in insect and Mammalian cells. Journal of virology *86*, 13486-13500.

Schuessler, A., Funk, A., Lazear, H.M., Cooper, D.A., Torres, S., Daffis, S., Jha, B.K., Kumagai, Y., Takeuchi, O., Hertzog, P.*, et al.* (2012). West Nile virus noncoding subgenomic RNA contributes to viral evasion of the type I interferon-mediated antiviral response. Journal of virology *86*, 5708-5718.

Schwanhausser, B., Busse, D., Li, N., Dittmar, G., Schuchhardt, J., Wolf, J., Chen, W., and Selbach, M. (2011). Global quantification of mammalian gene expression control. Nature *473*, 337-342.

Schwarz, D.S., and Blower, M.D. (2014). The calcium-dependent ribonuclease XendoU promotes ER network formation through local RNA degradation. The Journal of cell biology *207*, 41-57.

Schwarz, D.S., Hutvagner, G., Du, T., Xu, Z., Aronin, N., and Zamore, P.D. (2003). Asymmetry in the assembly of the RNAi enzyme complex. Cell *115*, 199-208.

Seiser, C., Posch, M., Thompson, N., and Kuhn, L.C. (1995). Effect of transcription inhibitors on the iron-dependent degradation of transferrin receptor mRNA. The Journal of biological chemistry *270*, 29400-29406.

Serman, A., Le Roy, F., Aigueperse, C., Kress, M., Dautry, F., and Weil, D. (2007). GW body disassembly triggered by siRNAs independently of their silencing activity. Nucleic acids research *35*, 4715-4727.

Shalem, O., Groisman, B., Choder, M., Dahan, O., and Pilpel, Y. (2011). Transcriptome kinetics is governed by a genome-wide coupling of mRNA production and degradation: a role for RNA Pol II. PLoS genetics *7*, e1002273.

Shaner, N.C., Steinbach, P.A., and Tsien, R.Y. (2005). A guide to choosing fluorescent proteins. Nature methods *2*, 905-909.

Shen, B., and Goodman, H.M. (2004). Uridine addition after microRNA-directed cleavage. Science *306*, 997.

Sheth, U., and Parker, R. (2003). Decapping and decay of messenger RNA occur in cytoplasmic processing bodies. Science *300*, 805-808.

Shimakami, T., Yamane, D., Jangra, R.K., Kempf, B.J., Spaniel, C., Barton, D.J., and Lemon, S.M. (2012). Stabilization of hepatitis C virus RNA by an Ago2-miR-122 complex. Proceedings of the National Academy of Sciences of the United States of America *109*, 941-946.

Siomi, M.C., Sato, K., Pezic, D., and Aravin, A.A. (2011). PIWI-interacting small RNAs: the vanguard of genome defence. Nature reviews Molecular cell biology *12*, 246-258.

Sivan, G., Kedersha, N., and Elroy-Stein, O. (2007). Ribosomal slowdown mediates translational arrest during cellular division. Molecular and cellular biology *27*, 6639-6646.

Sokoloski, K.J., Dickson, A.M., Chaskey, E.L., Garneau, N.L., Wilusz, C.J., and Wilusz, J. (2010). Sindbis virus usurps the cellular HuR protein to stabilize its transcripts and promote productive infections in mammalian and mosquito cells. Cell host & microbe *8*, 196-207.

Song, M.G., and Kiledjian, M. (2007). 3' Terminal oligo U-tract-mediated stimulation of decapping. Rna *13*, 2356-2365.

Spies, N., Burge, C.B., and Bartel, D.P. (2013). 3' UTR-isoform choice has limited influence on the stability and translational efficiency of most mRNAs in mouse fibroblasts. Genome research *23*, 2078-2090.

Stalder, L., Heusermann, W., Sokol, L., Trojer, D., Wirz, J., Hean, J., Fritzsche, A., Aeschimann, F., Pfanzagl, V., Basselet, P.*, et al.* (2013). The rough endoplasmatic reticulum is a central nucleation site of siRNA-mediated RNA silencing. The EMBO journal *32*, 1115-1127.

Stalder, L., and Muhlemann, O. (2009). Processing bodies are not required for mammalian nonsense-mediated mRNA decay. Rna *15*, 1265-1273.

Stevens, A. (1980). Purification and characterization of a Saccharomyces cerevisiae exoribonuclease which yields 5'-mononucleotides by a 5' leads to 3' mode of hydrolysis. The Journal of biological chemistry *255*, 3080-3085.

Stoecklin, G., Mayo, T., and Anderson, P. (2006). ARE-mRNA degradation requires the 5'-3' decay pathway. EMBO reports *7*, 72-77.

Stohr, N., Lederer, M., Reinke, C., Meyer, S., Hatzfeld, M., Singer, R.H., and Huttelmaier, S. (2006). ZBP1 regulates mRNA stability during cellular stress. The Journal of cell biology *175*, 527-534.

Su, H., Trombly, M.I., Chen, J., and Wang, X. (2009). Essential and overlapping functions for mammalian Argonautes in microRNA silencing. Genes & development *23*, 304-317.

Sun, M., Schwalb, B., Pirkl, N., Maier, K.C., Schenk, A., Failmezger, H., Tresch, A., and Cramer, P. (2013). Global analysis of eukaryotic mRNA degradation reveals Xrn1-dependent buffering of transcript levels. Molecular cell *52*, 52-62.

Sun, M., Schwalb, B., Schulz, D., Pirkl, N., Etzold, S., Lariviere, L., Maier, K.C., Seizl, M., Tresch, A., and Cramer, P. (2012). Comparative dynamic transcriptome analysis (cDTA) reveals mutual feedback between mRNA synthesis and degradation. Genome research *22*, 1350-1359.

Sun, R., Lin, S.F., Gradoville, L., and Miller, G. (1996). Polyadenylylated nuclear RNA encoded by Kaposi sarcoma-associated herpesvirus. Proceedings of the National Academy of Sciences of the United States of America *93*, 11883-11888.

Sweet, E.S., Previtera, M.L., Fernandez, J.R., Charych, E.I., Tseng, C.Y., Kwon, M., Starovoytov, V., Zheng, J.Q., and Firestein, B.L. (2011). PSD-95 alters microtubule dynamics via an association with EB3. The Journal of neuroscience : the official journal of the Society for Neuroscience *31*, 1038-1047.

Tadros, W., Goldman, A.L., Babak, T., Menzies, F., Vardy, L., Orr-Weaver, T., Hughes, T.R., Westwood, J.T., Smibert, C.A., and Lipshitz, H.D. (2007). SMAUG is a major regulator of maternal mRNA destabilization in Drosophila and its translation is activated by the PAN GU kinase. Developmental cell *12*, 143-155.

Tan, D., Marzluff, W.F., Dominski, Z., and Tong, L. (2013). Structure of histone mRNA stem-loop, human stem-loop binding protein, and 3'hExo ternary complex. Science *339*, 318-321.

Tani, H., Mizutani, R., Salam, K.A., Tano, K., Ijiri, K., Wakamatsu, A., Isogai, T., Suzuki, Y., and Akimitsu, N. (2012). Genome-wide determination of RNA stability reveals hundreds of short-lived noncoding transcripts in mammals. Genome research *22*, 947-956.

Teixeira, D., Sheth, U., Valencia-Sanchez, M.A., Brengues, M., and Parker, R. (2005). Processing bodies require RNA for assembly and contain nontranslating mRNAs. Rna *11*, 371-382.

Thapar, R., and Denmon, A.P. (2013). Signaling pathways that control mRNA turnover. Cellular signalling *25*, 1699-1710.

Thibault, P.A., Huys, A., Amador-Canizares, Y., Gailius, J.E., Pinel, D.E., and Wilson, J.A. (2015). Regulation of Hepatitis C Virus Genome Replication by Xrn1 and MicroRNA-122 Binding to Individual Sites in the 5' Untranslated Region. Journal of virology *89*, 6294-6311.

Tirasophon, W., Lee, K., Callaghan, B., Welihinda, A., and Kaufman, R.J. (2000). The endoribonuclease activity of mammalian IRE1 autoregulates its mRNA and is required for the unfolded protein response. Genes & development *14*, 2725-2736.

Tomecki, R., and Dziembowski, A. (2010). Novel endoribonucleases as central players in various pathways of eukaryotic RNA metabolism. Rna *16*, 1692-1724.

Tourriere, H., Gallouzi, I.E., Chebli, K., Capony, J.P., Mouaikel, J., van der Geer, P., and Tazi, J. (2001). RasGAP-associated endoribonuclease G3Bp: selective RNA degradation and phosphorylation-dependent localization. Molecular and cellular biology *21*, 7747-7760.

Trcek, T., Larson, D.R., Moldon, A., Query, C.C., and Singer, R.H. (2011). Single-molecule mRNA decay measurements reveal promoter- regulated mRNA stability in yeast. Cell *147*, 1484-1497.

Trcek, T., Sato, H., Singer, R.H., and Maquat, L.E. (2013). Temporal and spatial characterization of nonsense-mediated mRNA decay. Genes & development *27*, 541-551.

Ustianenko, D., Pasulka, J., Feketova, Z., Bednarik, L., Zigackova, D., Fortova, A., Zavolan, M., and Vanacova, S. (2016). TUT-DIS3L2 is a mammalian surveillance pathway for aberrant structured non-coding RNAs. The EMBO journal *35*, 2179-2191.

van Dijk, E., Cougot, N., Meyer, S., Babajko, S., Wahle, E., and Seraphin, B. (2002). Human Dcp2: a catalytically active mRNA decapping enzyme located in specific cytoplasmic structures. The EMBO journal *21*, 6915-6924.

van Dijk, E.L., Chen, C.L., d'Aubenton-Carafa, Y., Gourvennec, S., Kwapisz, M., Roche, V., Bertrand, C., Silvain, M., Legoix-Ne, P., Loeillet, S.*, et al.* (2011). XUTs are a class of Xrn1-sensitive antisense regulatory non-coding RNA in yeast. Nature *475*, 114-117.

Villordo, S.M., Filomatori, C.V., Sanchez-Vargas, I., Blair, C.D., and Gamarnik, A.V. (2015). Dengue virus RNA structure specialization facilitates host adaptation. PLoS pathogens *11*, e1004604.

Vlasova, I.A., Tahoe, N.M., Fan, D., Larsson, O., Rattenbacher, B., Sternjohn, J.R., Vasdewani, J., Karypis, G., Reilly, C.S., Bitterman, P.B.*, et al.* (2008). Conserved GU-rich elements mediate mRNA decay by binding to CUG-binding protein 1. Molecular cell *29*, 263-270.

Vlasova-St Louis, I., and Bohjanen, P.R. (2011). Coordinate regulation of mRNA decay networks by GU-rich elements and CELF1. Current opinion in genetics & development *21*, 444-451.

von Roretz, C., Di Marco, S., Mazroui, R., and Gallouzi, I.E. (2011). Turnover of AU-rich-containing mRNAs during stress: a matter of survival. Wiley interdisciplinary reviews RNA *2*, 336-347.

Waldron, J.A., Jones, C.I., Towler, B.P., Pashler, A.L., Grima, D.P., Hebbes, S., Crossman, S.H., Zabolotskaya, M.V., and Newbury, S.F. (2015). Xrn1/Pacman affects apoptosis and regulates expression of hid and reaper. Biology open *4*, 649-660.

Wang, C., Han, B., Zhou, R., and Zhuang, X. (2016). Real-Time Imaging of Translation on Single mRNA Transcripts in Live Cells. Cell *165*, 990-1001.

Wang, Z., and Kiledjian, M. (2000). Identification of an erythroid-enriched endoribonuclease activity involved in specific mRNA cleavage. The EMBO journal *19*, 295-305.

Weick, E.M., and Miska, E.A. (2014). piRNAs: from biogenesis to function. Development *141*, 3458-3471.

Weil, T.T., Parton, R.M., and Davis, I. (2010). Making the message clear: visualizing mRNA localization. Trends in cell biology *20*, 380-390.

Weinmann, L., Hock, J., Ivacevic, T., Ohrt, T., Mutze, J., Schwille, P., Kremmer, E., Benes, V., Urlaub, H., and Meister, G. (2009). Importin 8 is a gene silencing factor that targets argonaute proteins to distinct mRNAs. Cell *136*, 496-507.

Wells, S.E., Hillner, P.E., Vale, R.D., and Sachs, A.B. (1998). Circularization of mRNA by eukaryotic translation initiation factors. Molecular cell *2*, 135-140.

West, S., Gromak, N., and Proudfoot, N.J. (2004). Human 5' --> 3' exonuclease Xrn2 promotes transcription termination at co-transcriptional cleavage sites. Nature *432*, 522-525.

Wilczynska, A., Aigueperse, C., Kress, M., Dautry, F., and Weil, D. (2005). The translational regulator CPEB1 provides a link between dcp1 bodies and stress granules. Journal of cell science *118*, 981-992.

Wilson, G.M., Lu, J., Sutphen, K., Sun, Y., Huynh, Y., and Brewer, G. (2003). Regulation of A + U-rich element-directed mRNA turnover involving reversible phosphorylation of AUF1. The Journal of biological chemistry *278*, 33029-33038.

Wilusz, J.E., JnBaptiste, C.K., Lu, L.Y., Kuhn, C.D., Joshua-Tor, L., and Sharp, P.A. (2012). A triple helix stabilizes the 3' ends of long noncoding RNAs that lack poly(A) tails. Genes & development *26*, 2392-2407.

Wu, B., Eliscovich, C., Yoon, Y.J., and Singer, R.H. (2016). Translation dynamics of single mRNAs in live cells and neurons. Science *352*, 1430-1435.

Wu, L., Fan, J., and Belasco, J.G. (2006). MicroRNAs direct rapid deadenylation of mRNA. Proceedings of the National Academy of Sciences of the United States of America *103*, 4034-4039.

Wu, P.H., Isaji, M., and Carthew, R.W. (2013). Functionally diverse microRNA effector complexes are regulated by extracellular signaling. Molecular cell *52*, 113-123.

Wyers, F., Rougemaille, M., Badis, G., Rousselle, J.C., Dufour, M.E., Boulay, J., Regnault, B., Devaux, F., Namane, A., Seraphin, B.*, et al.* (2005). Cryptic pol II transcripts are degraded by a nuclear quality control pathway involving a new poly(A) polymerase. Cell *121*, 725-737.

Xu, K., Lin, J., Zandi, R., Roth, J.A., and Ji, L. (2016). MicroRNA-mediated target mRNA cleavage and 3'-uridylation in human cells. Scientific reports *6*, 30242.

Xu, N., Loflin, P., Chen, C.Y., and Shyu, A.B. (1998). A broader role for AU-rich element-mediated mRNA turnover revealed by a new transcriptional pulse strategy. Nucleic acids research *26*, 558-565.

Yamagishi, R., Hosoda, N., and Hoshino, S. (2014). Arsenite inhibits mRNA deadenylation through proteolytic degradation of Tob and Pan3. Biochemical and biophysical research communications *455*, 323-331.

Yamashita, A., Chang, T.C., Yamashita, Y., Zhu, W., Zhong, Z., Chen, C.Y., and Shyu, A.B. (2005). Concerted action of poly(A) nucleases and decapping enzyme in mammalian mRNA turnover. Nature structural & molecular biology *12*, 1054-1063.

Yan, X., Hoek, T.A., Vale, R.D., and Tanenbaum, M.E. (2016). Dynamics of Translation of Single mRNA Molecules In Vivo. Cell *165*, 976-989.

Yang, E., van Nimwegen, E., Zavolan, M., Rajewsky, N., Schroeder, M., Magnasco, M., and Darnell, J.E., Jr. (2003). Decay rates of human mRNAs: correlation with functional characteristics and sequence attributes. Genome research *13*, 1863-1872.

Yang, F., and Schoenberg, D.R. (2004). Endonuclease-mediated mRNA decay involves the selective targeting of PMR1 to polyribosome-bound substrate mRNA. Molecular cell *14*, 435-445.

Yang, N., and Kazazian, H.H., Jr. (2006). L1 retrotransposition is suppressed by endogenously encoded small interfering RNAs in human cultured cells. Nature structural & molecular biology *13*, 763-771.

Yang, Z., Jakymiw, A., Wood, M.R., Eystathioy, T., Rubin, R.L., Fritzler, M.J., and Chan, E.K. (2004). GW182 is critical for the stability of GW bodies expressed during the cell cycle and cell proliferation. Journal of cell science *117*, 5567-5578.

Yartseva, V., and Giraldez, A.J. (2015). The Maternal-to-Zygotic Transition During Vertebrate Development: A Model for Reprogramming. Current topics in developmental biology *113*, 191-232.

Yekta, S., Shih, I.H., and Bartel, D.P. (2004). MicroRNA-directed cleavage of HOXB8 mRNA. Science *304*, 594-596.

Zabolotskaya, M.V., Grima, D.P., Lin, M.D., Chou, T.B., and Newbury, S.F. (2008). The 5'-3' exoribonuclease Pacman is required for normal male fertility and is dynamically localized in cytoplasmic particles in Drosophila testis cells. The Biochemical journal *416*, 327-335.

Zenklusen, D., Larson, D.R., and Singer, R.H. (2008). Single-RNA counting reveals alternative modes of gene expression in yeast. Nature structural & molecular biology *15*, 1263-1271.

Zhang, K., Dion, N., Fuchs, B., Damron, T., Gitelis, S., Irwin, R., O'Connor, M., Schwartz, H., Scully, S.P., Rock, M.G.*, et al.* (2002). The human homolog of yeast SEP1 is a novel candidate tumor suppressor gene in osteogenic sarcoma. Gene *298*, 121-127.

Zheng, D., Ezzeddine, N., Chen, C.Y., Zhu, W., He, X., and Shyu, A.B. (2008). Deadenylation is prerequisite for P-body formation and mRNA decay in mammalian cells. The Journal of cell biology *182*, 89-101.

Zhou, J., Wan, J., Gao, X., Zhang, X., Jaffrey, S.R., and Qian, S.B. (2015). Dynamic m(6)A mRNA methylation directs translational control of heat shock response. Nature *526*, 591-594.

Zimyanin, V.L., Belaya, K., Pecreaux, J., Gilchrist, M.J., Clark, A., Davis, I., and St Johnston, D. (2008). In vivo imaging of oskar mRNA transport reveals the mechanism of posterior localization. Cell *134*, 843-853.